

Development of 3D filter made by stereolithography

Yoann Marchives

▶ **To cite this version:**

Yoann Marchives. Development of 3D filter made by stereolithography. Electronics. Université de Limoges, 2016. English. NNT : 2016LIMO0073 . tel-01482287

HAL Id: tel-01482287
https://theses.hal.science/tel-01482287

Submitted on 3 Mar 2017

HAL is a multi-disciplinary open access archive for the deposit and dissemination of scientific research documents, whether they are published or not. The documents may come from teaching and research institutions in France or abroad, or from public or private research centers.

L'archive ouverte pluridisciplinaire **HAL**, est destinée au dépôt et à la diffusion de documents scientifiques de niveau recherche, publiés ou non, émanant des établissements d'enseignement et de recherche français ou étrangers, des laboratoires publics ou privés.

Thèse de doctorat

UNIVERSITE DE LIMOGES

ECOLE DOCTORALE N°521

Science et Ingénierie pour la recherche

Laboratoire Xlim, Faculté des Sciences et Techniques de Limoges

Thèse

pour obtenir le grade de

DOCTEUR DE L'UNIVERSITÉ DE LIMOGES

Discipline / Spécialité : Electronique des hautes fréquences,

Optoélectronique et Photonique

présentée et soutenue par

Yoann MARCHIVES

le 12 octobre 2016

Development of 3D filter made by stereolithography

Thèse dirigée par Serge Verdeyme et Nicolas Delhote

JURY :

Président du jury

M. Pierre Blondy, Professeur, Laboratoire Xlim, Université de Limoges

Rapporteurs

M. Eric Rius, Professeur, Lab-STICC, Université de Bretagne Occidentale

M. Bruno Sauviac, Professeur, Laboratoire Hubert Curien, Université Jean Monnet

Examinateurs

M. Petronilo Martin Iglesias, Ingénieur Hyperfréquences, ESA/ESTEC

M. Massimiliano Simeoni, Docteur en Hyperfréquences, ESA/ESTEC

M. Serge Verdeyme, Professeur, Laboratoire Xlim, Université de Limoges

M. Nicolas Delhote, Maître de conférence, Laboratoire Xlim, Université de Limoges

Invités

M. Stéphane Bila, CR-HDR, Laboratoire Xlim, Université de Limoges

Université de Limoges

To my great-grandmother,

To my grandfather,

“Si vous voulez que la vie vous sourie, apportez-lui d'abord votre bonne humeur”

Spinoza

“

“La musique donne une âme à nos coeurs et des ailes à la pensée.”

Platon

“Nous ne savons jamais si nous ne sommes pas en train de manquer notre vie.”

Marcel Proust

Remerciements

Les travaux présentés dans ce manuscrit ont été effectués au sein de l'équipe MACAO du département MINACOM de l'institut de recherche XLIM. UMR CNRS n°7252 à l'Université de Limoges. Je remercie dans un premier temps Monsieur Dominique CROS, précédent directeur du laboratoire et professeur de l'Université de Limoges pour m'avoir permis de réaliser ces travaux .

Je remercie sincérement Monsieur Pierre Blondy d'avoir accepté de présider le jury de ma soutenance de thèse.

Je remercie également Messieur Eric RIUS et Bruno SAUVIAC d'avoir accepté d'être les rapporteurs de mes travaux de thèse.

J'adresse un profond remerciement à mes encadrants principaux Monsieur Nicolas DELHOTE qui a été à mes côtés tout au long de ce prériple et Monsieur Petronilo MARTIN IGLESIAS notamment pour le support qu'il m'a apporté lors de mes séjours au sein d'ESTEC (ESA) aux Pays-bas et à tous ses précieux conseils.

Je profite également de ces lignes pour remercier dans une plus grande mesure les différentes personnes qui m'ont aidé lors de ma présence à ESTEC, et en particulier Messieurs Cesar MIQUEL ESPANA et Christoph ERNST.

Je souhaite également remercie l'équipe dirigeante de MACAO, et plus particulièrement Messieurs Serge VERDEYME, Stephane BILA et Olivier TANTOT.

Je remercie aussi le CTTC en la personne de Monsieur Jérôme CLAUS pour les discutions et son aide pour la fabrication de mes différents prototypes en céramique notamment par le procédé de stéréolithographie.

Je tiens aussi à remercier Monsieur Aurélien PERIGAUD pour toute son aide et tous ses conseils que j'ai pu lui quémander durant mes recherches.

Je remerice également Monsieur Damien PASSERIEUX pour toute son assistance lors de mes différentes campagnes de mesure et à sa disponibilité. Je remercie également Monsieur Clément HALLEPEE qui m'a aidé dans mes dernières mesures.

Sur le plan personnel et affectif, je remercie mes collégues de la première heure à savoir Docteur Nicolas J. (pas besoin d'écrire le nom en entier tout le monde voit de qui je parle) et le double docteur Paul LESHAURIS (le fils) qui est un peu la soeur que je n'ai jamais eu ! Je n'oublie pas le plus beau Samuel Stéphane NGOHO MOUNGOHO et Carlos Paragua qui ont gravi les marches pour s'évader de cette prison maléfique.

Tous mes collégues du bureau, Joahnn, Philippe, Aymen, Khalil, Ahmad qui doivent encore travailler dur !

Je remercie aussi mes différents collègues-amis, Arnaud (joueur de babyfoot hors pair), Agostino (ma qué) toujours en train de courir, Karthik, Clément, Clément, Etienne et j'en oublie.

Je remercie également tous les courageux qui étaient là pour réaliser ces parties de soccer5.

Une dédicace spéciale au président de Sigmadox, Emilien LEMOINE, pour ces délicieux croissants et pour nos retrouvailles aux Pays-bas !

Je tiens également à remercier mes collégues et amis d'ESTEC, et notamment Nuno, Audrey, Matthew et Simone mes anciens colloc et ces merveilleux repas !!!!

Je remercie aussi Fanny, Anthony, AdoniX, Florent, ma Rosie, Julian, Christophe, Jérémy, Baptiste, Aurélien, Marion, David, Quentin, Philippe, Anne, Axelle, Lolita, Clarisse et Laurene.

Je remercie Marie-Laure et Marie-Claude pour toute l'aide qu'elles ont pu m'apportée.

Mes plus chaleureux remerciements vont à ma famille qui m'ont permis de réaliser ce fabuleux parcours de vie. Je remercie également Alexis d'avoir été à mes côtés dans les différents moments qui se sont présentés.

Droits d’auteurs

*Cette création est mise à disposition selon le Contrat : « **Paternité-Pas d'Utilisation Commerciale-Pas de modification 3.0 France** » disponible en ligne :*

http://creativecommons.org/licenses/by-nc-nd/3.0/fr/

Table des matières

Remerciements....3
Droits d'auteurs....4

General Introduction....18

Chapter I....20
Introduction....21
I.Context....21
1Telecommunication satellite....21
2Satellite architecture....24
1The platform....24
2The payload....24
3The functioning of a communication satellite....25
II.The robustness of the satellites....26
III.The future needs of the satellite industry....27
IV.Filtering function....28
1Input filter....29
2Solutions based on metallic wideband cavities....31
1Combline filter:....32
1Wide bandwidth....32
2Thermal compensation....33
3Q-factor and combline filters....34
4Manufacturing sensitivity....34
2 Ridge filter....35
5Solutions based on dielectric resonator....35
1Monobloc filter....36
2Solutions based on the TM modes....40
3Solution based on dielectric combline filter....41
4Conclusion....42
6Conclusion....43
V.Manufacturing methods....44
1Traditional manufacturing process....44
1Material removal....44
2Injection molding....44
3Assembly....45
2Manufacturing process using additive technologies....45
1Vat photopolymerization: Stereolithography (SLA) and Digital Light Processing (DLP)....47
1Stereolithography process (SLA)....47
2Digital Light Processing (DLP)....48
2Material jetting: Polyjet and multijet....48
3Binder jetting: 3D printing....49
4Material extrusion: fused deposition modeling (FDM), fused filament fabrication (FFF)....50
5Selective Laser Sintering (SLS)....50
6Selective Laser Melting (SLM) and Direct Metal Laser Sintering (DMLS)…51
7Electron Beam Melting (EBM)....51
8Sheet Lamination: Laminated Object Manufacturing (LOM)....52

9Directed Energy Deposition (DED): Laser Engineered Net Shaping (LENS), Direct Metal Deposition (DMD), 3D Laser Cladding....53
3Conclusion....54
Conclusion....54

CHAPTER II....60
I.Introduction....61
II.Characterization of the materials....61
1Method to characterize the dielectric materials....61
1Characterization of the cavity....63
2Properties of the dielectric resonator....64
2Measurement of the properties of the different ceramics....64
1Zirconia....65
2BMT (Barium Magnesium Tantalate)....67
1First recipe....68
2Second recipe....68
3Alumina....68
III.Determination of the coupling between dielectric resonators:....70
IV.Determination of the coupling in Input/Output accesses....71
1Phase of the S11 parameter....71
2S21 parameter....72
V.Project software environment....73
VI.TE01δ mode....76
1Dielectric resonator....76
2Ring resonators....78
3Input/Output couplings....79
1Waveguide....80
2Magnetic loop....82
4Inter-resonator coupling....88
1First configuration....89
2Second configuration....91
3Third configuration....93
4Fourth configuration....95
5Conclusion....96
VII.TM010 mode....97
1Electromagnetic fields....97
2Reasons of our choice....98
3Designs for Input/output coupling....98
4Designs for coupling between resonators....100
1Variation of the length of dielectric element (axis z)....101
2Variation of the gap between the dielectric element and the cavity....103
5Conclusion....104
VIII.Conclusion....105

CHAPTER III....109
Introduction....110
I.Manufacturing process....110
1Technology used in the CTTC....110
2Manufacturing....112
3Mechanical support for part under fabrication....114

4Shrinkage....115
5Conclusion....116
II.2-pole filter....117
1Characteristics....117
2Simulation....118
3Manufacturing dispersion on permittivity....120
4Manufacturing....121
1support for the manufacturing and dielectric manufacturing....121
2housing....123
5Measurements....124
III.4 pole Tchebitchev filter....126
1Characteristics....126
2Simulation....127
3Manufacturing....130
1support for the manufacturing....130
2Housings....131
4Measurements....132
5Post fabrication simulation....135
6Tuning screws: return of experience....136
Conclusion....136

CHAPTER IV....139
Introduction....140
I.2-pole filter with new Input/Output system....140
1Characteristics....140
2Simulation....141
1New Input/Output coupling system....141
2complete structure....144
3Manufacturing....146
4Measurements....147
II.2-pole filter with tuning system....148
1Characteristics....148
2Simulation....149
3Manufacturing....153
1Dielectric part and support for the manufacturing....153
2Dielectric rings....153
3Housing....154
4Measurements....154
1First set of rings made of Aluminia material....154
2Second set of rings made of Zirconia material....157
III.4-pole filter with improvements....159
1Characteristics....159
2Simulation....160
3Manufacturing....161
1Dielectric part....161
2cavity....162
4Measurements....162
IV.Filter with silver-plated dielectric part....164
13-pole silver-plated filter....165
1Characteristics....165

2Manufacturing.....166
1Dielectric part.....166
2Housing.....167
3Measurements.....167
32-pole filter covered by silver paint.....169
4Conclusion.....170
V.Conclusion.....171

Conclusion and perspectives.....173

List of Figures

Figure 1: Echo, the first satellite....18
Figure 2: Telstar 1 : the first active satellite and commercial payload....18
Figure 3: GOCE satellite....22
Figure 4: simplified payload synoptic of a communication satellite....22
Figure 5: Ariane 5 -ECA launch vehicle....23
Figure 6: artistic view of the mars colonization....25
Figure 7: technologies for wideband filters....26
Figure 8: technologies for narrow bandwidth....26
Figure 9: bandwidth as a function of the technologies....27
Figure 10: design example for combline and ridge filters....28
Figure 11: combline filter - wide band filter....28
Figure 12: Tunable combline filter....29
Figure 13: Tunable combline filter - Measurements....29
Figure 14: combline filters -thermal compensation....30
Figure 15: combline filters - high-Q and tunable filter....30
Figure 16: combline filters - conical resonators....31
Figure 17: dielectric filter - monobloc filter....33
Figure 18: dielectric filter - response of the monobloc filter....33
Figure 19: view of the quarter-cut TE01δ Image resonator filter....34
Figure 20: result of the quarter-cut TE01δ Image resonator....34
Figure 21: mushroom dielectric resonator (right) versus traditional shape (left)....35
Figure 22: Design of the 2-pole filter - Semicircular resonator....35
Figure 23: Response of the dual mode dual bandpass filter using semicircular resonators....37
Figure 24: DR filter using TM mode - 4-pole filter....37
Figure 25: DR filter using TM mode - 4-pole filter - results....38
Figure 26: DR filter based on TM mode....38
Figure 27: DR filter based on TM mode - results....39
Figure 28: Dielectric combline filter (left : design and right : fabrication)....39
Figure 29: Dielectric combline filter - left : measure and right : simulation....40
Figure 30: example of mold for injection [34]....42
Figure 31: artist view of a lunar station built by 3D printing....44
Figure 32: Principle of stereolithography process....45
Figure 33: Principle of the Polyjet printing....46
Figure 34: Principle of the binder jetting....47
Figure 35: principle of FDM....48
Figure 36: principle of SLS....49
Figure 37: principle of EBM....51
Figure 38: principle of LOM....52
Figure 39: A cavity to characterize a dielectric resonator on a Teflon support....61
Figure 40: determination of the Qc factor....63
Figure 41: powder of Zirconia (Zirconium oxide)....65
Figure 42: Characterization of the Zirconia material - 4GHz resonator....67
Figure 43: The behavior of the Zirconia permittivity as a function of the frequency....67
Figure 44: The behavior of the Zirconia loss tangent as a function of the frequency....68
Figure 45: Characterization of the Zirconia material - recipe 1 (left) , recipe 2 (right) - 10GHz resonator....69
Figure 46: powder of alumina (Aluminum Oxide)....70
Figure 47: Alumina resonators....70

Figure 48: Aluminia permittivity as a function of the frequency.....70
Figure 49: Alumina loss tangent as a function of the resonance frequency.....70
Figure 50: initial structure to calculate the K12 coupling.....71
Figure 51: one half of the previous structure.....71
Figure 52: Determination of the Qe factor between the cavity and the waveguide.....72
Figure 53: determination of the Qe-factor with the phase of the S11 parameter.....73
Figure 54: determination of the Qe-factor with the S21 parameter.....74
Figure 55: front panel of the FELO software.....74
Figure 56: example of a filter response with the FELO software.....76
Figure 57: coupling matrix obtained by FELO software.....76
Figure 58: front panel of the PRESTO software.....77
Figure 59: Values of the coupling coefficients of the simulated filter (bottom matrix) and of the theoretical one that is expected (top matric).....77
Figure 60: Zirconia DR inside a cavity.....78
Figure 61: Electric and magnetic field inside a cavity loaded by a dielectric resonator.....79
Figure 62: resonator and support with a hole - one single material.....80
Figure 63: Impact of the hole radius inside a dielectric resonator.....81
Figure 64: resonator excited by waveguide.....82
Figure 65: Waveguide - Input coupling - Height of the iris.....82
Figure 66: Waveguide - Input coupling -Width of the iris.....83
Figure 67: Waveguide - Input coupling -Thickness of the iris.....83
Figure 68: orientation of the magnetic field in the cavity.....84
Figure 69: Magnetic loops close to the DR.....85
Figure 70: Qe-factor of this design as a function of the length of the probe.....85
Figure 71: configuration B for Input/Output with magnetic loops inside the dielectric resonator 86
Figure 72: Variation of the gap between the two arms of the coaxial probe.....86
Figure 73: Result for the variation of the gap between the two arms of the coaxial probe.....87
Figure 74: Example of different lengths for the coaxial probe.....87
Figure 75: Result for the length variation of the coaxial probe.....88
Figure 76: excitation system - coaxial probe inside a cavity with a 90° bend.....88
Figure 77: Presentation of the two studied parameters for the Input coupling.....89
Figure 78: Behavior of the Qe-factor as a function the distance between the DR and the probe 89
Figure 79: Behavior of the Qe-factor as a function of the position of the coaxial probe.....90
Figure 80: electromagnetic field inside the cavity.....90
Figure 81: first configuration.....91
Figure 82: first configuration - TE01δ mode with modifications of the connecting cylinder radius (r).....91
Figure 83: Variation of the K12 coupling -first configuration.....92
Figure 84: first configuration - Electromagnetic field inside the DR and the cavity.....93
Figure 85: second configuration – TE01δ mode.....93
Figure 86: electric field – second configuration – TE01δ mode.....94
Figure 87: K12 coupling depending of the axis x dimension - second configuration – TE01δ mode.....94
Figure 88: K12 coupling depending of the axis z dimension - second configuration – TE01δ mode.....95
Figure 89: third configuration - TE01δ mode.....96
Figure 90: electric field – third configuration - TE01δ mode.....96
Figure 91: fourth configuration TE01δ mode.....97

Figure 92: fourth configuration - electric and magnetic fields.....98
Figure 93: dielectric resonator using the TM010 mode.....99
Figure 94: electric (left) and magnetic (right) fields – strong field: red; low field: blue – TM010 mode.....99
Figure 95: Input/Output coupling system.....100
Figure 96: Electric and magnetic fields - interaction between the dielectric resonator and the coaxial probe.....102
Figure 97: Evolution of the Qe-factor depending of the length of the coaxial probe.....103
Figure 98: dielectric element for strong coupling and connecting two resonators.....103
Figure 99: configuration to have a strong K12 coupling – TM010 mode.....104
Figure 100: K12 coupling versus the length of the dielectric coupling element.....105
Figure 101: K12 coupling versus the dimensions a and b of the dielectric coupling element 105
Figure 102: K12 coupling versus the gap metallic housing/dielectric element.....106
Figure 103: Summary of the different configurations using TE01δ mode dielectric resonators 108
Figure 104: paste making for stereolithography process (cttc.fr).....114
Figure 105: stereolithography process - view of the scraper and the work area.....115
Figure 106: stereolithography process - lightening of the paste.....116
Figure 107: stereolithography process - diluent bath and dielectric part before firing.....116
Figure 108: the different steps of the stereolithography process.....117
Figure 109: Example of a structure with support.....118
Figure 110: Example of gaps between the support and the element.....118
Figure 111: theoretical matrix of the 2-pole filter - f0=3.3GHz - bandwidth 14%.....120
Figure 112: theoretical response of the 2-pole filter - f0=3.3GHz - bandwidth 14%.....121
Figure 113: design on HFSS of the 2-pole filter.....121
Figure 114: design of the 2-pole filter with tuning screws.....122
Figure 115: full wave response of the 2-pole filter.....122
Figure 116: study of the permittivity value on the 2-pole filter response - S11 parameters....123
Figure 117: study of the permittivity value on the 2-pole filter response - S21 parameters…124
Figure 118: dielectric part with the support made during the manufacturing.....124
Figure 119: dielectric part of the 2-pole filter.....125
Figure 120: housing of the 2-pole filter.....126
Figure 121: copper housing for the 2-pole filter.....126
Figure 122: metallic housing for the 2-pole filter.....127
Figure 123: copper housing with the dielectric element between the Input/Output connectors 127
Figure 124: simulated and measured response of the 2-pole filter.....128
Figure 125: theoretical matrix of the 4-pole filter - f0=4GHz - bandwidth 10%.....129
Figure 126: theoretical response of the 4-pole filter-f0 = 4GHz -bandwidth 14%.....130
Figure 127: design on HFSS of the 4-pole filter.....130
Figure 128: closer view of the tuning screw placed between two resonators.....131
Figure 129: tuning screws for the central cavity of each cavity.....131
Figure 130: simulated response of the 4-pole filter and comparison with the electric model.132
Figure 131: extracted matrix of the 4-pole filter - f0=4GHz - bandwidth 10%.....132
Figure 132: simulated wideband response of the 4-pole filter.....133
Figure 133: 4-pole filter with tuning screws.....133
Figure 134: designed and manufactured dielectric part of the filter with support.....134
Figure 135: manufactured Aluminum housing for the 4-pole filter.....134
Figure 136: plastic housing for the 4-pole filter.....134
Figure 137: plastic housing covered by the silver paint.....135

Figure 138: measurement of the 4-pole filter.....135
Figure 139: simulated and measured response of the 4-pole filter.....136
Figure 140: extracted coupling matrix of the 4-pole filter.....136
Figure 141: crack on the dielectric element of the 4-pole filter.....137
Figure 142: measured dimensions of the 4-pole filter.....138
Figure 143: spurious mode created by the screws - 4-pole filter.....139
Figure 144: Theoretical coupling matrix of the 2-pole filter - f0=4GHz - BW=1.5GHz.....143
Figure 145: New Input/Output coupling.....143
Figure 146: Kin coupling versus metallic radius.....144
Figure 147: Kin coupling versus the gap between the dielectric and metallic radii.....145
Figure 148: Kin coupling versus the radius of the dielectric disk.....145
Figure 149: design of the 2-pole filter with the new Input/Output system.....146
Figure 150: 2-pole filter - new Input/Output coupling system - simulated response.....147
Figure 151: 2-pole filter - new Input/Output coupling system - dielectric element on this support.....147
Figure 152: coaxial probe for the new Input/Output system.....148
Figure 153: 2-pole filter - new Input/Output coupling system - manufactured structure without top plate.....148
Figure 154: Response of the 2-pole filter with the new Input/Output system.....149
Figure 155: Design for the tuning system with regular section (circular) and tuning one (cubic) 150
Figure 156: Coupling matrix for the 2-pole filter with tuning system.....151
Figure 157: 2-pole filter with the extra rings tuning system.....151
Figure 158: Behavior of the frequencies of the modes as a function of the radius of the hole 152
Figure 159: Variation of the Q-factor as a function of the radius of the hole.....152
Figure 160: dimensions of the 2-pole filter with tuning system.....153
Figure 161: Simulated response of the 2-pole filter with tuning system.....153
Figure 162: Manufactured dielectric part - 2-pole filter with tuning system.....154
Figure 163: a set of dielectric rings for the 2-pole filter with tuning.....155
Figure 164: 2-pole filter with tuning system - manufactured elements.....155
Figure 165: S21 parameters for different radius of the tuning rings (thickness = 3mm) – Alumina -2-pole filter with tuning system.....156
Figure 166: S11 parameters for different radius of the tuning rings (thickness = 3mm) – Alumina - 2-pole filter with tuning system.....157
Figure 167: S21 parameters for different thickness of the tuning rings (radius = 9mm) – Alumina - 2-pole filter with tuning system.....158
Figure 168: S21 parameters for different thickness of the tuning rings (radius = 9mm) - Zirconia - 2-pole filter with tuning system.....159
Figure 169: S21 parameters for different radius of the tuning rings (thickness = 2mm) – Zirconia -2-pole filter with tuning system.....159
Figure 170: Theoretical coupling matrix of the 4-pole filter - f0=4GHz - Bd=1.8GHz.....161
Figure 171: design of the 4-pole filter - new generation.....162
Figure 172: dimensions of the 4-pole filter new generation.....162
Figure 173: Simulated response of the 4-pole filter - new generation.....163
Figure 174: dielectric 4-pole filter with the Teflon supports.....163
Figure 175: measurement of the 4-pole filter.....164
Figure 176: Measured response of the 4-pole filter -new generation.....164
Figure 177: Behavior of the filter as a function of the temperature.....166
Figure 178: coupling matrix of the 3-pole silver-plated filter.....167

Figure 179: 3-pole filter covered by silver paint.....167
Figure 180: Simulated response - 3-pole filter covered by sylver paint.....168
Figure 181: Manufactured dielectric part and covered by a silver layer - 3-pole filter.....168
Figure 182: Plastic housing for the 3-pole filter silver-plated.....169
Figure 183: Dielectric silver-plated part inside the plastic housing cover of silver lacquer…169
Figure 184: Measured response of the 3-pole silver-plated filter.....170
Figure 185: 2-pole dielectric part covered by silver lacquer.....170
Figure 186: 2-pole silver-plated dielectric part inside the metallic housing.....171
Figure 187: 2-pole filter covered by silver paint - measurement.....171

List of Tables

Table I: frequency distribution and using in the satellite communications.....20
Table II: measured characteristics of the quarter-cut TE01δ Image resonator.....35
Table III: advantages and drawbacks of the combline and dielectric filters.....40
Table IV: frequency response of the dielectric resonator.....80
Table V: spurious modes for the first configuration - TE01δ mode.....92
Table VI: modes of the second configuration.....95
Table VII: modes of the third configuration.....96
Table VIII: modes for the fourth configuration.....97
Table IX: characteristics of the 2-pole filter.....128
Table X: characteristics of the 4-pole filter.....136
Table XI: Results of the measured 2-pole filter.....149
Table XII: Impact of the dielectric rings in the bandwidth - 2-pole filter with tuning system 156
Table XIII: bandwidths depending of the thickness of the tuning rings - 2_pole filter with tuning system.....158
Table XIV: bandwidths for different thickness of dielectric rings - Zirconia - 2-pole filter with tuning system.....159
Table XV: Banwidths depending of the radius of the tuning rings - Zirconia - 2-pole filter with tuning system.....160
Table XVI: Comparison between measure and simulation for the 4-pole filter new generation 165

General Introduction

The telecommunications are present in every moment of our life with smartphones and upcoming Internet of things all around us. These devices make possible to keep in touch with our family, our friends, and everything that happens in the world. Our phone has greatly evolved since Alexander Graham Bell era. It is now possible to have video call with someone everywhere on the planet. Our digital documents, movies and books can be now accessible from the Cloud at any moment and from anywhere. This evolution was partly possible thanks to the telecommunication satellites. The data exchanges are greatly growing up due to the need of a better worldwide access to the Internet and some projects propose to cover the last blind spots using drones, balloon or mega constellations of low Earth orbit (LEO) satellites. For these reasons, we need to increase the characteristics of our telecommunication transmission to have a better output to satisfy the customers. One way is to increase the bandpass of the signal to have the possibilities to transmit more information.

This thesis has been done in the frame of a European Space Agency (ESA) Networking/Partnering Initiative (NPI) program. In a very close relation with the European Space Research and Technology Center (ESTEC) based in Noordwijk (The Netherlands), this ESA sponsored project named "Development of 3D filters made by 3D ceramic stereolithography" is searching for innovative solutions to create bandpass filters in low frequency bands (L, C, …). Specific objectives are here researched:

- creating unusually wide bandwidth (>10%)
- keeping a high level of compactness
- remaining as low loss as possible
- limiting the number of assembled parts, one part as a desirable goal
- using ceramic materials and compatible additive manufacturing as provider of breakthrough solutions

Focusing this work on the input filters which can be found in the input section of the telecommunication satellite, our original approach is to use highly coupled cavities loaded with dielectric resonators (DR). Known for their low loss and good compactness, they usually are not the obvious choice when wide bandwidth are required. In other words, thanks to the fabrication freedom offered by the additive manufacturing and innovative designs, we seek new intermediate solutions between low loss and compact filters based on DR and somehow bulky wide bandwidth waveguide filters.

In the Chapter I, we will first present the context of the telecommunication satellite and the future needs related to this activity. The typical solutions used nowadays to get very wide bandwidth will be overviewed as well as filters based on DR. Different manufacturing techniques will then be reviewed with a specific focus on additive manufacturing (AM). We will thus describe several types of 3D printing technologies and select the most promising one for the creation of the DR based filters we are looking for.

Chapter II will firstly present the ceramic materials compatible with the AM technologies we will use. After presenting the used characterization method, the properties of the ceramics will be measured around 4 GHz, this frequency being chosen as a typical operating frequency for this project. A specific research about the couplings strategies that can be developed to create the wide bandwidth we are looking for will be performed. This chapter will also be focused on the TE01δ and TM010 modes for our dielectric resonators. Different geometrical configurations will be tested to meet our expectations with an original baseline: the resonating elements would be made within one single part. The final objective of this chapter is to select the most promising designs for the filter Input/Output couplings and for the couplings existing between the different DR for the next coming filters.

Chapter III, using the obtained results from the previous chapter, is dedicated to a deeper presentation of the specific technology used for the fabrication of the 3D dielectric part. The stereolithography process and its properties will thus be detailed and used for the creation of this chapter's filter. 2nd and 4th order filters are thus designed and tested using this technology.

Based on the lessons learned, the Chapter IV will target three issues which have been identified:

- getting a better excitation system based on coplanar probes
- trying to improve the filter tuning after assembly
- making sure to maintain low manufacturing tolerances for the dielectric part

New generations of the 2nd and 4th order filters will be thus proposed as upgraded version in order to finally achieve the project objectives. This chapter will finally draw some very promising perspectives with an experimental demonstration of super wide bandwidth using a single silver plated dielectric part. 2nd and 3rd order bandpass filters will here be presented as the project final demonstrators.
Several conclusions and perspectives will ultimately be given at the end of the manuscript.

Chapter I

General characteristics

I. Introduction

The telecommunication satellite area begun in 1960 by the first launch of an artificial satellite. Since this event, the technologies and missions of a satellite have greatly increased in complexity as well as the traveled distance since we have reached Mars and even some comets. After a description of this context, this chapter will focus on the transmission function and more precisely on the Input filters and Multiplexers. They are important elements because they permit to select a specific signal amongst many others. Today's needs of increasing data output through satellites require a use of wider bandwidth. Since weight and volume are critical in a satellite, we aim to realize wide bandpass filters without sacrificing compactness. Moreover, we want a filter with low insertion loss, making a high need of high Q-factor resonators within such filters. First, we will study different existing solutions for filters with the required wide bandpass and the aforementioned properties, and also solutions to maximize compactness and high Q-factor.

In a last part, we will present different additive manufacturing processes because of their broad availability and compatible materials, but particularly because they can provide boundary free manufacturing properties for the challenge we are looking for.

These different parts will help us choosing the most promising filters technologies, solutions and manufacturing processes that can make us reach the targeted wide bandpass filters for space telecommunications.

II. Context

1 Telecommunication satellite

A telecommunication satellite is an artificial satellite located in space to relay information to different locations in earth or between different satellites. A satellite has a predetermined lifespan due to its fuel tank size. Indeed, the satellite is built with a certain fuel quantity. It will be used to realize two principal missions, the first one is to hold the satellite on the right orbit (because of the earth's pull) and the second one is to avoid the other elements present in space like other satellites, debris, etc.

The first communication satellite [1] was launched the 12th of august in 1960 by the NASA. It was a spherical balloon of 30.5m diameter and 68kg called Echo. It was launched thanks to

18.144kg of air required to inflate the sphere. Echo was a passive communication satellite which reflected radio and radar signals. It was also used, over a period of time and with accurate tracking, to plot the variations of air density at the top of the atmosphere by following the vagaries of its orbit.

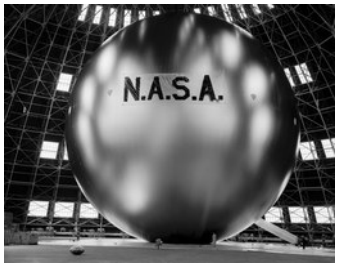


Figure 1: Echo, the first satellite

We had to wait the 10th of July 1962 to have the first active communication satellite with Telstar 1 [2] launched from Cape Canaveral, the American launch center. It relayed two days later the first transatlantic television signal between Andover Earth Station in Maine and the Pleumeur-bodou Telecom center in France. Then, it was the first commercial payload to prove the feasibility of the information transmission by satellite. However, the satellite permit to manage 400 transmissions of telephone, telegraph, facsimile and television. The lifespan finished in November of the same year due to the effects of radiation.
It was a good opportunity to understand and to comprehend the difficulties related to the launch of a satellite in orbit and its behavior in a space environment in order to give him a better protection.



Figure 2: Telstar 1 : the first active satellite and commercial payload

Since this first success, the complexity of the system had increased a lot and they have become heavier. We can notice that the current trends are nowadays to try to decrease this weight as much as possible for cost reasons.

This kind of satellite are actually used in the next domains:

- international communication
- radio and television
- GPS
- high output data transmission
- military communications

These satellites are mainly used to relay a radio signal over an allocated frequency range depending of the application. Every band has its own characteristics (spreading properties). However, the present demands require more and more frequencies allocations for the different applications.

The International Telecommunication Union (ITU) [3] is an agency from the United Nations and is in charge of validating the different frequency bands assignment and to normalize the applications. It is one of the most older intergovernmental organization since its previous name was the International Telegraph Union created in 1865 in Paris.

The ITU divides the different frequencies as shown in Table I.

Name of the band	**Frequency range (GHz)**		**Applications**
	Uplink	**Downlink**	
L-band	1.626 – 1.660	1.525 – 1.559	Radio navigation, cell phone by satellite
S-band	2.665 – 2.690	2.500 – 2.655	Cell phone by satellite (UMTS)
C-band	5.725 – 7.075	3.400 – 4.200 4.500 – 4.800	Phone transmission, broadcasting
X-band	7.900 – 8.400	7.250 – 7.750	Military coded communication
Ku-band	12.750 – 13.250 14.000 – 14.800 17.300 – 18.100	10.700 – 12.750	Television diffusion, multimedia applications
Ka-band	27.500 – 31.000	18.100 – 21.200	High output civil communication

Table I: frequency distribution and using in the satellite communications

The uplink represents the signal patch from Earth to the satellite and the downlink the opposite way. The frequency ranges are different for each way to avoid interference between them. In this report, our study is focused on input filters, the application being a front-end receiver for a frequency range from 300 MHz to 30 GHz. Then, three bandwidths can typically be used:

- C-Band: up to full band
- Ku-Band: with 250/500 MHz bands
- Ka-Band: with 250/500 MHz bands

and different examples of input filters on these bands will be given in part IV.1.1.

2 Satellite architecture

1 The platform

The platform is the name for all the elements that ensure the functionality of the satellite in space like:

- thermal control: to maintain a temperature range of the payload between -20°C and 60°C (the external temperature of the satellite can be 150°C during direct sun exposure and -160°C in the shadow of the sun light),
- positioning system: to hold the right position and orbit,
- power supply thanks to solar panels, energy storage and delivery.

2 The payload

It is the part that fulfills the missions of the satellite. The functions of this element is to exchange data information of the mission (observation, radio navigation, meteorology) with the ground. Usually, it is 30% of the entire mass of the satellite. For example, the Gravity Field and Steady-State Ocean Circulation Explorer satellite (GOCE) [4] is a scientific ESA satellite launched in 2009. Its mission is to study the gravity field of earth. Indeed, this field is not homogenous and it can be changed due to the relief under and over the sea. Then it is affected by the material distribution inside the earth: the earth's crust and mantle thicknesses vary and they are not also homogenous. The principal measurement device of the payload is a gradiometer composed of many accelerometers. All these scientific equipments occupy an important volume and mass, just as all the hardware we can find in a telecommunication satellite.



Figure 3: GOCE satellite

3 The functioning of a communication satellite

The payload traditional mission is to relay a signal between ground stations. Two elements are necessary, antennas and repeater systems. The satellite through its input antenna receives a signal and this latter is transposed in frequency and amplified before being transmitted again by the Output antenna. The signal information are still the same, they are not modified by the process, making that type of satellite being named “transparent” satellites.

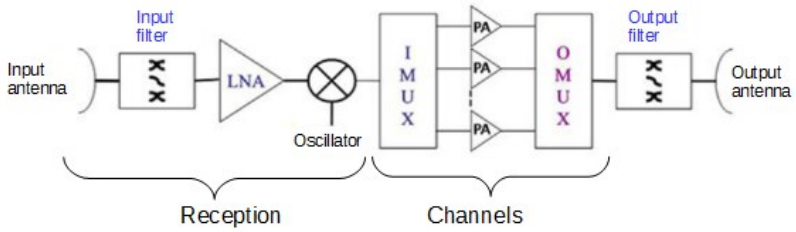


Figure 4: simplified payload synoptic of a communication satellite

We will present now the principal elements of this payload (Figure 4). The input antenna receives the signal from the ground station. The typical power level is low (from 100pW to 1nW at this stage). Following this part we have the reception stage that permits to select the right signal thanks to the filter and to amplify this one keeping a low noise level. The oscillator transposes the carrier frequency for the transmission. After this step, the channel stage cut the input bandwidth in several ones through the IMUX (Input Multiplexer), each cut signal going through one channel where it will be amplified for their transmission (around 100W for the output power). At the end, all the cut signals are combined together by way of the OMUX (Output Multiplexer) before going to the Output antenna that transmits the signal toward another ground station or another satellite.

III. The robustness of the satellites

To be installed in orbit, the satellite uses a launch vehicle. For example, the European launch vehicle is Ariane 5 developed by Arianespace [5]. In the Figure 5, we have a view of the Ariane 5 vehicle with two satellites EUTELSAT 8 West B [6] and Intelsat 34 [7]. The possibility to launch two elements at the same time is the principal advantage of this launch vehicle, allowing to share and decrease the launch cost.

The first flight of the Ariane family happened the 4th of June 1996 and failed. Since this first event, Ariane had launch 81 (at 2015-08-20) and the fiability ratio is 96,3%.

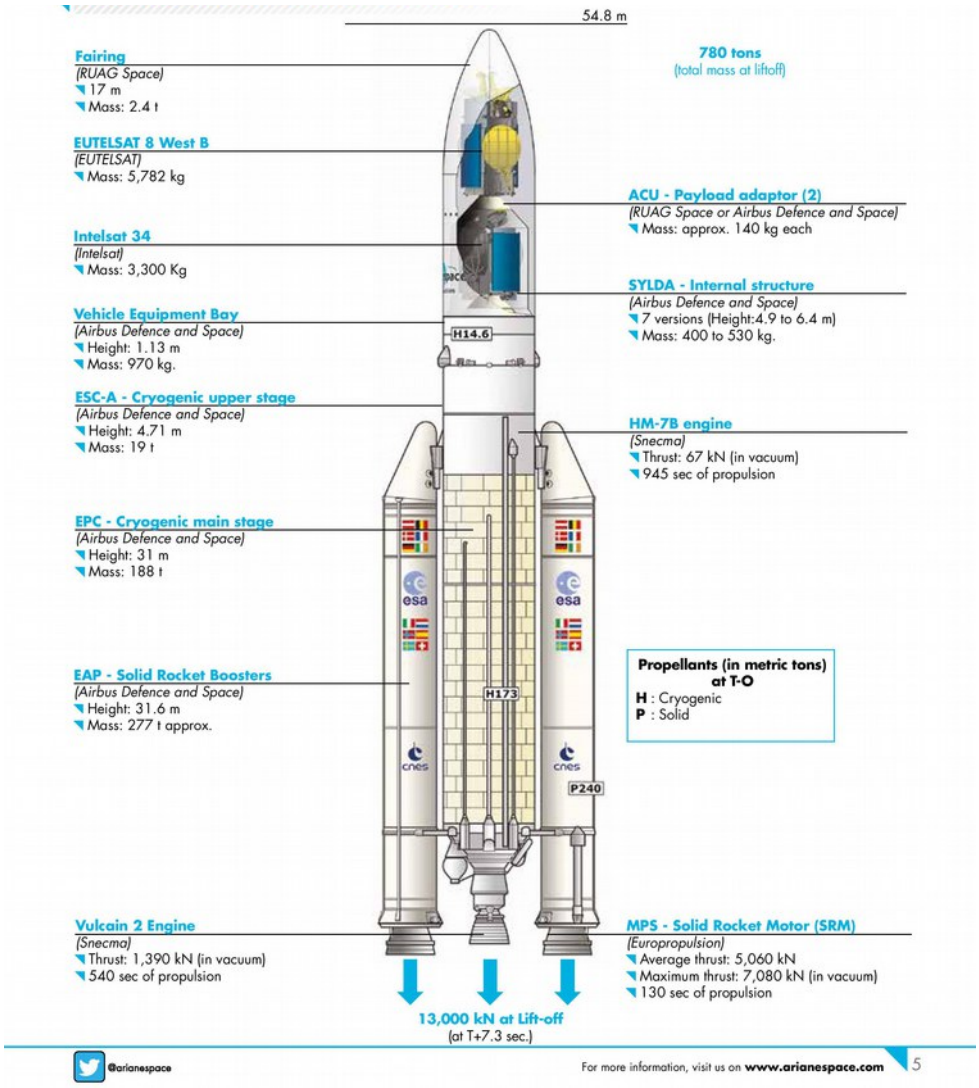


Figure 5: Ariane 5 -ECA launch vehicle

The launch center is based in Kourou, French Guiana, because it is close to the equator so it benefits from an additional velocity of 460m/s due to the Earth rotation. It is the best latitude

to send geostationary satellites. Moreover, this base can be used by a lot of launch vehicle (Vega, Soyouz, etc) so it is a very interesting location for space activities.
The satellites are located in the nose of the booster rocket and they will have to resist to the different launch steps (acceleration, floor splitting) and to support the different mechanical vibrations. Moreover, when the satellite arrives in the right orbit it will be submitted to the space temperature variation from -160°C (shadow) to 150°C (direct sunlight). However, the different elements of the satellite protect the payload to bring back the temperature range between -20°C and 60°C. We can notice that the payload is not protected from the cosmic and solar rays.

IV. The future needs of the satellite industry.

For the next decade, the satellite market represents $255 Billions for manufacturing and launch (estimated cost is for 1400 satellites). 75% of this amount of money come from government of 60 countries. The principal countries of this market are the U.S.A., Russia, Europe (France, Germany, the U.K., Italy and Spain), China, Japan and India where are located the main of the satellite manufacturers.
550 satellites would be launched in the next decade for the commercial space sector. Indeed, the actual space fleet is old and has to be replaced by new one. 80% of these elements will be installed in the geostationary orbit (35786 km from Earth surface).

The manned missions find a revival thanks to some people like Elon musk and Bas Lansdorp.
The first one is known as the founder of SpaceX and a cofounder of Tesla Motors. SpaceX (Space Exploration Technologies Corporation) is an American aerospace manufacturer. The main goal of this firm is to give an access to everyone to the space technologies. One of its launch vehicle, Falcon 9 permit to put in place payloads in orbit (13,15t to low Earth orbit and 4,8t to geostationary transfer orbit) [8]. Then it is used to resupply the ISS. To decrease the cost of this rocket, the choice was made to reuse some part of the vehicle for several launches. However a failure happened in June 2015 and the launch have stopped since the needed inquiries.
A common point between the two men is their interest in the colonization of the Mars planet (Figure 6). The Netherlander engineer Bas Lansdorp assured it was possible in 2024. However, several experts and the NASA doubt on that. Indeed, some technical and human problematics are still not solved. We can give some examples: for technical reasons is not

possible today to land a vehicle with a weight superior to 1t due to the Mars atmosphere. Then, the autonomous production of the different vital elements are in the experimental step such as oxygen or food production. As a difference with the ISS, no convoy is possible due to the travel time.



Figure 6: artistic view of the mars colonization

Regarding the human constraints, we can notice that it will be the first long space travel (seven months), and the astronaut will be exposed to strong psychological problems. Then, the lack of gravity will decrease the efficiency of the people when they will land on Mars. Finally, the effect of such a long flight is not known (actual travel duration is around six months).
However this kind of project has the benefits to focus advanced research activities in the space domain.

V. Filtering function

The hyperfrequency filters have been key components for the signal processing in the receiver/transmitter system since they are operating a sensitive process during the extraction of a given signal over a frequency range. Then, the flexibility and the complexity of the payload require more and more advanced technology and specific characteristics. Two main and required improvements are the dimensions and the weight of such device. Indeed, the launch cost is depending on the total weight of the satellite and having smaller devices result in more of them in a satellite. We will focus in the next section on the actual filters used and some solutions to decrease the size of these components.

1 Input filter

The first main filtering step of a payload is realized by Input filters. Their characteristics are to cover all the frequencies received by the satellite, that is why we may need to use wideband filter. In the Figure 7, we have the typical different technologies used to achieved this function depending of the frequency band. For example, in L/S-band, we give priority to combline filter, whereas in C-band we also have the possibility to use ridge filter. The principle of the combline filter is a metallic cavity loaded by metallic resonators, the structure will be explained in detail later.

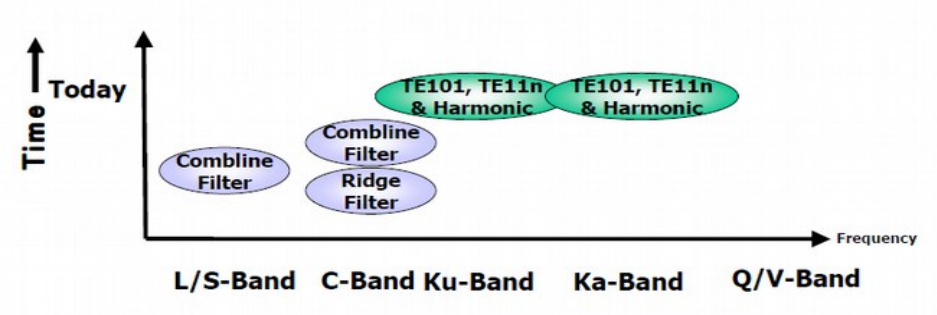


Figure 7: technologies for wideband filters

The next main filtering step is for the Input Multiplexer (IMUX). The signal is divided at this stage in different channels. The next section will highlight some of their main characteristics.

IMUX filter

The specifications of this kind of filters are not the same as the previous ones because the signal is covering much narrower bandwidths making flatness and insertion loss crucial. The typical specifications of such IMUX channel filters which have to be taken into account are:

- Narrow bandpass (<1%)
- Low ripple: less than 0.5dB on the bandpass
- Wide spurious free range
- Very low insertion losses
- Compactness

The Figure 8 depicts the particular case of narrow band filters. We remarks we have technologies that are not used for Input filters such as filters using dielectric material and TE01δ mode dielectric resonators. Indeed, with this elements, it is possible to have a good compactness with high permittivity material while keeping low insertion losses.

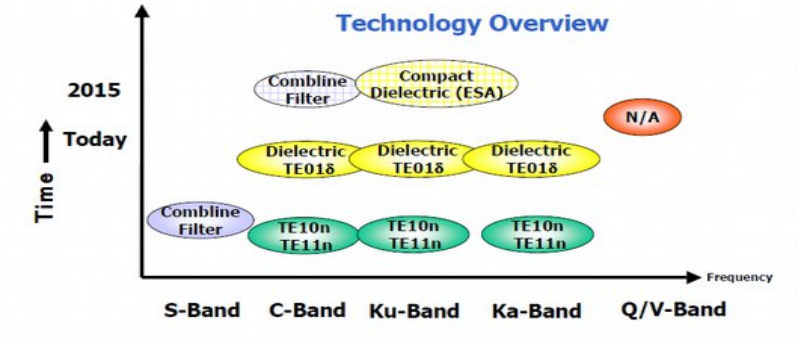


Figure 8: technologies for narrow bandwidth

Regarding these specifications, a pseudo-elliptic response is most of the time necessary to realize these filters. Regarding filters in lower band (C-band for example), dielectric resonators are commonly and placed in a metallic housing. Firstly, high permittivity materials are used and permit to strongly concentrate the electromagnetic fields inside the dielectric element making them capable to reduce the dimensions and the weight of the filter. Secondly, a strong attention has to be paid on the dielectric loss tangent if we want to ensure a high enough unloaded quality factor (Q-factor).

To be notice that another solution to decrease the volume of such filters is to use dual mode resonators.

In this manuscript, we would like to combine high Q-factor (low losses) and compactness (obtained with DR) with the wideband of the Input filter. To sum up combline and ridge filters are mainly used for wideband filters, however these filters do not permit is to have a small package and a very high Q-factor. Therefore we propose to study other technologies to fulfill the filter requirements in a better way. Ceramic materials, because of their high permittivity and low loss tangent can fill that requirements if the proper couplings between dielectric resonators can be reached.

Using this primary overview, we have two principal technologies for C-band applications: combline and dielectric resonators. Figure 9 resumes the typical relative bandwidth that can be reached with the main filtering technologies.

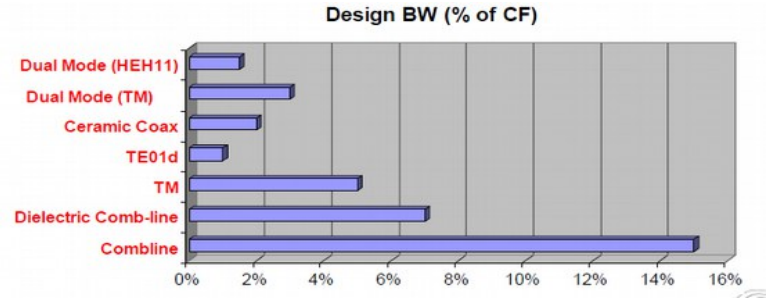


Figure 9: bandwidth as a function of the technologies

Because of their properties to highly concentrate the electric field, DR based filters are commonly limited to very small bandwidths (1 or 2%). Challenging the coupling limitation between regular DR, we can propose a resonator showing a better Q/size ratio than a typical combline resonator for wide bandpass application (10% and more)

After the presentation of these technologies, the next paragraph will give a deeper overview of the standard solutions for Input filters with a specific focus on the solutions able to provide wide bandpass of about 10% and more.

2 Solutions based on metallic wideband cavities

Usually, we use combline or ridge filters for Input filters that typically need wide bandwidth.

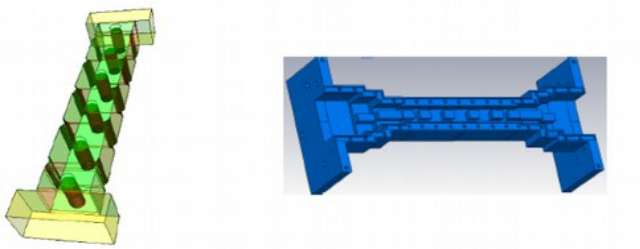


Figure 10: design example for combline and ridge filters

These well known filters are now easy to design [9] thanks to existing optimization tools and composed of a few and easily assembled number of mechanical parts. Moreover metallic material are used like Aluminum making these structures not very expensive. As seen before (Figure 9), it is possible to achieve a high bandwidth (10%) with such filters but they are not the most compact structure and do not have the highest Q-factor.

1 Combline filter:

The principle of a combline filter is similar to a stepped digital filter [10]. The difference is that the inductors are replaced by interdigital lines (short-circuited at one end). By this way, the filter can be reduced to a λ/12.

1 Wide bandwidth

Adam Abramowicz [11] proposes a method to design wide band combline filters. This method has been illustrated with a 2-pole filter with a central frequency of 1,7 GHz and a relative bandwidth of 54%. The dimensions of the complete structure are 15×20.3×30.3mm^3. The filter is shown in Figure 11.

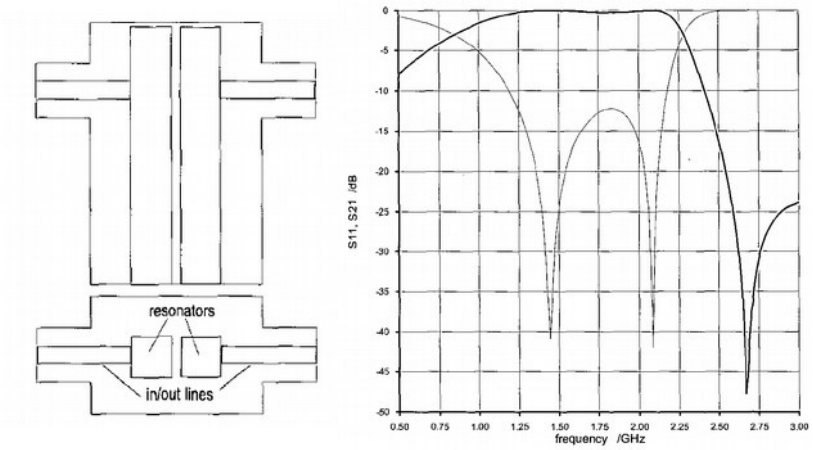


Figure 11: combline filter - wide band filter

The result of this filter shows the possibility to realize wide bandwidth using combline filter. However, we do not have information about the spurious free range and the Q-factor of this filter.

In [12], we have the presentation of a combline filter with a tunable bandwidth and central frequency. A 4-pole filter (Figure 12) is designed to describe this application. The capacitive effect brought by the metallic rods are tuned in order to modify the bandwidth of the lower passband. The bandwidth can be tune up to 200% from 11MHz to 33MHz.

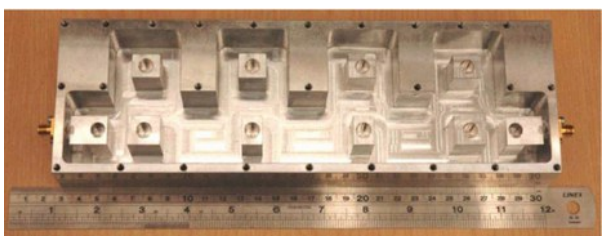


Figure 12: Tunable combline filter

The central frequency range is tuned from 1.5 to 1.8 GHz depending of the bandwidth. The results are shown in Figure 13. The insertion loss is not precised but they are apparently between 0.5 and 1dB.

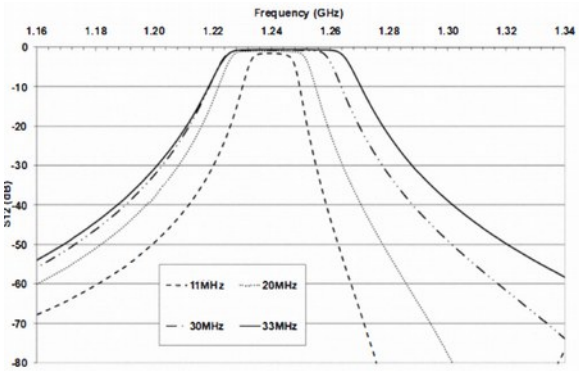


Figure 13: Tunable combline filter - Measurements

2 Thermal compensation

One of the most problematic aspect of the combline filter is the material expansion. Indeed, the space subjects the satellite to extreme temperature changes so the dimensions of the filter are not the same leading to a dysfunction of such filter. In this way, several techniques exists to avoid the expansion, one of them is to use different materials to design the filter as presented in the paper [13] of Hui-Wen Yao. Three materials are implemented: the first one with a very low coefficient of thermal expansion(Titanium: τ_r=8.5ppm/°C or Invar: τ_r=1.0ppm/°C, or a combination of the both: τ_r=4.0ppm/°C) for the resonator rod, the second one (steel) for the tuning screw and the last one (Aluminum) for the housing.

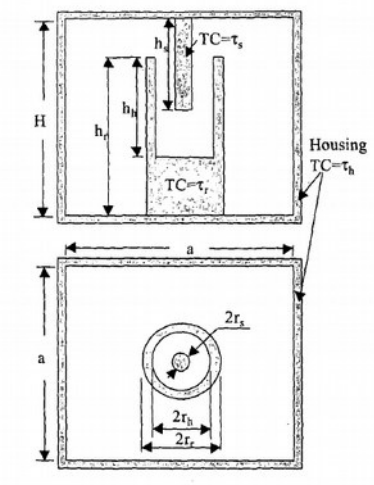


Figure 14: combline filters -thermal compensation

The simulations permit to find the right placement of the different elements. However, a study is necessary for each case and the impurities in the materials can modify the coefficient of thermal expansion and modify the expected behavior over temperature.

3 Q-factor and combline filters

The paper [14] presents the design and the implementation of a high-Q bandpass filter. This filter is tunable, consequently the Q-factor will be not the same due to the tuning system. The characteristics of the proposed 2-pole filter are: a central frequency at 3.6 GHz with a bandwidth of 11.9%. The material used for the housing and the metal perturber is Copper. The Figure 15 presents the design of the filter. The tuning system is realized by a metallic part (pink element) that can rotate by means of a motor on the top of the filter.

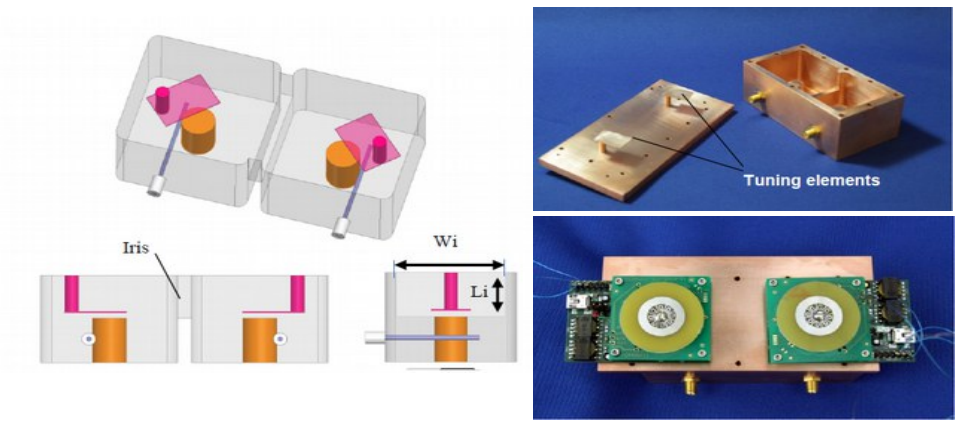


Figure 15: combline filters - high-Q and tunable filter

The simulation of the filter gives for the tuning range from 3.29 to 3.77 GHz a Q-factor around 5976. the insertion loss is less than 0.11dB. It is an interesting way to realize wide bandwidth filter with high Q-factor, however the used material (Copper) is not the lightest one and the dimensions are not specified.

We notice that the tunability of the filter [15]-[16] is another critical research thematic in order to remotely reconfigure the functions of one satellite.

4 Manufacturing sensitivity

Professor G Macchiarella [17] presents a solution to decrease the manufacturing sensitivity of the combline filter. The characteristics of the filter are a bandpass of 70 MHz at 854MHz, 3 poles and the return loss around -28dB. The dimensions of the complete filter are

$36x77x46mm^3$. To decrease the impact of the fabrication, he studied a conical shape for the resonators instead of a traditional cylindrical geometry (Figure 16).

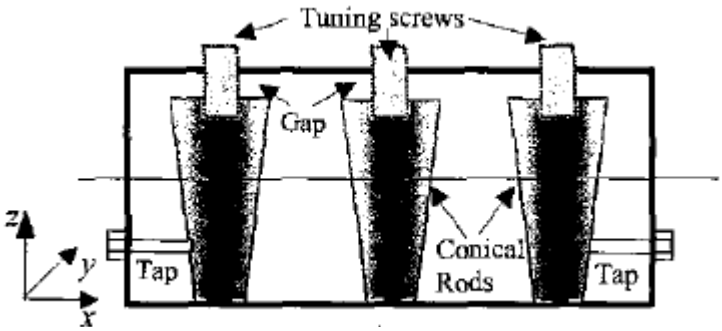


Figure 16: combline filters - conical resonators

Thank to this new shape, the needed tuning capacitance of the conical resonators is lower than the cylindrical one. Moreover, the manufacturing sensitivity has been demonstrated to be lower than with cylindrical rods.

2 Ridge filter

This kind of filter [18]-[19]-[20]- is based on waveguide elements. It is composed of a series of constrictions and cavities. The waveguide contains some constrictions that cause a capacitive effect. This effect decreases the fundamental mode (TE_{10} mode) frequency compared to a structure without these elements. Then, the frequency of the first superior mode (TE_{20} mode) is not strongly affected by the constrictions. Indeed, the ridge is located where the electric field of the TE_{10} mode is maximal whereas the one of the TE_{20} mode is minimal. That is why we can have an augmentation of the bandpass for the fundamental mode.
This kind of filter can not be used for very high power applications and has more losses compared to a traditional waveguide. For the rest of this study a more particular attention will be given to combline filters.

5 Solutions based on dielectric resonator

The first study of the dielectric resonator appears in the sixties with Titanium Oxide (TiO_2) based resonator which provide a very high Q-factor (10000) [21]. The progress of the technology made possible very high Q-factor (200 000) at ambient temperature [22] by using Sapphire Bragg reflectors. To realize the filtering function, a metallic housing is used and the

dielectric resonators are place in the center. This housing is used to avoid electromagnetic leakage and to contain the field in well defined places. To couple different resonators together and thus creating the filtering function coupling iris can be used between walls separating the DRs.

This kind of filter can be excited by many different ways as for example microstrip [23], waveguide [24], coaxial probe [25], etc.

1 Monobloc filter

Xi Wang [26] described a TM01 mode monobloc dielectric filter. It is composed of only one ceramic element with silver-plated external surfaces and metallic lid for hosting tuning screws. A 4-pole prototype filter (Figure 17) is made at 2.6 GHZ with a 50MHz equal ripple bandwidth. The dimensions of this structure are 54×54×17.5 mm^3. The name of the material is not precised but it has the following properties: ε_r=20.5 and tanδ=2.5 10^{-5} (certainly a BMT[1] ceramic).

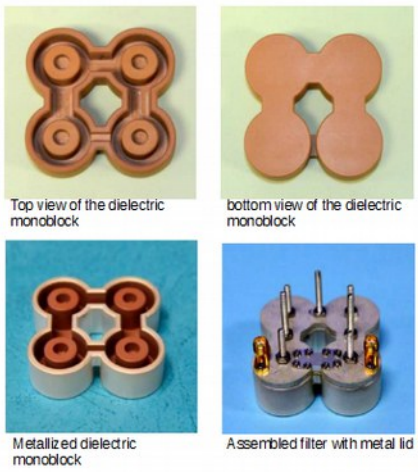


Figure 17: dielectric filter - monobloc filter

A temperature study of this filter is realized from 20°C to 60°C. The result is shown in Figure 18. The response is stable for the both extreme temperatures thanks to the very low TCF[2] of the ceramic material.

1 Barium Magnesium Tantalate
2 Temperature Coefficient of resonant Frequency

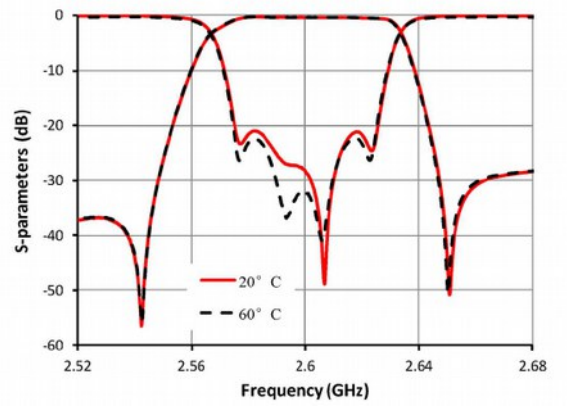


Figure 18: dielectric filter - response of the monobloc filter

The Q-factor of this filter is around 1800. It is a low value considering the properties of the dielectric material (tan δ=2.5 10^{-5}). The painting on the dielectric part seems thus to strongly limit the Q-factor of this filter.

In conclusion, we can notice that the insertion losses are lower than with a metallic structure taking into account the temperature changes. We have with this structure a better ratio $\frac{\text{Size}, \textit{Weight}}{Q}$ and we have a temperature stable response. However, the spurious modes are closer using the dielectric element than the metallic one.

In [27], a high power bandpass filter is presented. The characteristics of the filter are: f_0 = 880 MHz, BW = 20 MHz (2% of f_0), insertion loss < 0.45dB and Input power < 500W. To obtain these values an 8-pole elliptic function filter is designed using quarter cut TE01δ resonator. This special resonator shape permit to decrease the dimensions and to reduce the weight of the total structure while keeping good results. Two ceramic materials have been used for this

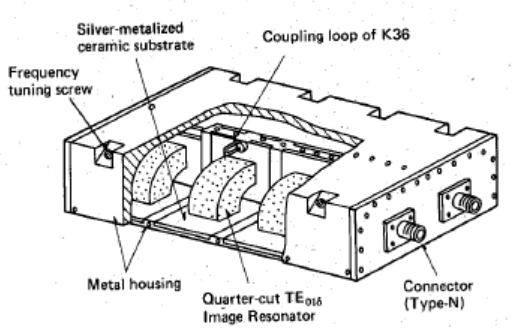


Figure 19: view of the quarter-cut $TE_{01\delta}$ Image resonator filter

application. They have for formulas : $(Zr, Sn)TiO_4$ (εr = 37.5 , tanδ = 2.5 .10^{-5} at 800 MHz) and $2MgOSi0_2 - ZrSiO_4$ (ε_r = 8.5). Then, dielectric materials are interesting for high power applications because usually they have a correct thermal conductivity and they do not become distorted over temperature changes due to the very low coefficient of thermal expansion (CTE).

The results of the filter are presented in Figure 20 and in Table II.

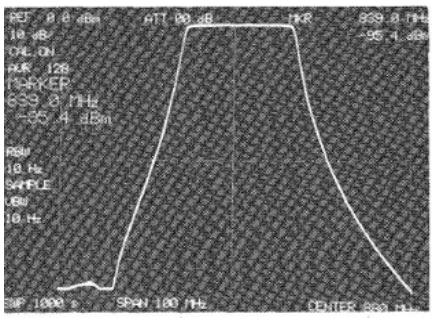


Figure 20: result of the quarter-cut $TE_{01\delta}$ Image resonator

Center frequency (f0)	880 MHz
Bandwidth (BW)	20 MHz
Insertion loss	0.37 dB
Size	280×135×65 mm^3

Table II: measured characteristics of the quarter-cut TE01δ Image resonator

This filter based on DR is relatively compact and with a high Q-factor of about 7100. However the bandwidth is very small (2%) due to a low coupling coefficient between them.

One of the easiest way to change the performances of the dielectric resonator is to modify this

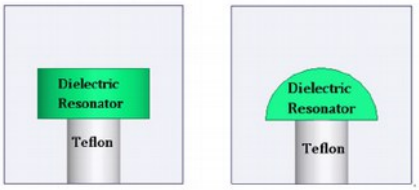


Figure 21: mushroom dielectric resonator (right) versus traditional shape (left)

shape. In [28], the DR looks like a mushroom (Figure 21). Thanks to this shape, dual mode resonators are used for this filter.

This design permits to increase the bandwidth of a filter. Then, we obtained, in this case, $\frac{1}{2}HEE_{11}$ and $\frac{1}{2}HEH_{11}$ mode because the resonator is half cut then one mode from each pair vanishes.

A 2-pole dual bandpass filter is designed as presented in Figure 22. The resonators are excited by coaxial probe and several tuning screws are designed in order to have a better control of the different parameters: intra-cavity coupling for each mode, source and load coupling, frequency of the mode inside the dielectric resonators.

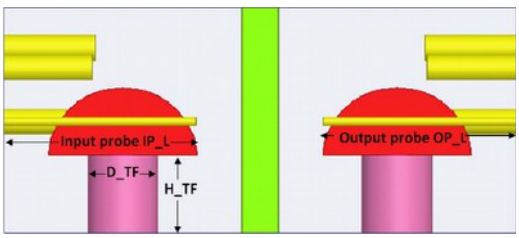


Figure 22: Design of the 2-pole filter - Semicircular resonator

The Figure 23 shows the simulated response of this filter, and we identify the two bandpass filter, the first one is at 5.32GHz with a relative bandwidth of 1.83% and the second one is at 5.56GHz with a relative bandwidth of 1.65%.

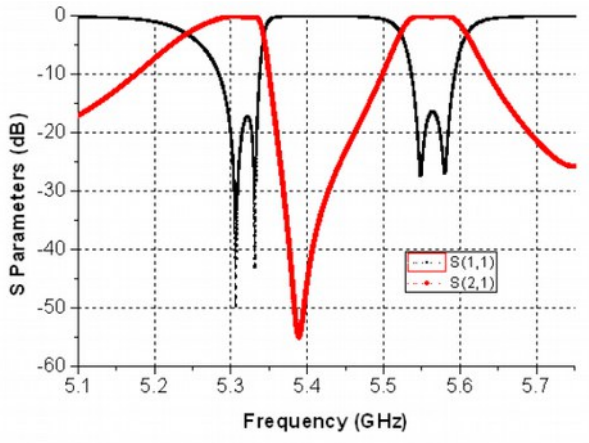


Figure 23: Response of the dual mode dual bandpass filter using semicircular resonators

The Q-factor and the spurious free range are not precised for this configuration. Then, it is difficult to evaluate the relevance of this design

2 Solutions based on the TM modes

One of the first researcher who studied the filter using TM mode is Prof. Kobayashi [29]. He realized a 4-pole filter composed of four dielectric rod resonators as shown in the Figure 24. The specifications of this application (Japanese broadcast satellite) are: a central frequency of 11.958GHz with a bandwidth of 50MHz. The dielectric resonators are made of BMT material (ε_r = 24 and tanδ = 4.10^{-5} at 12GHz), and the metallic housing is realized using Copper-plated brass.

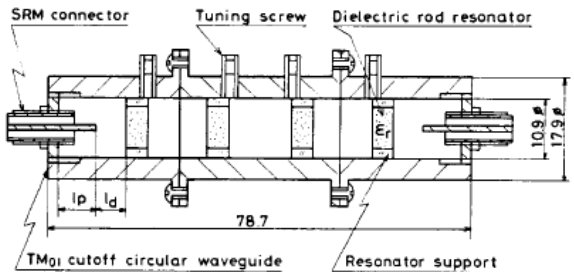


Figure 24: DR filter using TM mode - 4-pole filter

Each resonator frequency can be adjusted by tuning screws. Thus it was possible to have a good response and we can see in the Figure 25 that we have a good agreement between the simulated and the measured results. The measured Q_factor is about 18000.

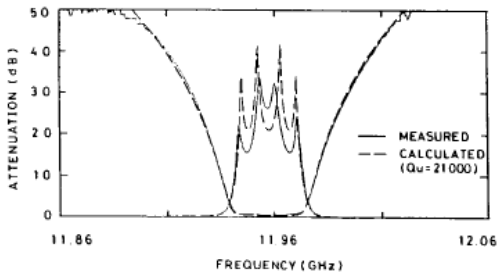


Figure 25: DR filter using TM mode - 4-pole filter - results

L. Pellicia [30] proposed a 4-pole filter using TM dual-mode with four transmission zeros. Dielectric resonators are used to increase the compactness of this kind of filter. The central frequency is 4.35GHz with a relative bandwidth of 3%.

The housing is made of Aluminum and the dielectric resonators are made of NGK/NTK-F31 ($\varepsilon_r = 34$ and $\tan\delta = 5.10^{-5}$) as shown in Figure 26.

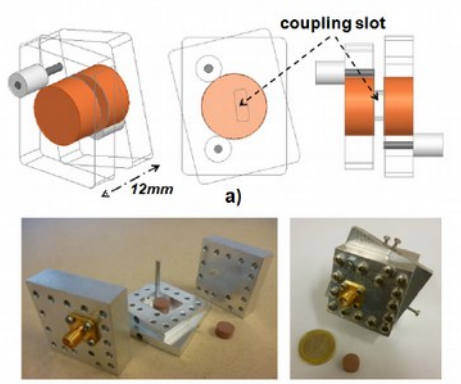


Figure 26: DR filter based on TM mode

The measurement of this filter has a good agreement with the simulated response (Figure 27). The measured Q-factor is 1750 but it is possible to obtain 3000 by silver plating the metallic housing. The size of the filter is $40\times40\times12mm^3$ without including the SMA connector dimensions.

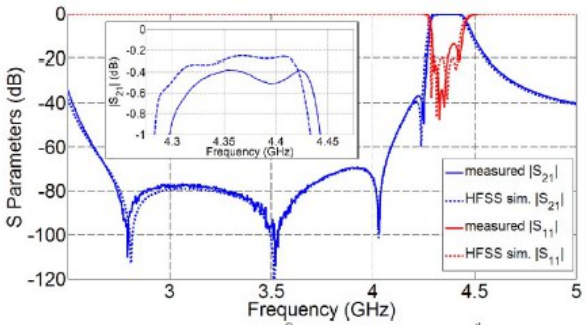


Figure 27: DR filter based on TM mode - results

This filter offers a good compactness and a high Q-factor (with silver-plated cavities), however the bandwidth is limited to 3% of the central frequency.

3 Solution based on dielectric combline filter

In [31], we have the description of a combline filter using dielectric resonators. Indeed, the traditional usually metallic resonator for this kind of filter is bordered by a dielectric ring resonator. Thus, the size of the filter [32] decreases due to the high permittivity of the dielectric material (not precised). A 4-pole filter with two transmission zeros was designed as we see in Figure 28. The central frequency is 1,747GHz with a bandwidth of 75MHz (4%).

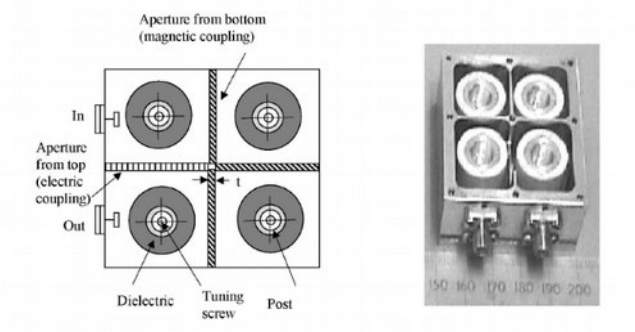


Figure 28: Dielectric combline filter (left : design and right : fabrication)

Thanks to the dielectric material, the size is reduced by 75%. compared to a commercial airfilled counterpart.

The simulated and measured responses are presented in Figure 29. We have a good agreement between both responses. The insertion loss is about 0,46dB and the higher order mode is at 3.5GHz.

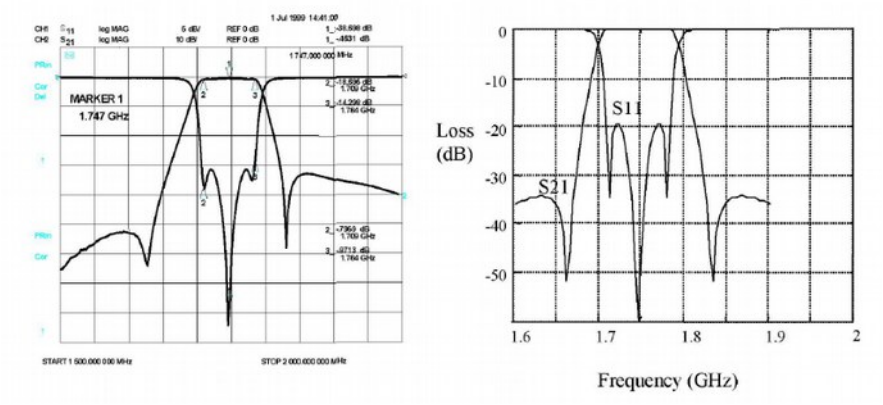


Figure 29: Dielectric combline filter - left : measure and right : simulation

4 Conclusion

Based on this initial overview, we can summarize the principal advantages and drawbacks between metallic and dielectric combline filters and dielectric resonators based filters. These latter can use different modes such as TE01 that offers compactness and high Q-factor or TM mode that permits to have an important compactness with an interesting Q-factor. We have summarized in table III all these filters properties with the key requirements of the wideband bandpass filter (C-band) we want in this project.

Combline filters		**Filters based on dielectric resonators (DRs)**	
Advantages	**Drawbacks**	**Advantages**	**Drawbacks**
Easy to design	Not very compact	High Q-factor	Low spurious-free range
Cheap	Low Q-factor	Compactness	Expensive material for DRs
Wide bandwidth	Thermal compensation need external elements	Thermal compensation	Low bandwidth
Easy to assembly			More difficult to assembly

Table III: advantages and drawbacks of the combline and dielectric filters

With this Table III, we see that combline filters are more interesting than the DRs based filters (cheaper, less assembly, etc), but for the key requirements (size, Q factor), DR based filters are

hard to beat but they lack the possibility to achieve the 10% (and more) bandwidth we are looking for.

6 Conclusion

Based on these considerations, we will try to find an intermediate way where we could combine the key features of the DRs based filters (compact size, high Q factor, temperature stable dielectric materials) with the very wide bandwidth that can be obtained only with combline filters thanks to the very strong couplings that can be generated in these components. This way will drive the studies proposed in Chapter II. We expect at this stage to need rather complex geometries to for the need DRs in order to get the high couplings require for very wide bandpass filters. A choice of appropriate technologies has to be done and we chose to firstly focus our attention to traditional subtractive and more exotic additive manufacturing technologies. The next section of this first Chapter will thus make an overview of the current technologies which can be used to realize the DRs based filters of this thesis as well as their advantages and properties.

VI. Manufacturing methods

1 Traditional manufacturing process

In this part, we will present some manufacturing process to have a first idea of their capability to create dielectric elements. A very large choice of techniques exist that is why we will on purpose limit the studied technologies to the ones available to the Xlim laboratory and ESTEC workshop.

1 Material removal

For this technique, we need first a block of material and we will machine this block to remove the material to obtain our element.

Usually, machining is the most common process to achieve a typical cavity filter. A tool, like a drill bit or cutter, is fixed on a rotation axis and removes the material. This method is recommended to build the key line of the element, to drill hole, etc. We can machine mold for another process such as injection molding. The manufacturing tolerances that can be achieved are ±12µm and we are not limited in the use of one material. Polymer, metal, ceramic can be used. However, the design is limited by the different dimensions of the tools and their

movements. The steps are more numerous and complex, the tool costs are more important because we need a wide variety of them (different diameters, different lengths, etc) and we have to take into account the wear of them. Then, we lose a lot of material following the removal of material.

2 Injection molding

For this process we need to create a mold of the element we want to manufacture. This mold have to be sealed because we will inject a liquid material or a paste inside.



Figure 30: example of mold for injection [34]

Thanks to the gravity and the pressure of the injection, the paste fill the entire mold and the empty space with the liquid. Then, we wait that the paste is solidified to open the mold to extract our element. An example of mold and object created by injection is presented in Figure 30. The process can be also destructive for the mold.

A lot of techniques and of molds exist in industry. Different materials can be used to realize the mold such as metal, polymer, wax, clay, etc. Then, different process can be applied to fill the mold depending on the number of elements to create (for an important quantity, a metallic mold could be more recommended to resist the different fabrications), of the exactitude, of the surface finish, of the mechanical properties and also the compatibility between the material of the mold and the one of the paste (to avoid merger between them).

Following the important process range, it is difficult to give the advantages and the drawbacks of each one but we can highlight that the typical the manufacturing tolerances are around 50µm. It is possible to realize complex design with this technique. It is an interesting process for an assembly-line production because the mold is used several times (hundreds, thousands, etc times). However, these techniques require time to design the object, to create the mold of this one and be sure it is feasible, to manufacture the mold and finally fabricate our object.

3 Assembly

This technique gathers several process together as the methods using screws, adhesive, weld, or other ways to unite different parts together. This process is difficult to manage because we have to take into account the compatibility of the different assembled materials and their dilatation. The manufacturing tolerances are composed of several factor, firstly the fabrication tolerances of each element, and secondly the positioning tolerances.

2 Manufacturing process using additive technologies

The additive manufacturing technologies were created in the 1970's. They gather together the manufacturing techniques using a CAD file to create layer by layer an element in three dimensions. The advantages of these process are the possibility to design original pieces and to create unique elements. Then, the realization can be very fast and the sample can be designed and manufactured in the same day. Moreover, we can save the used material because in this this case we do not machine a block but we put the material where it is necessary. For some appliances, several materials can be used and we do not need to change the tools to create our pieces, so we can use a machine for many applications, a big saving takes place.

The material range is still limited but we can predict a strong increasement of the choice in the next years or decades. Additive manufacturing is used in a lot of fields such as in electronic, medicine, telephony, motor vehicle, aeronautics, art, and general public use (toys, custom parts,...).

The first use of this technology was the realization of prototypes. Indeed, we can make a preliminary part very quickly and for a low cost, and we can study the potential defects before creating the final piece. In this way, we can decrease very quickly the probability to have an invalid object.

Since this prototype step, a lot of researches have been realized in this area to increase the repeatability and the mechanical performances of the process to compete with the traditional manufacturing.

As an example, an ESA program [33] is proposing to build a lunar station thanks to a 3D printer using the material of the ground (Figure 31). Agencies and other entities are now thinking to create very big structure using this new way of manufacturing.

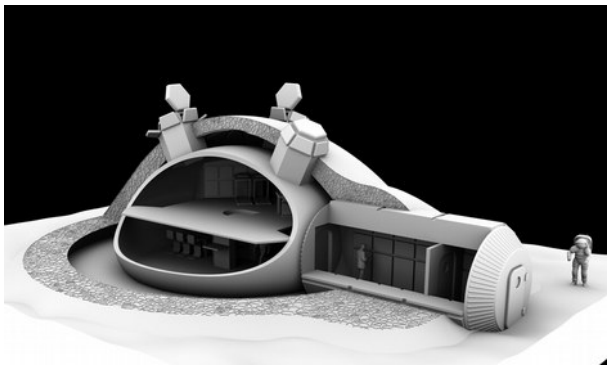


Figure 31: artist view of a lunar station built by 3D printing

The common point of that kind of manufacturing process which will be developed in the next parts is the CAD[3] file. We design our complete object using a 3D design software. Then, the file is saved in a special format that transforms our design's surfaces in a multitude of triangles. Then, another software cuts the structure in layers and this file is transferred to the 3D printer to be manufactured.

The interest of this technology is to have a single object specific to an application for a low cost and a brief period.

The ASTM F42 comity [35] classifies the different additive manufacturing process in seven groups which will be described in the next paragraphs:

-Vat photopolymerization

-Material jetting

-Binder jetting

-Powder bed fusion

-Sheet lamination

-Directed energy deposition

1 Vat photopolymerization: Stereolithography (SLA) and Digital Light Processing (DLP)

1 Stereolithography process (SLA)

The stereolithography was developed first by J.C André from the DCPR laboratory of ENSIC, then by Hull. Stereolithography process [36] was one of the first rapid prototyping device that

3 CAD : Computer-aided design

was commercialized. The first principle as presented in Figure 32 is to turn a liquid photosensitive monomer into a solid polymer thanks to a UV laser beam.

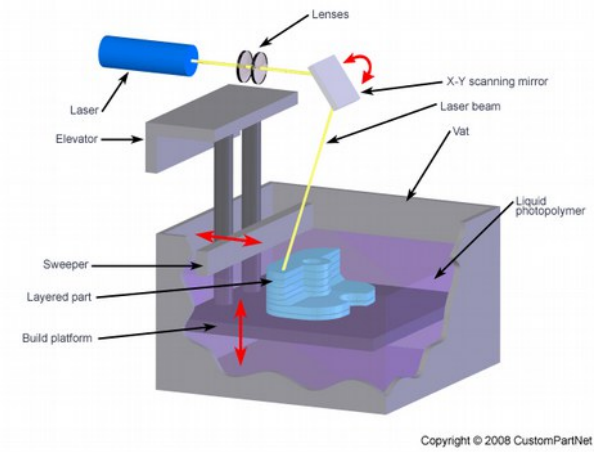


Figure 32: Principle of stereolithography process

The first people interested by this technology was the dental prosthetic technician, surgeons, architects, etc. Indeed, thanks to this process, it is possible to design a piece for a special applications. In hyperfrequency field, this process, and more specially when using ceramic materials, is very interesting because ceramics have very good electromagnetic properties. The most used ceramics are Alumina, Zirconia and BMT with a typical accuracy of 50 to 100 µm depending on the size of the manufactured part.

The ceramic stereolithography process will be more deeply described in Chapter III.

2 Digital Light Processing (DLP)

This method used by Lithoz GmbH [37] and Admatec Europe [38] is practically the same as the SLA. The different point concerns the way the liquid monomer is exposed to the light. We do not use a laser but a lamp associated with micro-mirror matrix composed of millions of them. Every mirror represents a pixel of the XY manufacturing plan. The mirror reflects (or not) the light on the paste to expose to the light (or not) the equivalent pixel of the fabricated element. The layers are created one after another. The interesting part of this process is its time saving factor compared to the SLA because it does not require a laser to move to polymerize the entire surface. Then, the displacement of the micro-mirrors is very fast and the implementation of this technique is less complex. The resolution is directly linked to the size of a single micro-mirror (few tenths of µm).

2 Material jetting: Polyjet and multijet

The polyjet (Figure 33) approach is similar to the previous technologies because here again an ultraviolet light polymerizes a resin. The difference concerns the paste deposition. The material is injected by nozzles with an inkjet printer. The used light illuminates the complete working surface. In this way, the resolution of our element is not the dimension of a laser spot but the dimensions of the droplets. Moreover an artificial and structural plastic is added to support our element during the process. This latter can be simply removed by water jet.

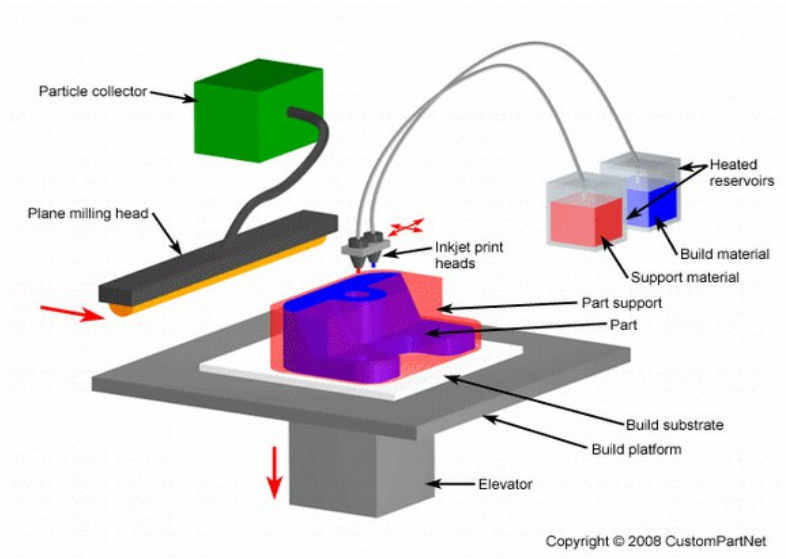


Figure 33: Principle of the Polyjet printing

The advantages of this process are the association of different materials and the possibility to obtain parts with several colors. A lot of materials can be used with different properties: high temperature resistance, opaque, transparent, unbendable, bio-compatible, etc.
However, the mechanical strength is low and the heat and the natural light (UV) exposure decrease the lifespan.

3 Binder jetting: 3D printing

This 3D printing process [39] is interesting to have multicolored objects in a short time. The Figure 34 describes the principle of this manufacturing method. A powder is spread uniformly by means of a piston and a roller. The inkjet print head releases a colored liquid binder to assembly the different particles of the powder together. Furthermore, it is possible to have several colors on the same layer.

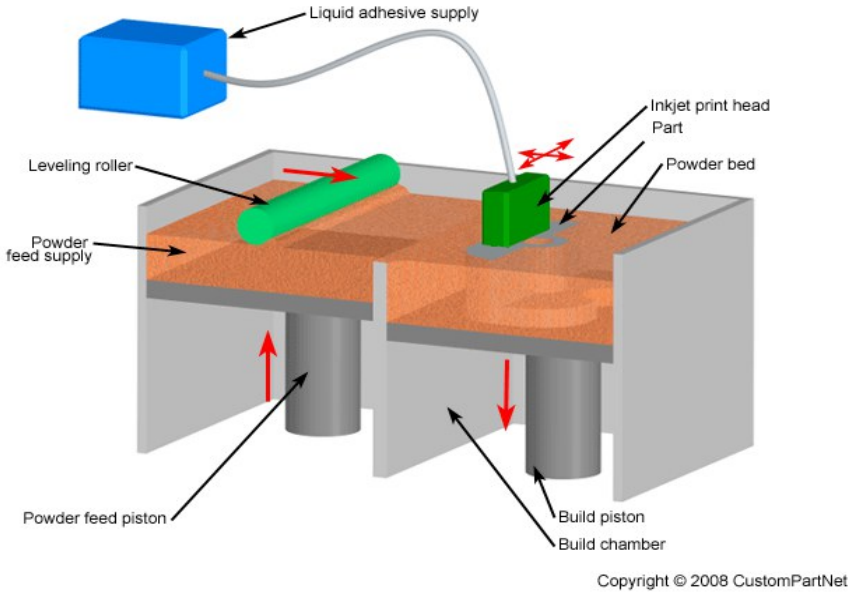


Figure 34: Principle of the binder jetting

Two to four layers per minute can be realized with this printer. Then, the powder is used for the support of the fabricated element. However, a cleaning step is necessary to remove the useless powder and we have to inject an adhesive compound to strengthen the piece. Then, the element is cured to increase its mechanical properties.

Nevertheless, we do not have a good surface finish, exactitude and solidity with this method. The binder jetting is a cheap and fast process but it is more useful for a prototype activity.

4 Material extrusion: fused deposition modeling (FDM), fused filament fabrication (FFF)

The FDM [40] is a very cheap and reachable technology for general public. A fused polymer wire is droped on a mobile platform by extrusion nozzles. A schematic view is presented in Figure 35. The object is created very fast layer by layer. A support material is deposited in the same time to hold our element and can be removed after fabrication by a Sodium chlorate[4].

Several nozzles can be used to have different colors of polymers in the same piece. The manufacturing tolerances depends on the diameter of the melted wire, usually it is about hundreds of micrometer.

4 Sodium chlorate : Na_2ClO_3

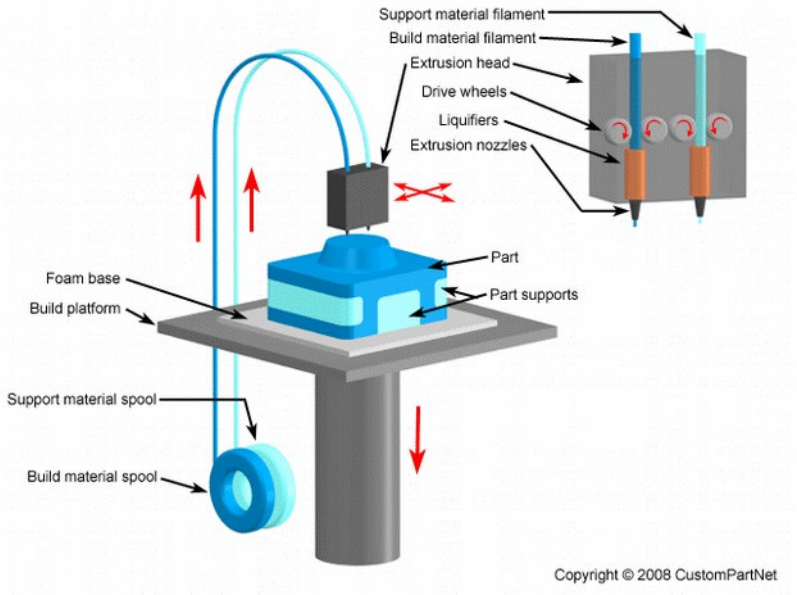


Figure 35: principle of FDM

The next materials can be used with this process: thermoplastics (ABS, PLA), polycarbonates, elastomers, wax, ceramics [41] and many others.

5 Powder bed fusion: selective laser sintering (SLS), selective laser melting (SLM), Direct metal laser sintering (DMLS), electron beam melting (EBM)

1 Selective Laser Sintering (SLS)

For this process, we can use powder of polymer, ceramic or glass. The difference with the previous method is the powder is aggregated by a laser [42] (Figure 36). Indeed, the laser warms up the particles and they will fuse to create a layer of the 3D object. Then, the work area moves down and another powder layer is spread. This process takes place in a closed and heated enclosure.

For the same reason as the binder jetting, the powder is also the support of the manufactured element. The cleaning step is very easy to do and we can achieve complex structure with this process. The advantages are the mechanical strength of the fabricated piece and a lower cost than the SLA but the exactitude is lower. We notice that it is possible to realize articulated objects. The roughness of the surfaces are bigger than the SLA because of the porosity and the dimensions of the powder particles needed to ensure a proper spreading of them.

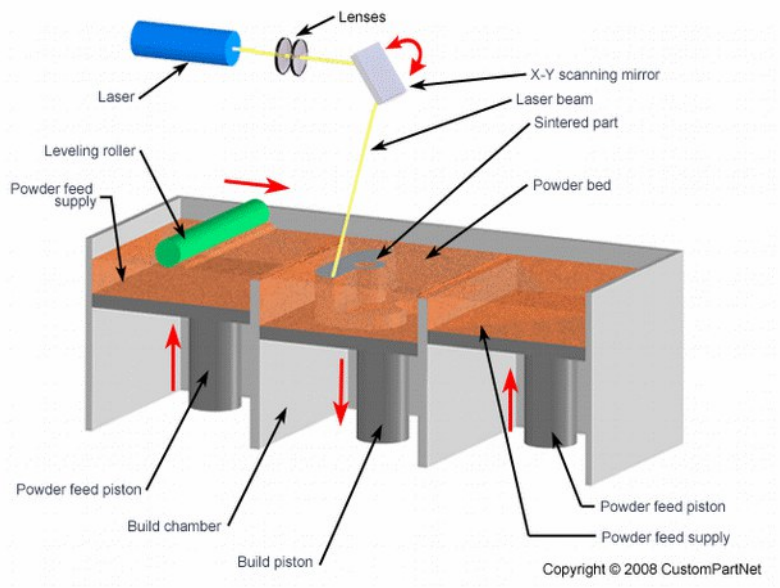


Figure 36: principle of SLS

2 Selective Laser Melting (SLM) and Direct Metal Laser Sintering (DMLS)

They are the same process as SLS but they are using powders composed of metallic particles. Then the difference [43] between SLM and DMLS is that in SLM the material is fully melted rather than sintered.

3 Electron Beam Melting (EBM)

This method [44] uses also metallic powder but to aggregate it an electron beam at high temperature (700 to 1000°C) melts the powder and merges the metallic particles together. The density of this kind of element can achieved 100%, consequently the mechanical properties are maximal. However, the process (Figure 37) takes place in a vacuum enclosure with an antioxidant atmosphere to conserve the metallic powder in a good conditions. It is an interesting way to realize mold fabrication and the object can claim to be space applications compatible due to its excellent mechanical properties.

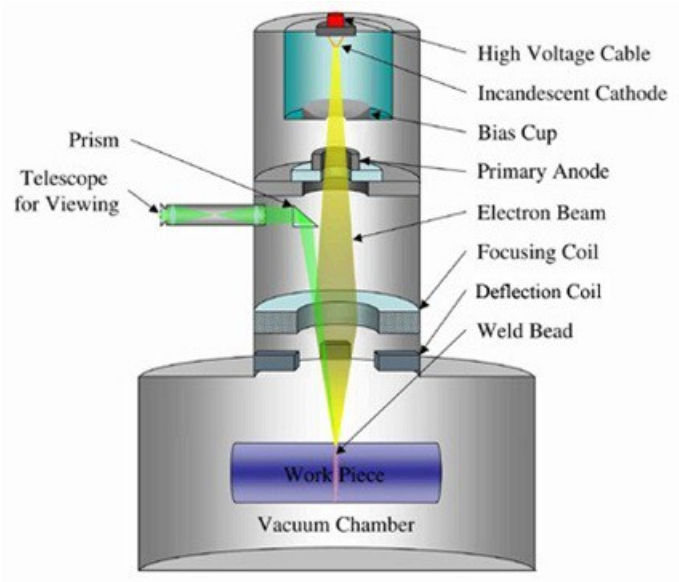


Figure 37: principle of EBM

4 Sheet Lamination: Laminated Object Manufacturing (LOM)

This process (Figure 38) is based on a solid layer of polymer, paper or metal that is cut out thanks to a laser [45]. Then, the platform moves down and another layer is rolled out and sticks to the previous one.

This method presents a low intern tightness of the materials, as a result we have less strain of the object. The lifespan is longer and the element are less fragile. They can also present huge dimensions (500×800×500 mm^3). It is a very cheap process as demonstrated with the paper material. However, we can not have a good exactitude and homogenous mechanical and thermal properties due to the contact between two layers. Thus, a finishing step must be programmed.

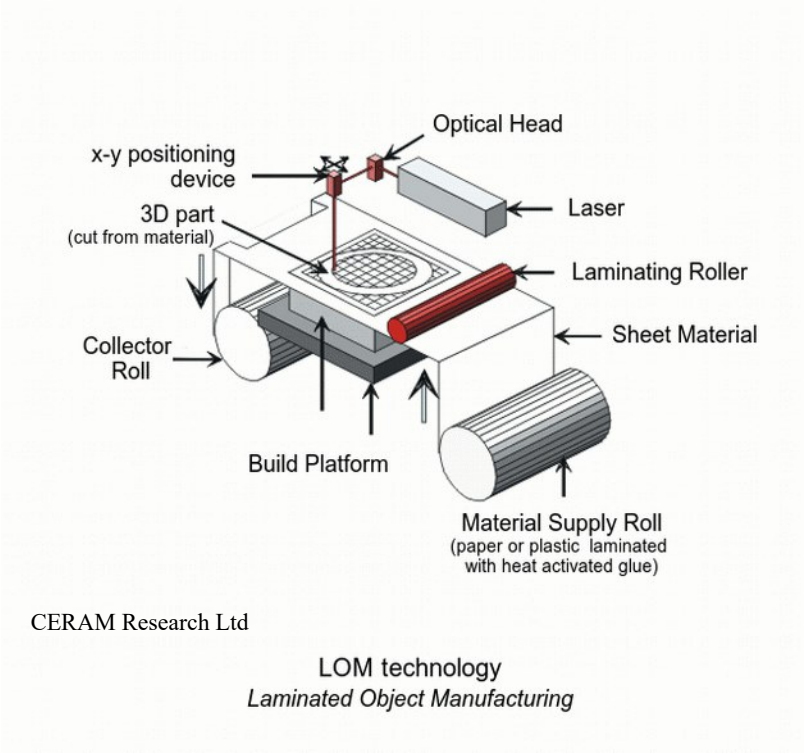


Figure 38: principle of LOM

6 Directed Energy Deposition (DED): Laser Engineered Net Shaping (LENS), Direct Metal Deposition (DMD), 3D Laser Cladding

For this kind of application, the matter is directly deposited to the wished location [46]. The metallic powder or wire is warmed up using a laser, an electron beam or an ionized gas before being thrown to the working area. To avoid oxidization, this process takes place in an enclosure low on oxygen. When the first layer is completed, the printing head rises by layer thickness and realizes the second one.

This process permits to have voluminous object with a strong density up to 100%. Then, the fusion can change the properties of the material and creates special characteristics for one application. It is possible to repair specifically an element with this method.

However, a finishing step is necessary to obtain a low roughness, then, the used quantity of material is important and we are more limited for the design of complex piece.

Since our application based on DRs is extremely dependent on the material properties and the need to be capable to produce complex (ideally ceramic parts), we have chosen the 3D stereolithography process (SLA) because of the previous points, and because we can have the

same results as for a classic manufacturing with more rapidity. Then, the possibilities with this method are practically infinite, so the complicated shapes are not a limitation.
Because of the very demanding performances required by this thesis components for space applications, the compatible materials (Zirconia, Alumina, BMT) present very interesting properties (permittivity, loss tangent, etc) and are relevant candidates for filters and resonators that are working in millimetric and submillimetric frequencies.
To realize the different pieces by stereolithography process, we will work with the CTTC, Centre de Transfert de Technologie Céramique located in Limoges.

3 Conclusion

The additive manufacturing processes are now one of the main evolution of this century. Indeed, they change the way to realize things from the customer that can make his own piece like replacing a broken part of his washing machine to the ESA that want to built a lunar station using the Moon's ground material. The different techniques permit to adapt the technologies to the element characteristics, we can made very small element (micrometer) to huge one (several meters). The range of material is also an advantage and every day new materials are created in order to be more efficient and adapted for the different function. The plastic was one of the first study material thanks to this malleable structure, but now it is possible to use metals, alloys or ceramics which are a very interesting candidates for the researched DRs based filters. Associated with the accuracy provided by the SLA as well as its capability to create complex shapes, the additive manufacturing appears to be suitable for our goal even if traditional means like high precision milling of ceramic blocks can still be a good back-up to keep.

Conclusion

The space knows a resurgence of interest with the last discoveries and programs. The Mars mission and Rosetta show us we still have so much things to accomplish. Some big companies are now realizing research in the spatial field. We have for example SpaceX that want to reduce the prices of the launch for small satellites by re-using some parts of the booster rocket. Then, original ideas appeared as to colonize the Mars planet (Mars-one [51]). Even if it is not currently possible, this project creates interest for the general public and for laboratories in many areas such as biology, heat science, etc.

In this chapter, we have defined the preliminary requirements for the wide band filter researched in this thesis. We want to realize an Input filter with a wide band and a high Q-factor. In this way, we have studied the existing solutions of wide band filters and we have identified two main technologies: combline and ridge filters. However the drawbacks of these kind of filters are the limited compactness and a low to medium Q-factor. That is why we were interested by the filters used for narrow bandwidth selection, these latter using dielectric resonators, because we know that with these components we can have high Q-factor and good compactness due to the properties of the used dielectric materials (loss tangent and permittivity). In this way, we have seen different configurations using this kind of dielectric elements and we saw that one main constraints is the limited coupling which can be used between DRs.
The purpose of this work is to achieve a wide bandpass filter using dielectric resonators in order to have also a high Q-factor and compactness, therefore to try to find an intermediate path between wide band combline filters and compact/ low loss DRs based filters.

Then, we have presented different additive manufacturing processes in order to have an overview of the different kinds of technologies that may be capable to build the researched DRs based filters. We have seen that these technologies are part of a greatly developing sector because, thanks to this new way of manufacturing, the only limit is our imagination. Indeed, all kinds of forms can be realized and many materials (plastics, ceramics, metal, etc) and colors can be used. We can also created by this way very small object but also voluminous one. For example, it is possible to built houses [52] with 3D printer.
Looking at our objective, the SLA process using low loss ceramics such as Alumina, Zirconia or even BMT looks like to be a very good candidate for the realization of the first prototypes which will be studied and developed in Chapter II.

Bibliography

[1] http://www.nasa.gov/centers/langley/about/project-echo_prt.html

[2] http://www.nasa.gov/topics/technology/features/telstar.html

[3] www.itu.int

[4] http://www.esa.int/Our_Activities/Observing_the_Earth/The_Living_Planet_Programme/Earth_Explorers/GOCE/Satellite

[5] http://www.arianespace.com/launch-services-ariane5/ariane-5-intro.asp

[6] http://www.eutelsat.com/en/satellites/EUTELSAT-8WB.html

[7] http://www.intelsat.com/blog/intelsat-34-our-next-satellite-set-to-launch/

[8] http://www.spacex.com/falcon9

[9] http://www.changpuak.ch/electronics/combline_bandpass_filter_designer.php

[10] J. D. Rhodes, "The Stepped Digital Elliptic Filter," in *IEEE Transactions on Microwave Theory and Techniques*, vol. 17, no. 4, pp. 178-184, Apr 1969

[11] Abramowicz, A., "Wide band combline filters," *Microwaves, Radar and Wireless Communications, 2004. MIKON-2004. 15th International Conference on,* vol.3, no., pp.1048,1051 Vol.3, 17-19 May 2004

[12] A. I. Abunjaileh and I. C. Hunter, "Combline filter with tunable bandwidth and central frequency," *Microwave Symposium Digest (MTT), 2010 IEEE MTT-S International*, Anaheim, CA, 2010, pp. 1476-1479

[13] Hui-Wen Yao; Atia, A.E., "Temperature characteristics of combline resonators and filters," *Microwave Symposium Digest, 2001 IEEE MTT-S International,* vol.3, no., pp.1475,1478 vol.3, 20-24 May 2001

[14] Iskander, M.A.; Nasresfahani, M.; Mansour, R.R., "A constant-Q tunable combline bandpass filter using angular tuning technique," *Microwave Conference (EuMC), 2014 44th European,* vol., no., pp.1103,1106, 6-9 Oct. 2014

[15] Anand, A.; Small, J.; Peroulis, D.; Xiaoguang Liu, "Theory and Design of Octave Tunable Filters With Lumped Tuning Elements," *Microwave Theory and Techniques, IEEE Transactions on,* vol.61, no.12, pp.4353,4364, Dec. 2013

[16] Savin, K.; Golubeva, I.; Prokopenko, Y., "A novel concept for the tunable cavity combline resonator," *Electronics and Nanotechnology (ELNANO), 2015 IEEE 35th International Conference on,* vol., no., pp.520,522, 21-24 April 2015

[17] Macchiarella, G.; Santoniccolo, Marco; Fumagalli, M.; Sartorio, Alessando, "Combline filters using conical resonators," *Microwave Conference, 2003. 33rd European,* vol.1, no., pp.167,169 Vol.1, 7-9 Oct. 2003

[18] Cohn, Seymour B., "Properties of ridge waveguide," *Proceedings of the IRE,* vol.35, pp.783,789, June 1947

[19] Cohn, Seymour B., "Analysis of a Wide-Band Waveguide Filter," *Proceedings of the IRE,* vol.37, no.6, pp.651,656, June 1949

[20] Pucci, E. ; Zaman, A. ; Rajo-Iglesias, E. (2013) "Study of Q-Factors of Ridge and Groove Gap Waveguide Resonators". IET Microwaves, Antennas & Propagation, vol. 7(11), pp.900-908

[21] Harrison, W.H., "A Miniature High-Q Bandpass Filter Employing Dielectric Resonators," in *Microwave Theory and Techniques, IEEE Transactions on,* vol.16, no.4, pp.210-218, Apr 1968

[22] O. Piquet, D. Cros et al, «*New design of high Q sapphire resonator with distributed bragg reflector*», IEEE Symposium on Microwave Theory and Techniques, Seattle, vol.3, pp. 1993-1996

[23] S. W. Chen and K. A. Zaki, "Dielectric ring resonators loaded in waveguide and on substrate," in *IEEE Transactions on Microwave Theory and Techniques*, vol. 39, no. 12, pp. 2069-2076, Dec 1991

[24] W. C. Tang, J. Sferrazza, B. Beggs and D. Siu, "Dielectric Resonator Output Multiplexer for C-Band Satellite Applications," *Microwave Symposium Digest, 1985 IEEE MTT-S International*, St. Louis, MO, USA, 1985, pp. 343-345.

[25] S. Vigneron and P. Guillon, "Input impedance and loaded quality factor of a probe exciting dielectric resonator," in *IEE Proceedings H – Microwaves, Antennas and Propagation*, vol. 135, no. 3, pp. 163-166, Jun 1988

[26] Xi Wang; Ke-Li Wu, "A TM_{01} Mode Monoblock Dielectric Filter," *Microwave Theory and Techniques, IEEE Transactions on,* vol.62, no.2, pp.275,281, Feb. 2014

[27] Nishikawa, T.; Wakino, K.; Tsunoda, K.; Nishikawa, T., "Dielectric High-Power Bandpass Filter Using Quarter-Cut TE/018/ Image Resonator for Cellular Base Stations," in *Microwave Theory and Techniques, IEEE Transactions on,* vol.35, no.12, pp.1150-1155, Dec 1987

[28] Baluni, P.; Awasthi, S.; Biswas, A., "Dual mode dual bandpass filter using semicircular Dielectric Resonator in mushroom configuration," in *Applied Electromagnetics Conference (AEMC), 2013 IEEE,* vol., no., pp.1-2, 18-20 Dec. 2013

[29] Kobayashi, Y.; Yoshida, S., "Bandpass Filters Using TM_{010} Dielectric Rod Resonators," in *Microwave Symposium Digest, 1978 IEEE-MTT-S International,* vol., no., pp.233-235, 27-29 June 1978

[30] L. Pelliccia, F. Cacciamani, C. Tomassoni and R. Sorrentino, "Ultra-compact filters using TM dual-mode dielectric-loaded cavities with asymmetric transmission zeros," *Microwave Symposium Digest (MTT), 2012 IEEE MTT-S International*, Montreal, QC, Canada, 2012, pp. 1-3.

[31] J. M. Chuma and D. Mirshekar-Syahkal, "Compact Dielectric Loaded Combline Filter with Low Insertion-loss," *Microwave Conference, 2000. 30th European*, Paris, France, 2000, pp. 1-4

[32] Chi Wang, K. A. Zaki, A. E. Atia and T. G. Dolan, "Dielectric combline resonators and filters," in *IEEE Transactions on Microwave Theory and Techniques*, vol. 46, no. 12, pp. 2501-2506, Dec 1998

[33] http://www.esa.int/Highlights/Lunar_3D_printing

[34] http://www.romalpindustries.com/fr/

[35] ASTM. ASTM F2792–10 standard terminology for additive manufacturing technologies

[36] Jacobs P F. Rapid Prototyping & Manufacturing: Fundamentals of Stereolithography. Dearborn: SME publication, 1992

[37] http://www.lithoz.com/

[38] http://www.admatec.nl/

[39] Sachs M E, Haggerty J S, Cima M J, Williams P A., "Three dimensional printing techniques." US Patent, 5204055, 1993

[40] James W. Comb, William R. Priedeman, Patrick W. Turley, FDM® TECHNOLOGY PROCESS IMPROVEMENTS, Stratasys, Inc., Eden Prairie, Minnesota

[41] M. Allahverdi, S.C. Danforth, M. Jafari, A. Safari, "Processing of advanced electroceramic components by fused deposition technique", Journal of the European Ceramic Society 21 (2001) 1485–1490

[42] A. Stwora, G. Skrabalak, "Influence of selected parameters of Selective Laser Sintering process on properties of sintered materials", Journal of achievements in materials and manufacturing engineering, vol 61, issue 2, december 2013

[43] https://en.wikipedia.org/wiki/Direct_metal_laser_sintering

[44] Ola L.A. Harrysson, Omer Cansizoglu, Denis J. Marcellin-Little ,Denis R. Cormier, Harvey A. West II, "Direct metal fabrication of titanium implants with tailored materials and mechanical properties using electron beam melting technology", Materials Science and Engineering C 28 (2008) 366–373

[45] Bernhard Mueller, Detlef Kochan, "Laminated object manufacturing for rapid tooling and patternmaking in foundry industry", Computers in Industry 39, 1999. 47–53

[46] J. Mazumder · A. Schifferer · J. Choi, "Direct materials deposition: designed macro and microstructure", Mat Res Innovat (1999) 3:118–131

[47] http://3dceram.com/en/category/biomedical/implants-et-substituts-osseux/

[48] http://www.iceram.fr/1ere-pose-dun-sternum-en-ceramique/

[49] http://www.iceram.fr/

[50] http://3dceram.com/

[51] http://www.mars-one.com/

[52] *http://www.wasproject.it/w/en/*

CHAPTER II

Strong Coupling Studies

Introduction

In this part, we will present a study dedicated to maximizing coupling between dielectric resonators (DR). We seek here to reach coupling values capable to create wide bandpass filter with a bandwidth superior to 10% of the central frequency, using dielectric resonators and around 4 GHz. Then, a typical spurious free range of 700MHz around 4 GHz is also part of our initial specifications.

For this work, we decided to study and characterize three different dielectric materials: Alumina because it is a common material used for telecommunication applications, Zirconia because it proposes a high permittivity (>30) and BMT for its low loss tangent (< 1 10^{-4}).

First, we will show how we will calculate the coupling between cavities loaded with DR and the coupling for the Input and the Output of a filter based on such resonators. Then, we will present the synthesis software we will use to facilitate the optimization of our designs.

The first DR mode chosen as a starting point will be the well established $TE_{01\delta}$ mode. We will have here a deep investigation on its electromagnetic field distribution, its characteristics, etc. With this mode we will try to answer our problematic that is to create very strong coupling with Input/Output probes and between two dielectric resonators of this kind. We will study more precisely several evolutions of its base geometry and we will give the advantages and the drawbacks of the proposed designs.

A very similar work will be done with the TM_{010} mode We will expose our solution to realize the strong coupling needed by this work.

Following this study, we will choose the more efficient and promising configuration for the next step that is to design and to build a wide bandpass filter.

VII. Characterization of the materials.

1 Method to characterize the dielectric materials

To measure the properties of the ceramic material, we first design a dielectric resonator at the wanted frequency and then place it inside a metallic cavity on a Teflon support (Figure 42). This support permits us to center the resonator in the middle of the cavity and it has usually a low permittivity to minimize its impact on the DR performances. We have a set of already

available cavities with various dimensions for the characterizations of cylinders of dielectric materials. These dielectric resonators should follow these next formulas in order to be placed in such cavities and to minimize the losses coming from the metal enclosure (metal cavities):

$R_c = 2\ R_{dr}$ $H_c = 3\ R_{dr}$

$H_{dr} = R_{dr}$ $H_s = R_{dr}$

with R_c: the radius of the cavity

H_c: the height of the cavity

R_{dr}: the radius of the dielectric resonator

H_{dr}: the height of the dielectric resonator

H_s : the height of the support

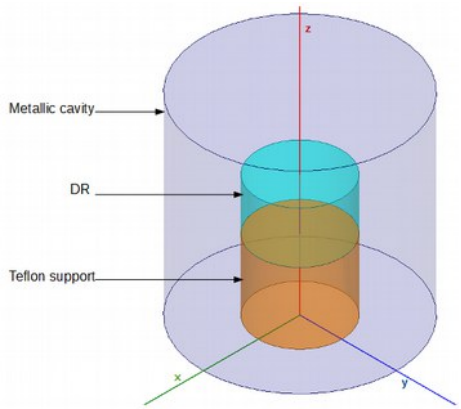


Figure 39: A cavity to characterize a dielectric resonator on a Teflon support

For example, we design a dielectric resonator working at 4GHz using Zirconia material in an available cavity. We optimized the DR as a function of the available cavity. In our case, we find a height of 8mm and a radius of 6.5mm for the DR using a cavity with a height of 15mm and a radius of 15mm.

This cavity is excited thanks to coaxial probes ended by a magnetic loop.

We measure the loaded Q-factor (Q_c) defined by the next equation:

$$Q_c = \frac{f_r}{\Delta f} \quad (1)$$

with f_r : the resonance frequency

Δf: f_2-f_1 as seen in Figure 43.

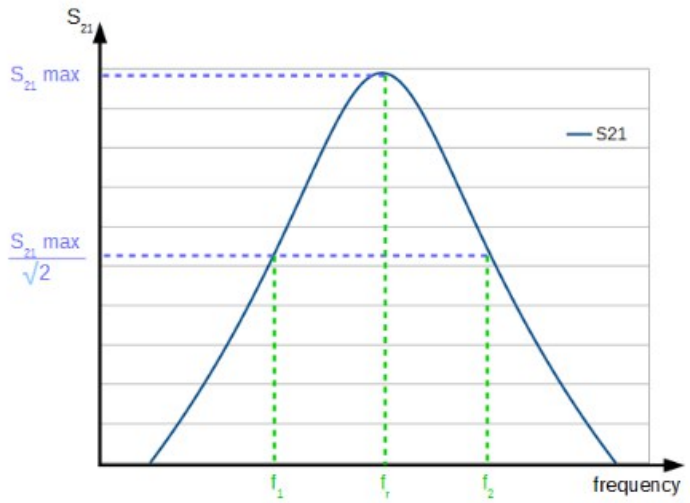


Figure 40: determination of the Q_c factor

Then, we determinate unloaded the Q-factor of the resonator and the cavity (Q_0) using the next relation:

$$Q_0 = \frac{Q_c}{1 - |S_{21}|_{\varpi=\varpi_0}} \quad (2)$$

with S21 the value of the transmission coefficient at the resonance frequency: $f_r = \varpi_0 / 2\pi$ (3)

We can link the Q_0-factor with the dielectric Q-factor (Q_d) with the following equation:

$$Q_0^{-1} = Q_d^{-1} + Q_m^{-1} + Q_s^{-1} \quad (4)$$

with Q_d: quality factor showing the dielectric losses

Q_m: quality factor showing the metallic losses

Q_s: quality factor showing the losses of the Teflon support

1 Characterization of the cavity

We measured the empty cavity with a very low Input/Output coupling ($|S21|_{fr}$<-30dB) to have the simplified relation: $Q_c = Q_0$ so we determine the Q_0-factor of the cavity without the support and the DR. Then, we have to calculate the conductivity of the walls of the cavity using these formulas:

$$Q_{0mes} = R_{Smes} \times G \quad (5) \text{ and } \quad Q_{0th} = R_{S1} \times G \quad (6)$$

With R_{Smes}: measured surface resistivity

R_{S1}: surface resistivity given by σ_{th} the theoretical conductivity

G: coefficient of the metallic losses

so $G = 1/(Q_{0th} \times R_{S1})$ (7) with $R_{S1} = 20\pi \times \sqrt{f_{r_{mes}} / \sigma_{mes}}$ (8)

we have: $\sigma_{mes} = \sigma_{th} \times \frac{f_{r_{mes}}}{f_{r_{th}}} \times \left(\frac{Q_{0mes}}{Q_{0th}}\right)^2$ (9)

and $R_{Smes} = 20\pi \times \sqrt{f_{r_{mes}} / \sigma_{mes}}$ (10)

At the end, we have determinate the properties of the empty cavity, R_S and σ_{mes}.

2 Properties of the dielectric resonator

Using a 2D FEM (Finite Element Method) of the cavity, support and DR and the dielectric material supplier supposed properties, we have a first information of the probable frequency of the DR $TE_{01\delta}$ mode. This information is important to have in order to find the right resonant mode when the cavity, support and DR will be connected to the VNA for its measurement.

Then, we have to determine ε_r' and ε_r'' of the complex permittivity ($\varepsilon_r = \varepsilon_r' - j\varepsilon_r''$) of our dielectric material under characterization. We use again the 2D FEM model to match the measured resonant mode frequency and Q factor (respectively f_{0mes} and Q_{0mes}) to the one simulated with the model.

To obtain the loss tangent ($\tan\delta = \varepsilon_r'' / \varepsilon_r'$), we use the following relation:

$$Q_0^{-1} = R_{Smes} \times G + \alpha \times \tan\delta_{mes} \quad (11)$$

with α: coefficient of the dielectric losses

G: coefficient of the metallic losses

$R_{Smes:}$ measured surface resistivity

So:

$$\tan\delta_{mes} = \frac{Q_{0mes}^{-1} - R_{Smes} \times G}{\alpha} \quad (12)$$

2 Measurement of the properties of the different ceramics

The resonators we used for these characterizations are all made by stereolithography.

1 Zirconia



Figure 41: powder of Zirconia (Zirconium oxide)

The chemical name is Zirconium dioxide with the formula ZrO_2. It is a white crystalline oxide of zirconium with a monolithic crystalline structure. The typical uses of the material are for jewelry. Indeed, the cubic Zirconia can be transparent and imitates the diamond, Medicine also uses this ceramic: for example, it is possible to realize teeth with high hardness and a low wear, or in another field to realize hip replacement because this material has a very good compatibility with the human body, reducing transplant rejection.

We have firstly characterized this material for the future design of our filter. Cylinders resonating around 4, 10 and 11GHz are manufactured by SLA in order to have a wideband characterization of their electrical properties. Their size are:

-for 4GHz: radius = 6.2mm and height = 8mm

-for 10GHz: radius = 2.1mm and height = 4mm

-for 11GHz: radius = 2mm and height = 4mmIn the graph shown in Figure 43, our characterization reveals that the permittivity decreases when the frequency increases. For our case, at 4GHz, we take the value of 33 for the permittivity.

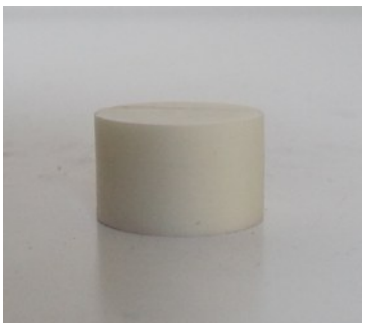


Figure 42: Characterization of the Zirconia material - 4GHz resonator

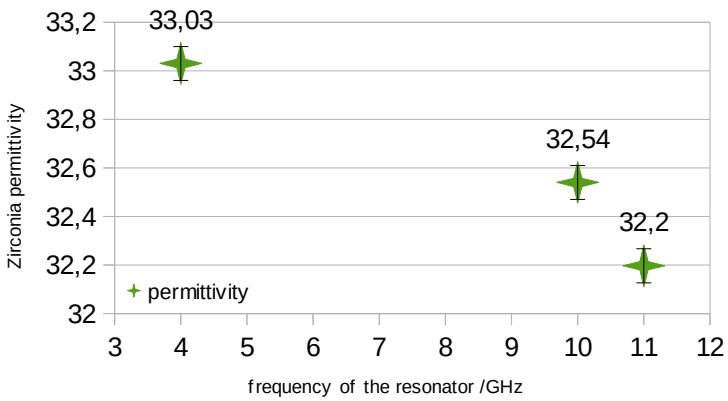


Figure 43: The behavior of the Zirconia permittivity as a function of the frequency

The characterization results of the material loss tangent are presented in the Figure 44. The variation over frequency is less important than with the permittivity, we will take the value of $\tan\delta = 1.10^{-3}$ for the simulation of our design working at 4GHz.

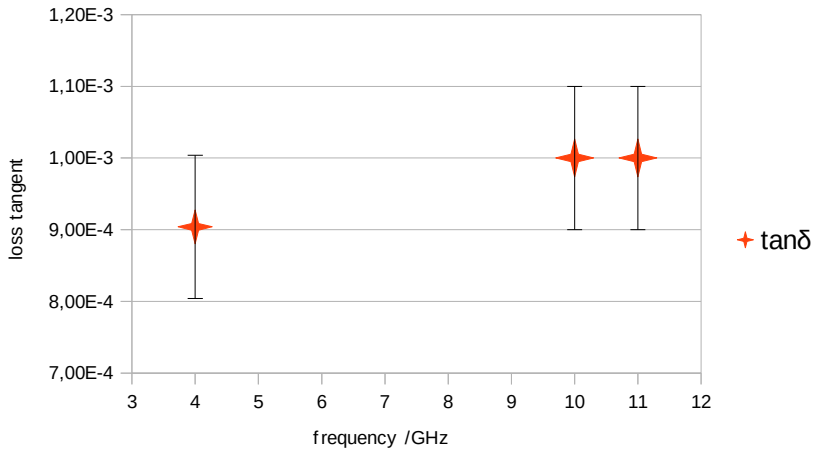


Figure 44: The behavior of the Zirconia loss tangent as a function of the frequency

Another parameter that is interesting to know is the Temperature Coefficient of resonant Frequency (TCF). This coefficient represents the deviation of the DR (or any resonator) resonant frequency over temperature (between T_0 and T_1). When the value is close to zero, it is meaning that the material electrical properties (resonance frequency) are stable over

temperature and does not have a strain due to the temperature. The formula of the TCF is shown below:

$$TCF\left(ppm.°C^{-1}\right)=\frac{f_r(T_1)-f_r(T_0)}{f_r(T_0)}\times\frac{10^6}{T_1-T_0} \quad (13)$$

with T1: low temperature value

fr(T): the frequency corresponding at the temperature T

T2: high temperature value

We calculate this coefficient for Zirconia material for a temperature range from 20 to 80°C and we obtain a TCF =-71 ppm.°C^{-1}. This value is not very close to 0 ppm.°C^{-1} as an ideal material for space application, but it could be used for prototype. As a consequence it does not have the ambition to go to space and to go through the temperature change.

Moreover, we notice that this material has a very high hardness (1200 Hv) and a low sensitivity to the humidity. Then, this material is compatible with different manufacturing process as milling, sintering, molding and stereolithography.

2 BMT (Barium Magnesium Tantalate)

The chemical formula is $Ba(Mg_{1/3}Ta_{2/3})O_3$.

We also realize the characterization of the BMT material with a first dielectric resonator designed to resonate at 10GHz on its $TE_{01\delta}$ mode. The usual properties of the BMT material are: ε_r = 24 and tanδ = 10^{-4} [10]. The characterization on BMT resonators fired with two different recipes were realized. Moreover the very low loss tangent, this material presents a temperature stability.

1 First recipe

The firing process of this first sample is done at 1500°C for 30 hours. In the Figure 45, we observe on the left resonator a small layer on the top which is lighter than the bottom part. It is a layer composed of pollutant elements where some particles have migrated during the firing. The measurement of this resonator gives us the following properties: the permittivity is 20,8 and a loss tangent of 0.9 10^{-4}. The TCF is -2.66 ppm.°C^{-1}.

We notice that the loss tangent is ten times better than Zirconia material, as a consequence we will have a better Q_0-factor because we will have less losses in our DRs.

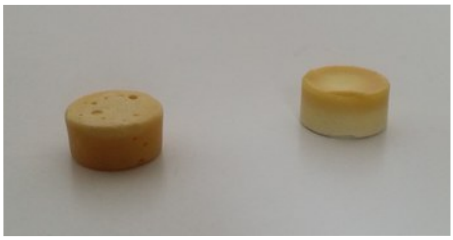


Figure 45: Characterization of the Zirconia material - recipe 1 (left) , recipe 2 (right) - 10GHz resonator

2 Second recipe

The firing of this second resonator is done at 1600°C for 2 hours. On the right of the Figure 45 we observe the obtained dielectric piece. We notice the same problem, a yellow layer composed of pollutants on the top. For this recipe, we obtain a permittivity of 21.1 and a loss tangent of 1.2 10^{-4}. The TCF is -0.085 ppm.°C^{-1}. We have mostly the same properties with a TCF remarkably close to 0 ppm.°C^{-1}. Thanks to that a filter using this material would not need thermal compensation for its dielectric part.

3 Alumina

This material is very common for the stereolithography process. The chemical name of this material is Aluminum Oxide with the chemical formula Al_2O_3.



Figure 46: powder of alumina (Aluminum Oxide)

The dielectric resonators are shown in the Figure 47.

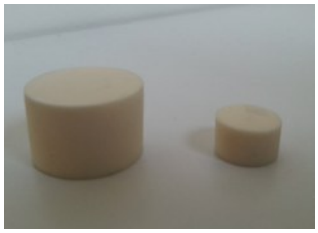


Figure 47: Alumina resonators

They are designed to resonate at 5 and 10 GHz on the $TE_{01\delta}$ mode.

The permittivity of the material as a function of the frequency is presented in the Figure 48.

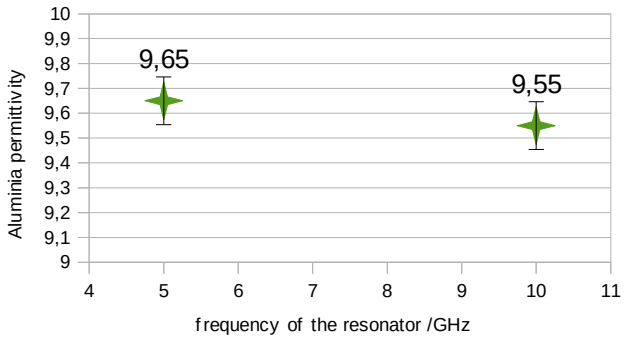


Figure 48: Aluminia permittivity as a function of the frequency

The loss tangent is also measured and shown in the Figure 49. We notice the loss tangent is more important than usual, we realized several time the measurement to eliminate the possible error due to the measure.

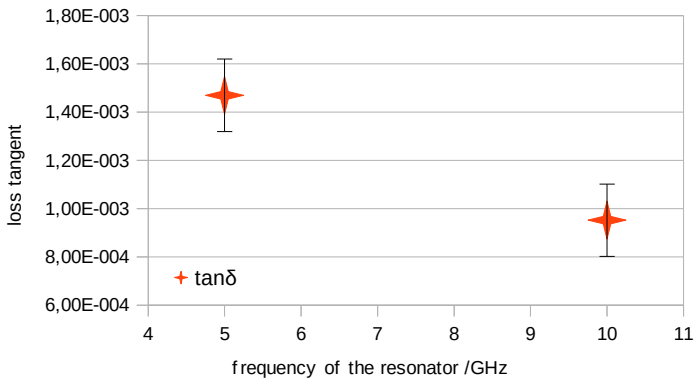


Figure 49: Alumina loss tangent as a function of the resonance frequency

A probable low density has been obtained for the biggest DR since the loss tangent is directly linked to density [1].

VIII. Determination of the coupling between dielectric resonators:

In this part, we present how to calculate the value of the coupling coefficient K_{12} between two cavities loaded in our case with dielectric resonators.

To determinate the K_{12} coupling between two cavities, we choose the eigenmode simulation mode in HFSS© and we apply different steps to obtain the value. We use for the explanation this structure (Figure 50):

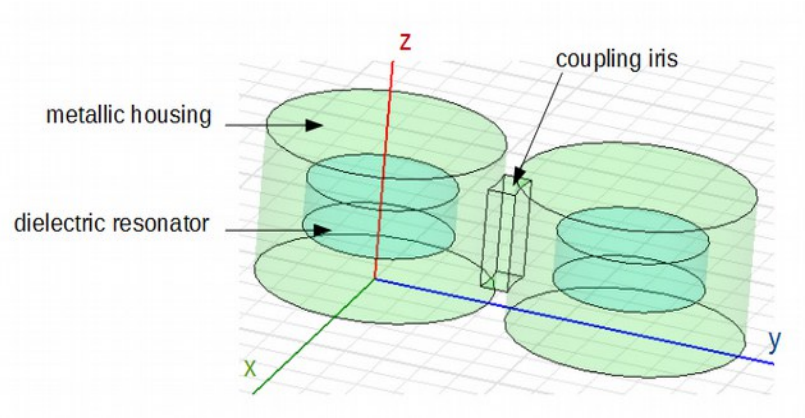


Figure 50: initial structure to calculate the K_{12} coupling

To calculate the coupling of this configuration, we take only a half structure because it is symmetrical, so we simulate this structure (Figure 51):

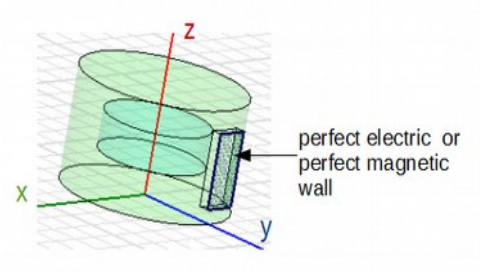


Figure 51: one half of the previous structure

In the HFSS© software, we apply a perfect electric wall on the blue area and we obtain a frequency which will be named f_e corresponding to the even mode. In the same way, we apply a perfect magnetic wall to obtain another frequency, f_m, corresponding to the odd mode of the cavity.

As a result, using this next formula we can calculate the K_{12} coupling:

$$k_{12}=\frac{f_e^2-f_m^2}{f_e^2+f_m^2} \quad [2]\ (15)$$

This parameter could be expressed as a function of MHz using this formula:

$$K_{12}(/MHz) = k_{12} \times bandwidth \quad (16)$$

This latter expression will be used in this chapter.

IX. Determination of the coupling in Input/Output accesses

1 Phase of the S_{11} parameter

To obtain the Input/Output coupling expressed as the Qe parameter, we have to measure the phase of the S_{11} parameter when a single resonator is excited. For example, in the Figure 52

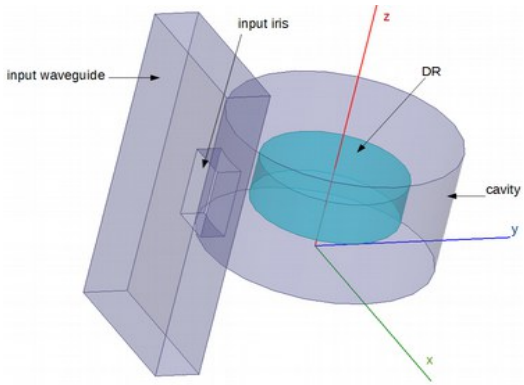


Figure 52: Determination of the Qe factor between the cavity and the waveguide

we change the dimensions of the iris between the cavity and the waveguide to see the impact on the Input/Output coupling. In this way, we study the phase as shown in Figure 53.

So we determinate the frequency f_r to the middle of the phase break and we measure the frequency interval for the values of $\varphi(f_r)+90°$ and we calculate Qe-factor as follow. When we realize a simulation without losses and finally we have:

$$\frac{1}{Q_L} = \frac{2}{Q_e} \quad (17) \Leftrightarrow \quad Q_e = 2Q_L \qquad \text{with} \quad Q_L = \frac{f_r}{\Delta f_{r_{\pm 90°}}} \quad (18) \text{ loaded Q-factor} \qquad \text{so}$$

$$Q_e = 2\frac{f_r}{\Delta f_{r_{\pm 90°}}} \quad (19)$$

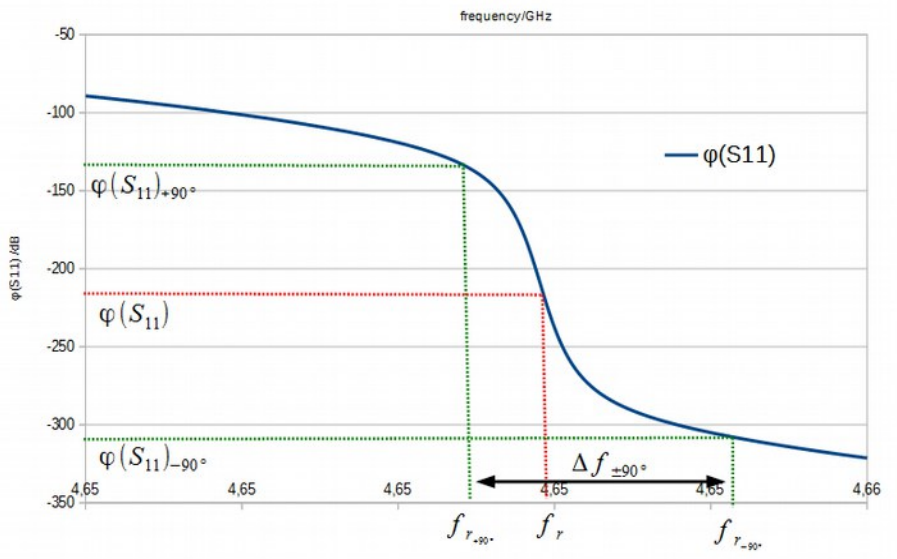


Figure 53: determination of the Qe-factor with the phase of the S_{11} parameter

2 S_{21} parameter

Another way to determinate the Qe-factor is to use the S_{21} parameter. In this case, we need to have input and output excitations. The calculation of this one is a little bit different with the next formula:

$$Q_e = 2\frac{f_r}{\Delta f_{-3dB}} \quad (20)$$ with: resonance frequency as illustrated in Figure 54

$$\Delta f_{-3dB} = f_{r2_{-3dB}} - f_{r1_{-3dB}}$$

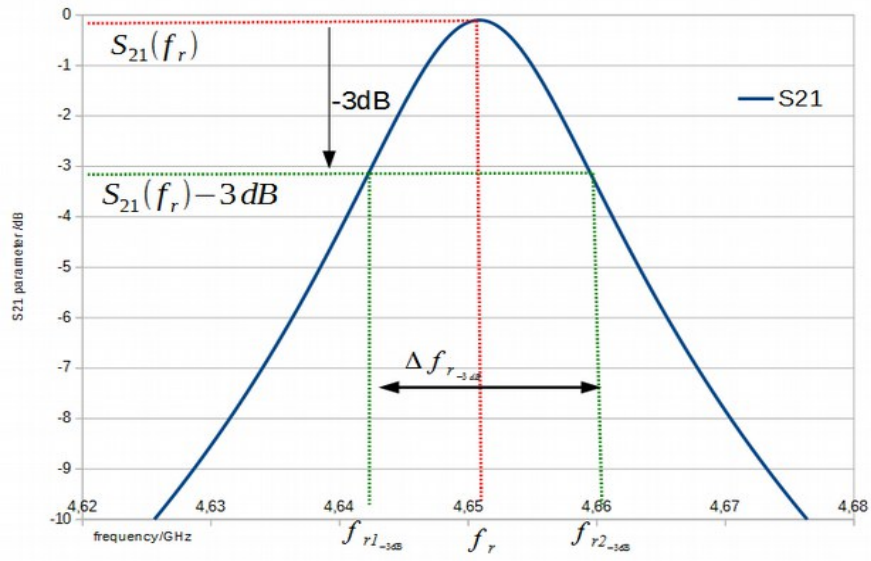


Figure 54: determination of the Qe-factor with the S_{21} parameter

In the Figure 54, we see the approach to calculate the Qe-factor with the S21 parameter.

X. Project software environment

A program called FELO© (Figure 55) is firstly used to obtain the theoretical coupling matrix of a filter for a given set of specifications (central frequency, the bandwidth, the number of poles, etc). We have also the possibility to choose the topology (Chebyshev, elliptical,..) and finally to retrieve the matrix that will be used for the design of the project filters. After

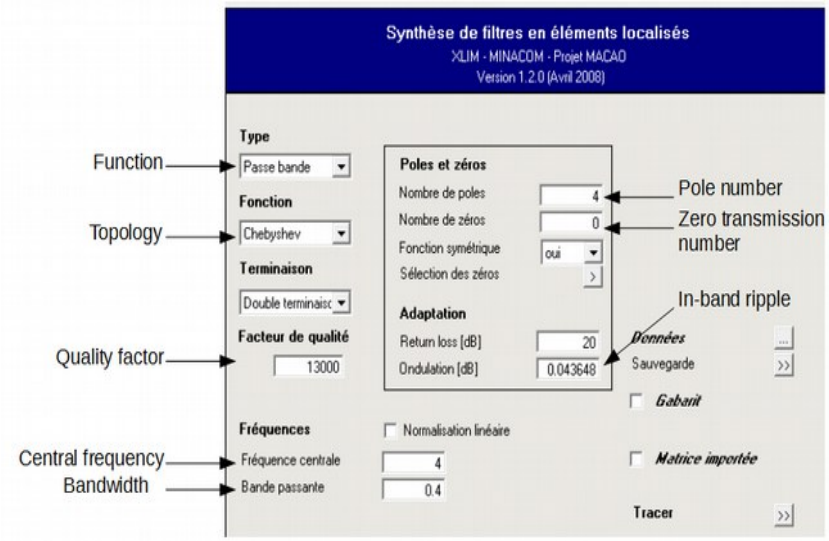


Figure 55: front panel of the FELO software

completing the software, the theoretical S parameters can be plot as well as the corresponding coupling matrix (Figure 57 and Figure 58).

Then, we plot the response (Figure 56) to check if it is the right one we want and we can collect the coupling matrix calculated by the software (Figure 57).

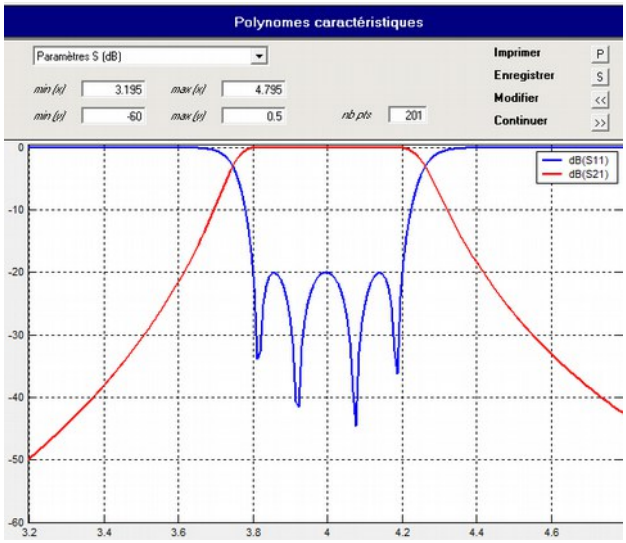


Figure 56: example of a filter response with the FELO software

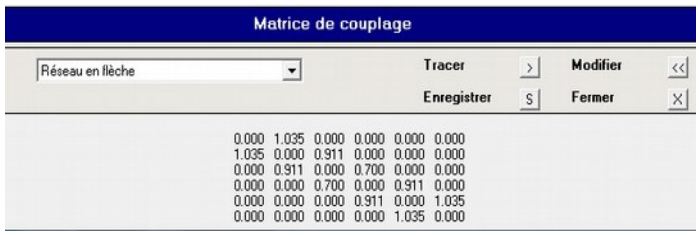


Figure 57: coupling matrix obtained by FELO software

We note that the matrix is normalized so it is not associated to a frequency or to a bandwidth in Hz but only to the shape of the response we want.

During the design process, we can use another software called PRESTO (Figure 58) to help us identifying the actual couplings and resonance frequencies of the resonators composing a filter under design (simulation). The response of the simulated filter is thus compared to the theoretical matrix, and this program identifies the couplings between the different poles that compose our filter. The software need us to precise the characteristics of our filter as the central frequency, the number of poles, etc. To increase the pertinence of the result, it is possible to shrink the study frequency interval to have a better identification of its coupling matrix. Thanks to PRESTO, the couplings within a given structure can be identified and their study and optimization can be very efficiently done.

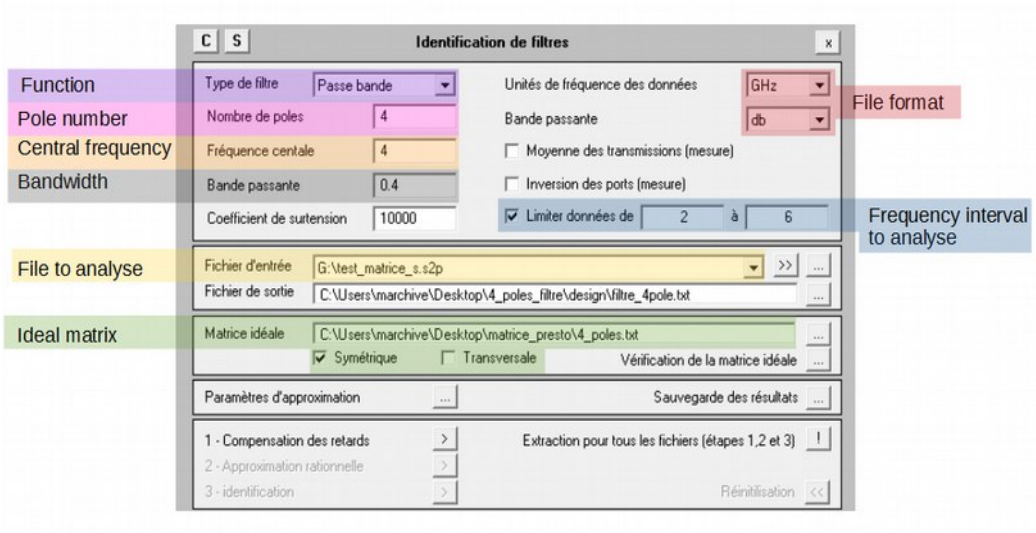


Figure 58: front panel of the PRESTO software

With this software, we can then study a given geometrical modification on the different couplings existing in the structure under study. In other words, we are able to identify the different coupling coefficients affected by this modification.

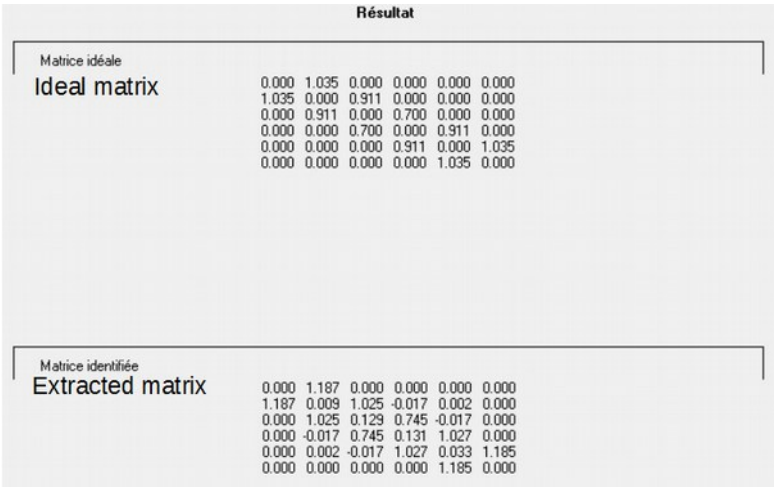


Figure 59: Values of the coupling coefficients of the simulated filter (bottom matrix) and of the theoretical one that is expected (top matric)

For practical reason, we will denormalize this matrix to have the coefficient expressed in MHz. Indeed, it will be more easier to identify how wide a bandwidth can be achieved using such couplings.

XI. TE01δ mode

1 Dielectric resonator

The first part of this study will be focused on a cylindrical cavity containing a cylindrical DR design to resonate on the $TE_{01\delta}$ mode [3]-[4]. This resonator permits us to increase the compactness of our design because the dielectric material allow to concentrate more efficiently the EM field inside this element due to the permittivity. However, we will have lower Q-factor than using only metallic cavity because we add some dielectric losses. As we saw in the first chapter, the $TE_{01\delta}$ mode is present in many input filters or in IMUX. Indeed, this single mode is very interesting because it offers the advantages of design simplicity, a good frequency free range, the possibility to couple with different technologies like micro-strip line [5], waveguide [6], probe [7], etc.

We will use two main dielectric materials in the project: Zirconia and BMT. The Zirconia (ZrO2) will be mainly used for prototyping purposes because of its lower price and easier availability. The BMT material will be rather used for advanced filters regarding its higher performances (temperature stability, better tanδ) but coming with a higher price and more limited availability in terms of quantity.

The starting point of this study is a single Zirconia resonator on the $TE_{01\delta}$ mode in a cavity at 4 GHz (Figure 60).

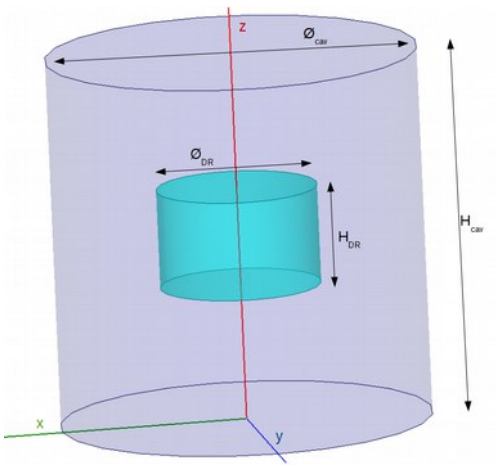


Figure 60: Zirconia DR inside a cavity

Then, the Figure 61 shows the electric and the magnetic field inside the cavity loaded by a dielectric resonator and the cavity. We notice it is concentrated in the dielectric material as expected. The $TE_{01\delta}$ mode is easily identifiable.

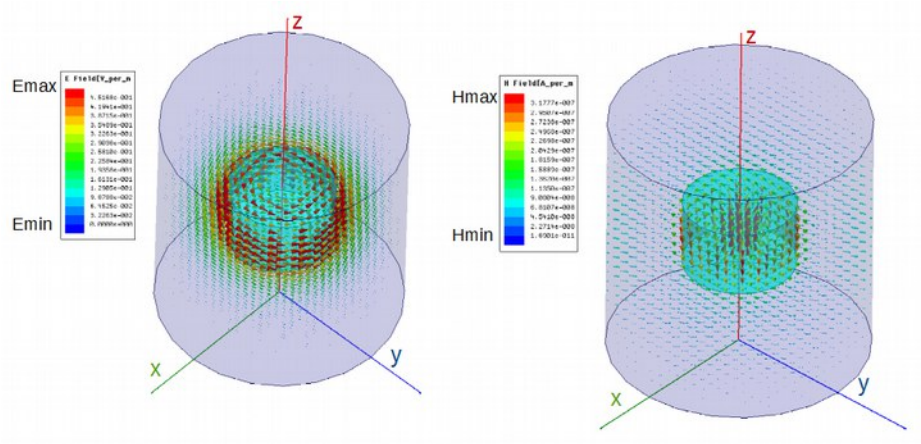


Figure 61: Electric and magnetic field inside a cavity loaded by a dielectric resonator

The diameter and the height of the DR are optimized to provide the $TE_{01\delta}$ mode at 4 GHz. After that, we choose the dimensions of the cavity to tune the spurious free range and to make it as wide as possible. We initially chose some arbitrary ratio between the DR and cavity dimensions such as:

- $R_{cav} = 2\ R_{DR}$
- $H_{cavity} = 3\ R_{DR}$

After optimization, we obtained the following dimensions to work at 4GHz:

1/ dielectric resonator:

- radius = 9.5 mm
- height = 6 mm

2/ cavity:

- radius = 15 mm
- height = 18mm

The response of this element is summarized in the Table IV considering a loss tangent for the Zirconia material and a cavity conductivity of 50 10^6 S/m (ideal case with a silver plating).

Eigenmode	Frequency /GHz	Q
$TE_{01\delta}$	4.049	1190
TE_{112}	4.551	1210
TE_{112}	4.551	1210
Spurious mode	5.20	1860
Spurious mode	5.20	1860

Table IV: frequency response of the dielectric resonator

We have the fundamental $TE_{01\delta}$ mode frequency at 4.049 GHz (close enough to our objective) and the next mode is at 4.55 GHz, providing a spurious free range higher than 500 MHz and the Q factor is 1190.

A more realistic geometry will include a Teflon support in order to maintain the DR in the middle of the cavity and therefore to maximize its Q-factor. Teflon is chosen because it has a low permittivity of 2,1 and a low loss tangent of 0.00028 (at 3 GHz).

The obtained dimensions for the cavity and DR will provide a baseline for the following study: based on a 2-pole configuration, we will try different strategies to obtain coupling high enough for a 10% or better bandpass filter.

2 Ring resonators

It is possible to modify the previous design of the DR in order to have a better Q-factor or/and a better spurious free range: we draw a dielectric ring resonator [8]-[9]. We add a hole in its center to increase the Q-factor as well and use a supporting element made with the same

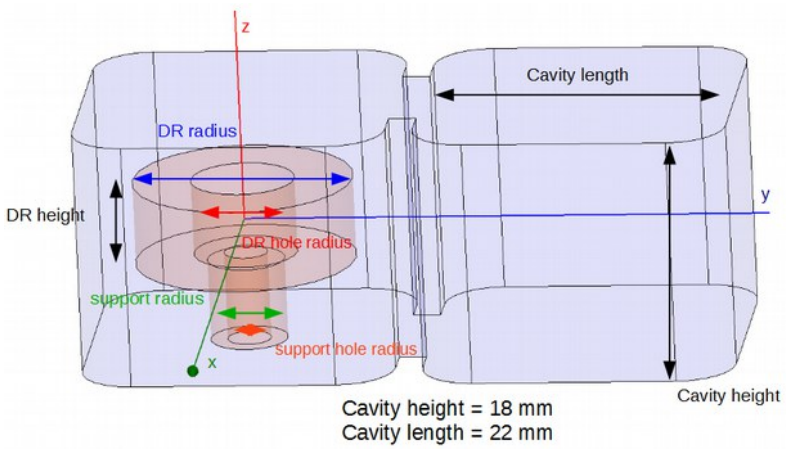


Figure 62: resonator and support with a hole - one single material

dielectric material as for dielectric resonators. The DR and its supporting element are designed to be only one part.

In the Figure 62, we identify the DR and its support which is used to center the DR in the middle of the cavity. Both DR and support have a central hole to limit the excitation of spurious modes. The dielectric material we use is Zirconia in the following parts.

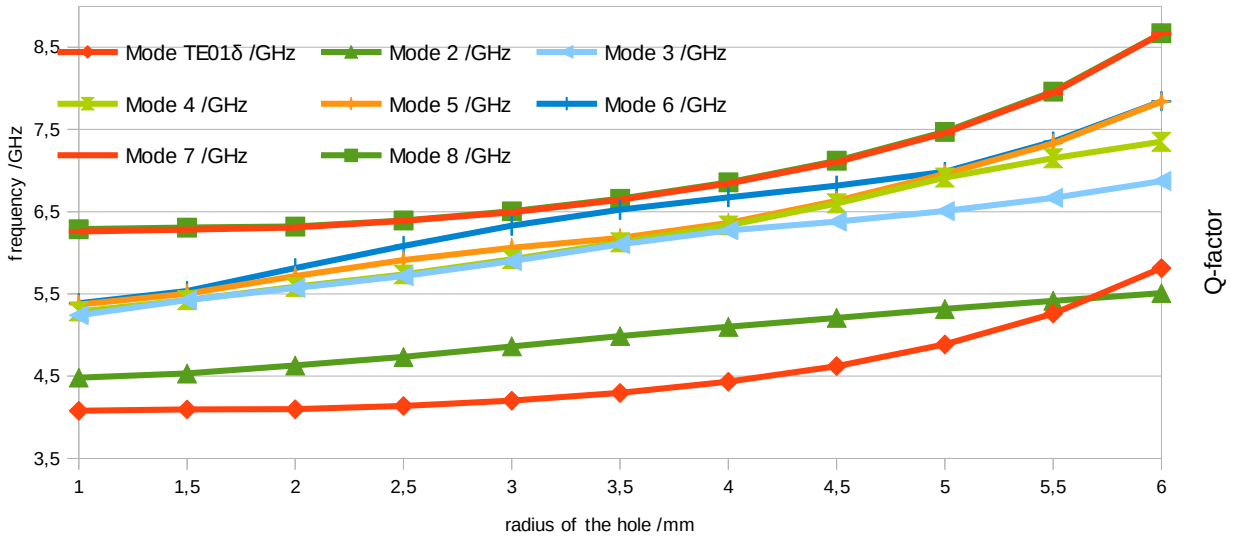


Figure 63: Impact of the hole radius inside a dielectric resonator

The Figure 63 shows the influence of the diameter of the hole inside the dielectric resonator for the first eight modes. These simulations are made using the following parameters:

$diameter_{cavity}$ =22mm $diameter_{DR}$ = 14,8mm

$height_{cavity}$ = 18mm $height_{DR}$ = 7mm

We can see that the best spurious free range is for a hole radius of 3.5mm. The frequency window between the TE mode and the next one is more than 700MHz in that case. It will be a solution for our future filter if we need to increase the spurious free range while using this single part component combining the DR and its support.

3 Input/Output couplings

In this part, we will present different Input/Output coupling system. To realize a wide bandwidth filter, we know that a strong Input/Output coupling will be necessary. In this way, we present several techniques to achieve this challenge. For the next designs, we work on the

$TE_{01\delta}$ mode. The targeted Qe-factor for our study will be 10 for the 10% bandwidth researched in this thesis.

1 Waveguide

This way is the usual one for cavity resonator. To determinate the Qe-factor (Input/Output coupling value), we need the argument of the S_{11} parameter, that is why we design only one waveguide connected to one cavity loaded with the DR (Figure 64). We widely open the Input iris to have a maximum coupling. The dielectric resonator and the cavity are designed to resonate at 4GHz.

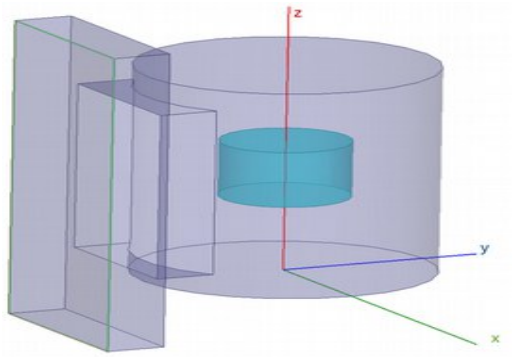


Figure 64: resonator excited by waveguide

We study the value of the coupling for different dimension for the Input coupling iris.

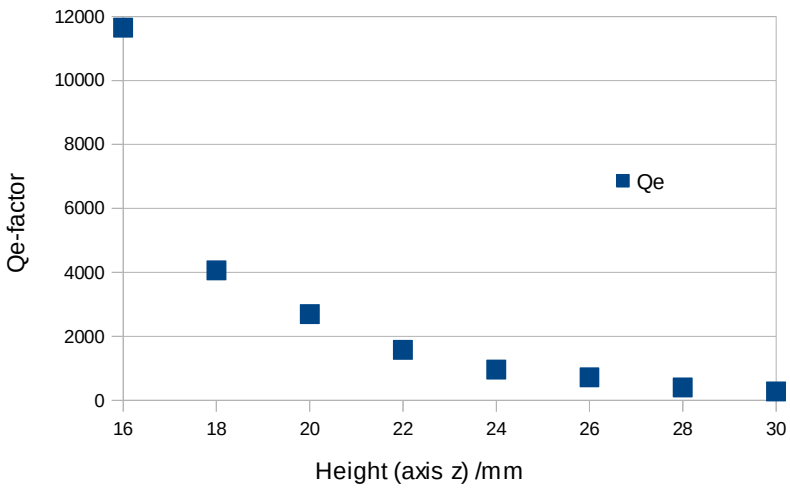


Figure 65: Waveguide - Input coupling - Height of the iris

We observe in the Figure 65 that the Qe-factor decreases when we increase the height of the Input iris, meaning that the coupling increases. Indeed, the opening is bigger so more electromagnetic fields can pass through this element.
In the Figure 66, we obtain the same comment about the variation of the Qe-factor. However, it is less sensitive.

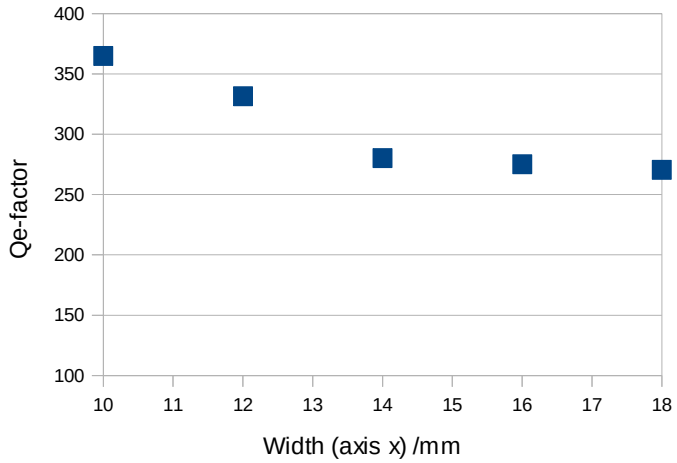


Figure 66: Waveguide - Input coupling -Width of the iris

Finally, we observe on the Figure 67 variation of the Input coupling as a function of the thickness of the coupling iris. It is the expected behavior. Indeed, when the thickness increases the Input/Output coupling decreases.

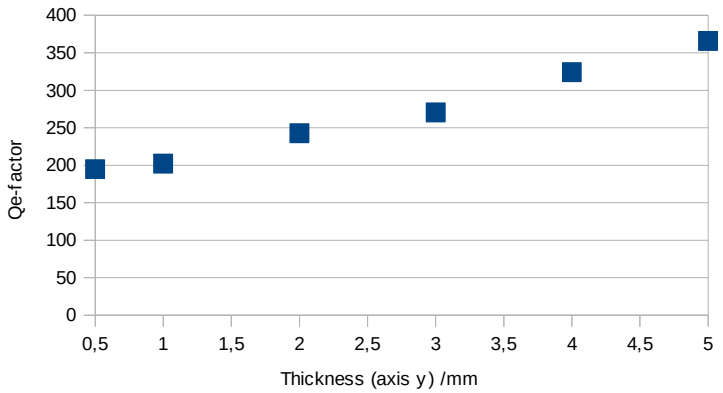


Figure 67: Waveguide - Input coupling -Thickness of the iris

In light of the obtained result, we have a very low Input/Output coupling using waveguides. As a reminder, the targeted value is around 10. In this way, we have to find another way to couple our dielectric resonator.

Then, we will use a magnetic loop because this excitation system will be closer to the dielectric resonator, so the coupling should be bigger.

2 Magnetic loop

We decide to try this system due to the orientation of the magnetic field inside the dielectric resonator, Figure 68. Indeed, if the probe is close to the dielectric element, it is possible to increase the energy transfer between the two parts. In this way, we study the behavior of a magnetic loop with the ceramic piece.

The dimensions of these elements are:

-for the cavity: height: 30mm
diameter: 30mm

-for the DR: height: 8mm
diameter: 13mm

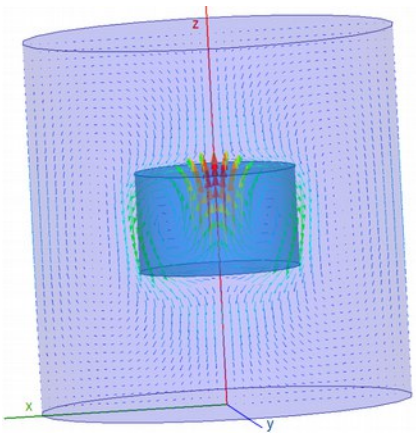


Figure 68: orientation of the magnetic field in the cavity

Firstly, we insert a coaxial probe with a loop close to the DR as presented in Figure 69.

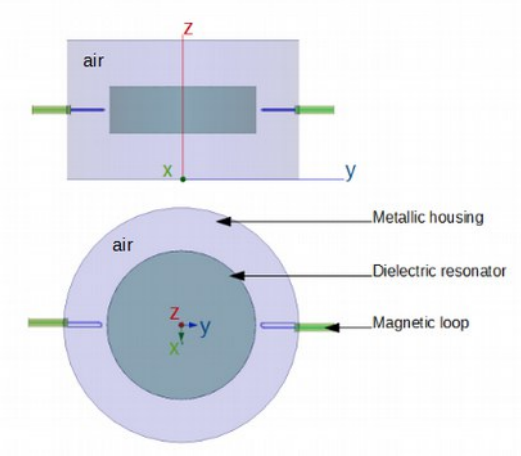


Figure 69: Magnetic loops close to the DR

We calculate the Qe-factor and with a long probe which is very close (touching) to the DR, we can obtain a low Qe-factor. In the Figure 70, we see when the probe length increases (so it becomes closer of the dielectric resonator) the Input/Output follows the same effect. However the lowest Qe-factor we obtain is 609. In this way, we can not use this solution to achieve strong coupling for the Input and Output accesses.

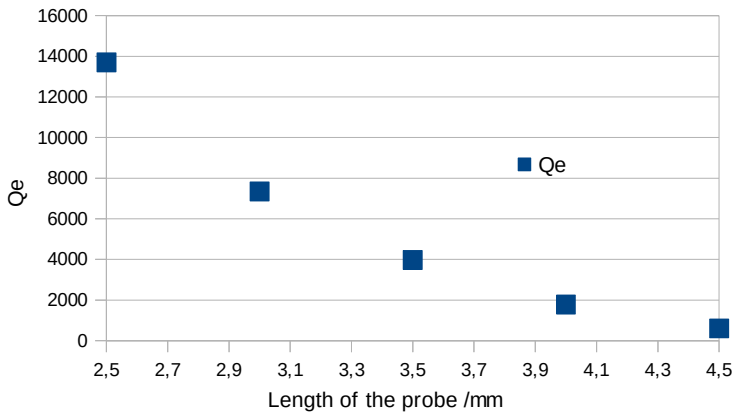


Figure 70: Qe-factor of this design as a function of the length of the probe

We have decided to follow this direction and we propose another configuration presented in the Figure 71. In order to increase the coupling provided by such system, we increase the size of the loops as well as their position and geometry (Figure 71).

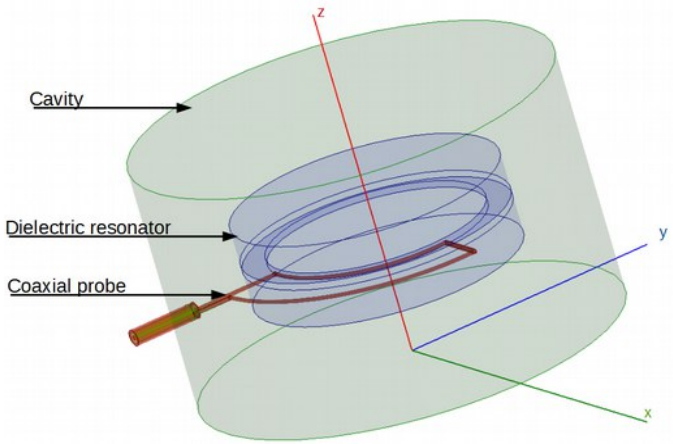


Figure 71: configuration B for Input/Output with magnetic loops inside the dielectric resonator

First, we study the impact of the gap between the two arms of the coaxial probe. The length of the excitation stays the same. It is presented in the Figure 72.

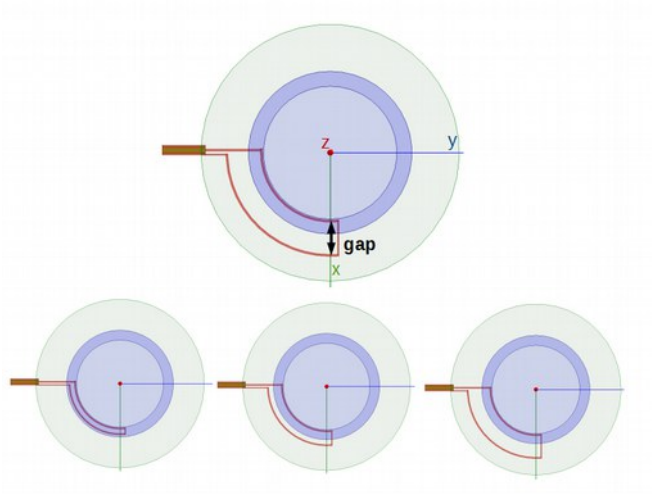


Figure 72: Variation of the gap between the two arms of the coaxial probe

The results are shown in the Figure 73. We observe that we have a maximal coupling for a gap of 1.5mm, the associated Qe-factor is 22. However, the value of the coupling has a small evolution. The Qe-factor stays around 25.

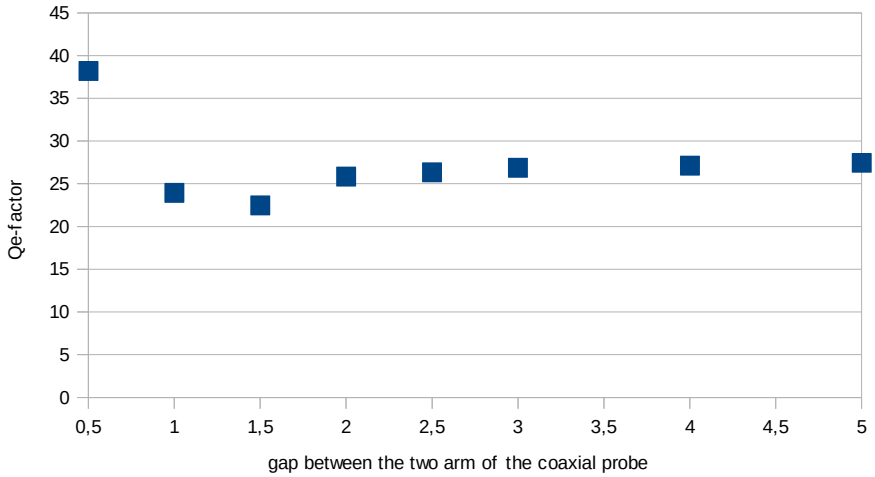


Figure 73: Result for the variation of the gap between the two arms of the coaxial probe

Then, we investigate the variation of the Qe-factor as a function of the length of the coaxial probe. In the Figure 74, we can see different lengths for the coaxial probe.

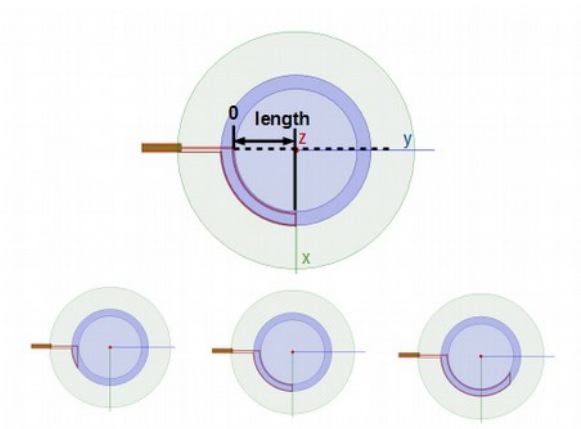


Figure 74: Example of different lengths for the coaxial probe

The values of the Input coupling obtained for the different lengths of the coaxial probe are presented in the Figure 75.

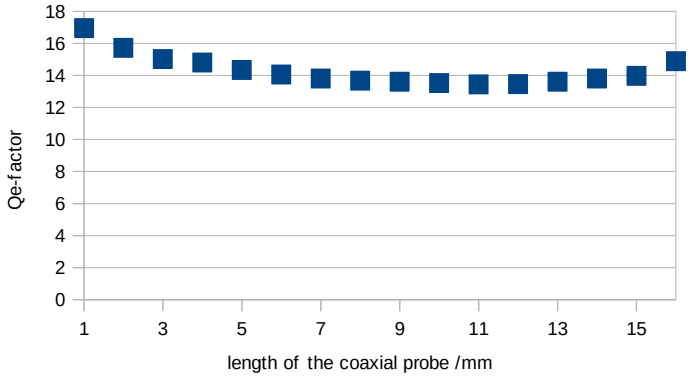


Figure 75: Result for the length variation of the coaxial probe

For this configuration we obtained a Qe-factor around 13. We see this excitation configuration we can achieve strong coupling even if we did not have less than 10. However, the complexity of this kind of coaxial probe is too important to apply it for our filter. Indeed, It will be difficult to have the right dimensions and gaps, then we have to design the dielectric resonator as a function of the diameter of the coaxial probe.

A last configuration with a coaxial probe in the cavity placed close to the DR is proposed (Figure 76). We modify the different dimensions to realize the wanted coupling value of 10. We can increase the diameter of the metallic probe and also the distance to the dielectric resonator.

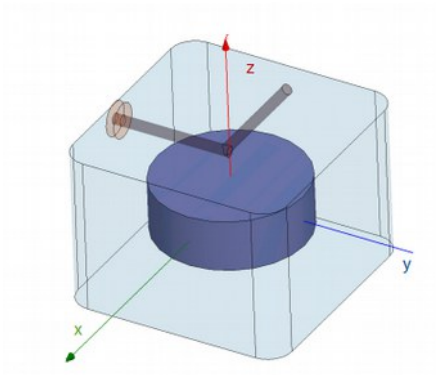


Figure 76: excitation system - coaxial probe inside a cavity with a 90° bend

We study the behavior of the Qe-factor as a function of the position and the length of the coaxial probe. The two parameters we will study are presented in the Figure 77.

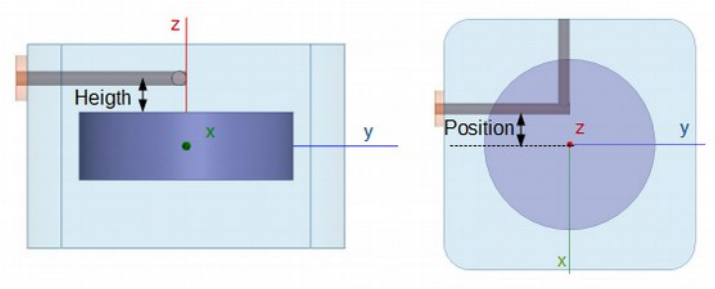


Figure 77: Presentation of the two studied parameters for the Input coupling

In the Figure 78, we have the variation of the Qe-factor as a function of the distance with the coaxial probe. We can deduce that the Input coupling increases when the coaxial probe is closer to the dielectric resonator as expected.

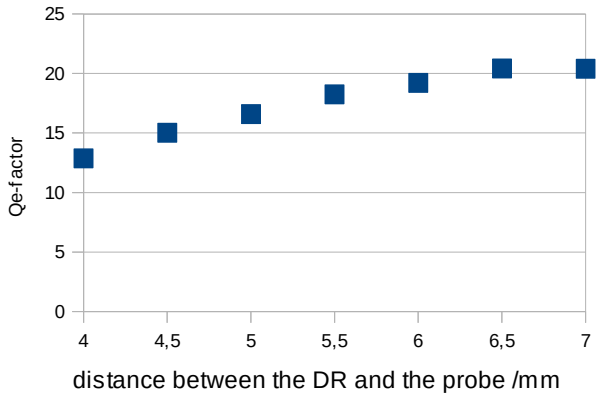


Figure 78: Behavior of the Qe-factor as a function the distance between the DR and the probe

The second parameter which is studied is the position of the coaxial probe. Upon changing its position, the length of the 90° bend changes (Figure 79). When the position of the probe moves to the highest positive values (0 mm means that the probe is above the DR center). the length of the 90° bend increases, and more surface are excited by the coaxial probe. Consequently, the Input coupling increases when the position goes up.

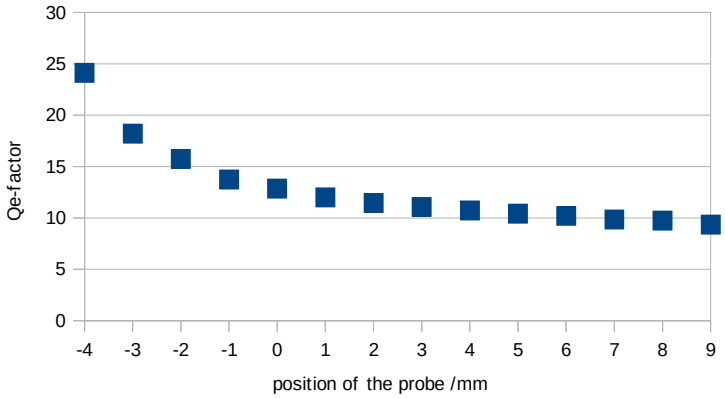


Figure 79: Behavior of the Qe-factor as a function of the position of the coaxial probe

With this kind of probe, we achieve a Qe-factor around 9. This last solution appears to be compatible with our needs. To have a better idea of the behavior of this coupling, we examine the electromagnetic fields to see the interaction between the coaxial probe and the dielectric resonator, as shown in Figure 80.

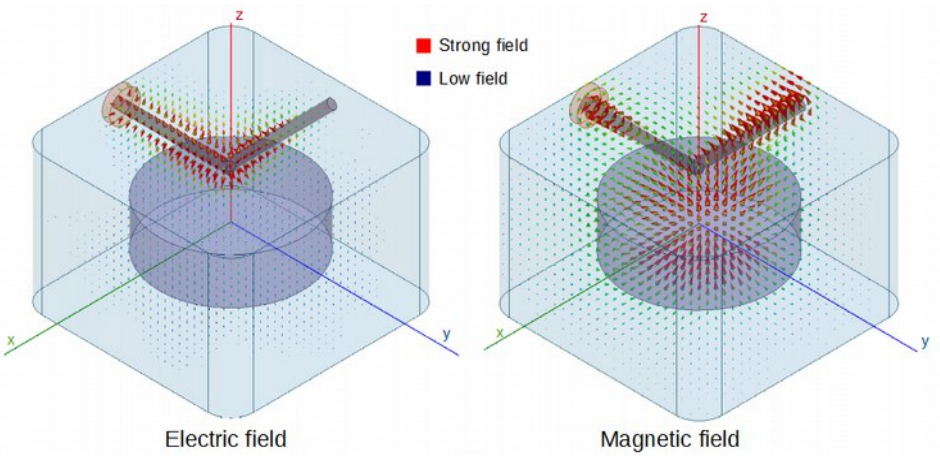


Figure 80: electromagnetic field inside the cavity

Now, we have to study the coupling between two resonators to move forward towards the creation of our 10% bandwidth filter around 4GHz.

4 Inter-resonator coupling

Keeping the TE mode, we have then tried different modifications of the base DR to maximize the coupling between adjacent dielectric resonators to reach the wanted value of 400MHz. The

dielectric material used for the next configurations is still Zirconia and we try to create monolithic ceramic components where all the resonators are merged together.

1 First configuration

The first modified structures used here are presented in Figure 81. It is composed of a cylindrical dielectric resonators with two cylinders (arms) connected to it. The purpose of these cylinders is to guide the electric field in these dielectric cylinders. The Figure 82 shows the variation of the radius of the connecting dielectric element.

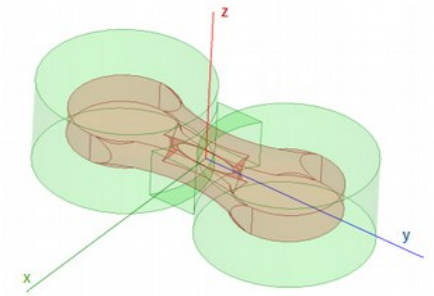


Figure 81: first configuration

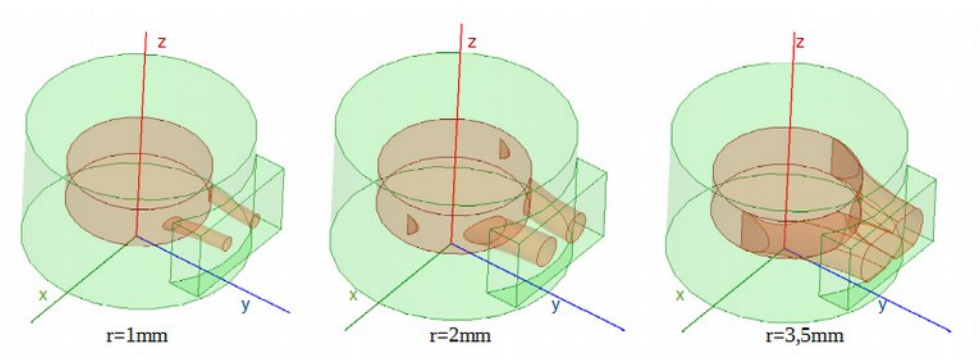


Figure 82: first configuration - $TE_{01\delta}$ mode with modifications of the connecting cylinder radius (r)

The K12 coupling is plotted as a function of the cylinder diameters. At the beginning, the K12 coupling increases with the radius to a maximum for 3.5mm because after this value, the two horizontal cylinders merge in just one big cylinders. The maximal coupling we obtain is 80 MHz far from the expected 400MHz.

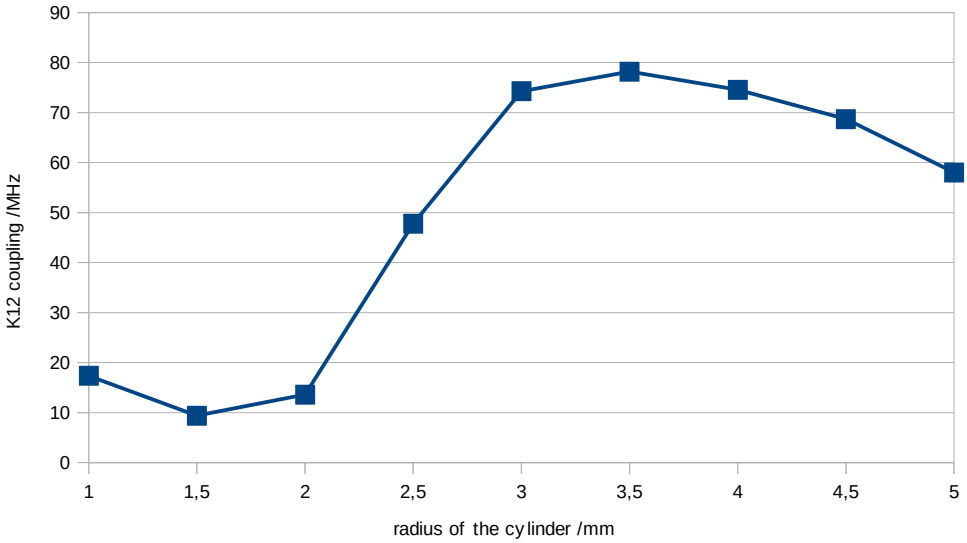


Figure 83: Variation of the K12 coupling -first configuration

In the Table V, we present one simulation for the radius r=5mm in the perfect magnetic wall configuration.

Eigenmode:	Frequency /GHz
Mode 1 – fundamental	3.69
Mode 2 – cavity	4.25
Mode 3 – cavity	4.30
Mode 4 – TE101	4.46
Mode 5 – cavity	5.23

Table V: spurious modes for the first configuration – TE01δ mode

In the Figure 84, we observe the electric and magnetic field inside the cavity and the dielectric element. The fields are strong at the level of the connecting element, however the appearance of the electric field is disturbed by this element.

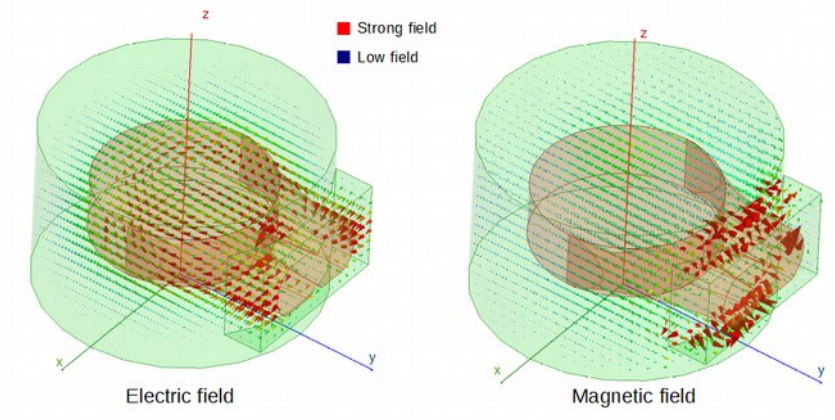


Figure 84: first configuration - Electromagnetic field inside the DR and the cavity

2 Second configuration

Another modification with the dielectric part connecting two close dielectric resonators is proposed (Figure 85).

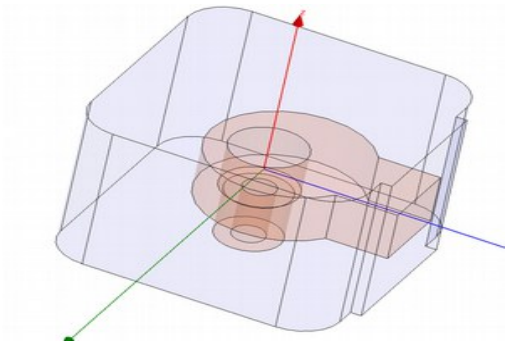


Figure 85: second configuration – $TE_{01\delta}$ mode

We put a hole in the center of the dielectric resonator to avoid some spurious modes and we have a rectangular shape for the dielectric element connecting the two DRs.

The electric field (Figure 86) is a little bit easier to identify than with the previous configuration. A spurious mode is unfortunately located in the iris close to 4GHz and it will be difficult to avoid its presence.

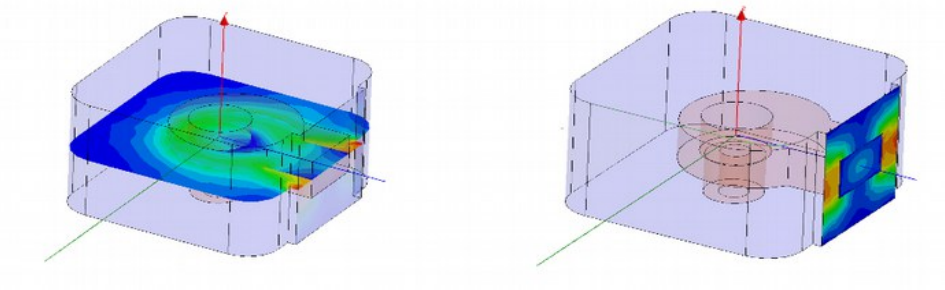


Figure 86: electric field – second configuration – $TE_{01\delta}$ mode

To determinate the K12 coupling provided by this structure, a parametric study of the dielectric iris dimensions has been done. The dielectric iris height (z axis) is here set to 6mm.

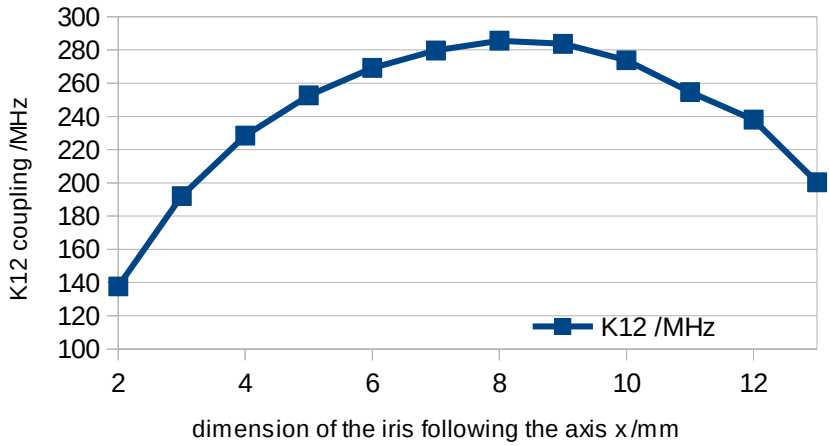


Figure 87: K12 coupling depending on the axis x dimension -
second configuration – $TE_{01\delta}$ mode

Thanks to this graph (Figure 87), we identify the maximal coupling we can have with this design, it is 280MHz. In this way, we do the same thing for the other dimensions (following the axis z) with the dimension for the axis x at 9mm.

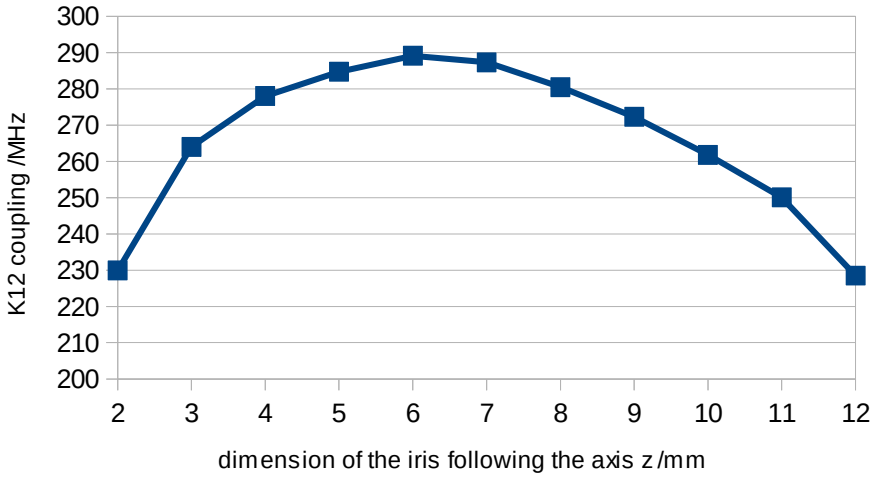


Figure 88: K12 coupling depending of the axis z dimension - second configuration – TE01δ mode

The variation according to the other axis (Figure 88) does not show a better K_{12} coupling. So with the concept we can achieve a coupling around 280 MHz.

We also study the different modes excited within the structure and we see that some spurious modes are close to our working frequency (Table VI) making it not satisfactory for our application.

Eigenmode –	Frequency /GHz	Q
Mode 1 – cavity	4.19	1290
Mode 2 – cavity	4.20	2270
Mode 3 – fundamental	5.01	1240
Mode 4 – iris/cavity	5.46	1330
Mode 5 – cavity	5.53	1240

Table VI: modes of the second configuration

3 Third configuration

We present another configuration with the $TE_{01\delta}$ mode on the Figure 89.

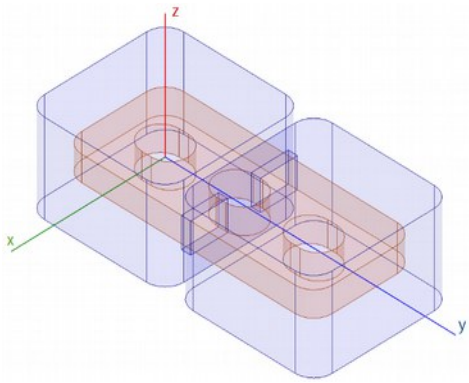


Figure 89: third configuration - $TE_{01\delta}$ mode

We keep the hole inside the dielectric resonator and add another on the dielectric element between the two cavities. The two rectangular shapes are located in the place where we have the maximum value of the electric field.

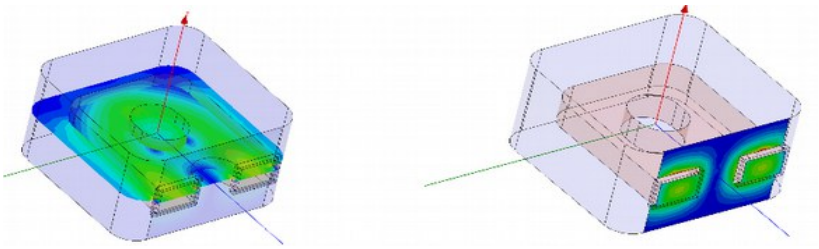


Figure 90: electric field – third configuration - $TE_{01\delta}$ mode

We do not have a clear result here when trying to identify the $TE_{01\delta}$ (Figure 90) and we are not sure to actually work on this mode. We also have a small coupling between cavities loaded by such dielectric part and spurious modes are very close to our working frequency (Table VII).

Eigenmode –	**Frequency /GHz**	**Q**
Mode 1 – fundamental	3.22	1200
Mode 2 – cavity/iris	3.40	1210
Mode 3 – cavity/iris	3.42	1870
Mode 4 – TM_{22}	4.65	1250
Mode 5 – TM_{22}	4.81	1550

Table VII: modes of the third configuration

4 Fourth configuration

We present a last design for the coupling between cavities based with the $TE_{01\delta}$ DR mode. To do this we take into account the previous results and we try to avoid as much as possible the spurious mode that could appear and we keep trying to maximize the K_{12} coupling factor. This last concept is shown in the Figure 91.

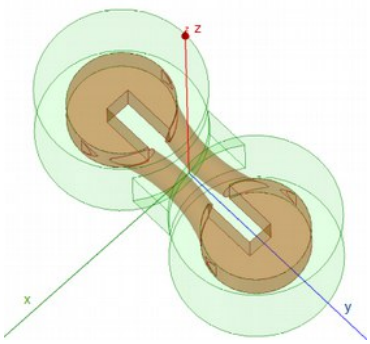


Figure 91: fourth configuration

$TE_{01\delta}$ mode

We have a first dielectric resonator with two arms connected to a second dielectric resonator. In this way, the dielectric material in the iris is more located where we mostly have the electric field for the $TE_{01\delta}$ mode and we avoid to excite spurious modes. We obtain the next modes for this structure:

Eigenmode	Frequency /GHz
Mode 1 – cavity	4.15
Mode 2 – fundamental	4.25
Mode 3 – cavity	5.21
Mode 4 – TE101	5.80
Mode 5 – TE101	5.90

Table VIII: modes for the fourth configuration

We see in Table VIII that the first mode is not the fundamental one but if we succeed to eliminate this one we will have a spurious free range around 1GHz. Moreover, the measured K_{12} coupling is around 270 MHz, so it is close to our goal.

In the Figure 92, we identify the structure of the electric and magnetic fields. The electric field is disturbed by the dielectric element at the level of the iris

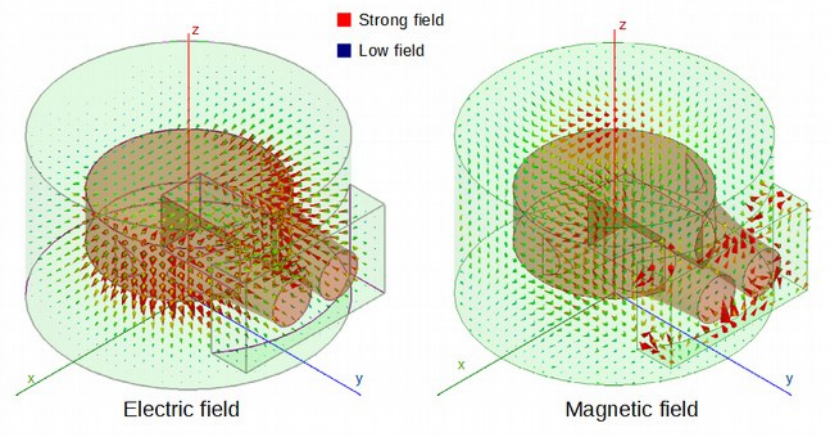


Figure 92: fourth configuration - electric and magnetic fields

However, two principal reasons make that design not feasible. The first one is it will be difficult to avoid the first mode of the cavity and to keep the actual spurious free range. The other reason is that we want to realize a typical Chebychev filter with an order higher than two (a 4th order typically). Because of the geometry of the proposed DR, the intermediate resonators (between resonators number 1 and 3 in the case of a 4th order filter for example) would be very complex and hard to make geometry that would certainly disturb our $TE_{01\delta}$ mode.

5 Conclusion

We have presented in this section resonators based on the $TE_{01\delta}$ mode and their different characteristics.

After all the studied configurations where modifications of these DRs have been tried, we have not succeed to have a strong enough K_{12} coupling with the $TE_{01\delta}$ mode DRs even if a proper Input/Output coupling can be achieved with bended coaxial probes. Indeed, the electric field can not be easily guided through dielectric arms connecting two close DRs. Even with potentially high K_{12} close to 300 MHz, the studied structures present a high number of spurious modes close to the DR working frequency, making that result not satisfactory.

XII. TM010 mode

1 Electromagnetic fields

We work with this mode to try to have 10% of bandwidth for our filter since the previous studies based on $TE_{01\delta}$ mode resonators were not satisfactory. First, we study a dielectric resonator in a cavity (Figure 93) using the selected TM01 mode proposed that Pr Kobayashi [11]

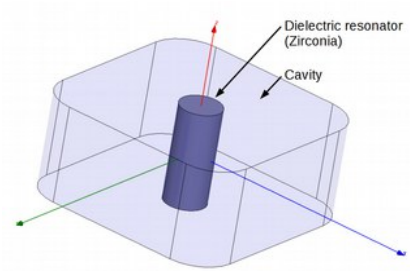


Figure 93: dielectric resonator
using the TM_{010} mode

We see the electric and the magnetic field inside the cavity:

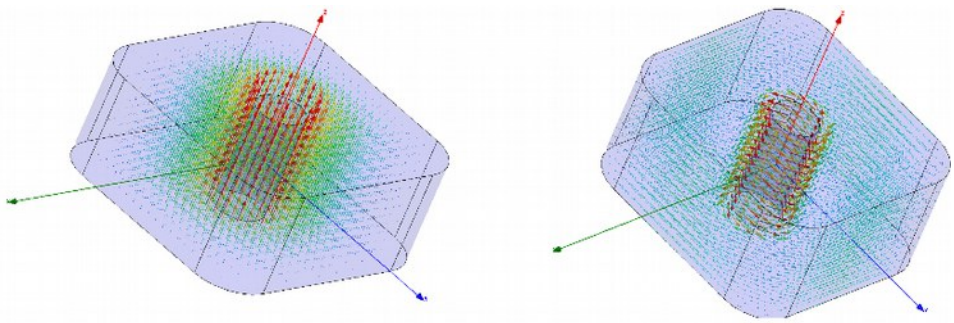


Figure 94: electric (left) and magnetic (right) fields – strong field: red;
low field: blue – TM_{010} mode

The electric field is contained inside of the dielectric resonator and we think it would be easier to very efficiently couple this field between two stacked resonators.

Considering the Zirconia properties and a metal housing conductivity of 50 S/m, a Q factor of 2100 can be obtained. Moreover, we have a very good spurious free range of 5GHz. The dimensions of the initial configuration used for this study are as follow:

1/ dielectric resonator:

- radius = 2,1mm
- height = 10 mm

2/ cavity:

- side (axis x and y) = 20 mm
- height = 18mm

2 Reasons of our choice

The study of the $TE_{01\delta}$ and TM_{010} modes gives us a good idea of which one will be more efficient to realize the wide band filter we want to achieve. Indeed, the different configurations for the $TE_{01\delta}$ mode shows that it is very difficult to obtain a strong coupling between two cavities and also to have a good spurious free range. Then, the electromagnetic fields are not easy to guide from one cavity to another, specially the electric field. That is why we decide to move to the TM_{010} mode. Furthermore, the orientation of the electric field makes us sure that it will be more easier to guide this mode between two resonators. Therefore, we study the way to obtain strong coupling with this mode.

As in the previous part, we will optimize an Input/Output and inter-resonator couplings dedicated to this TM_{010} mode.

3 Designs for Input/output coupling

To end up with a strong coupling, we decide to put a coaxial probe inside the dielectric resonator to have a maximum interaction between these two elements (Figure 95). Moreover, we can control the coupling value thanks to the length of the coaxial probe inside the

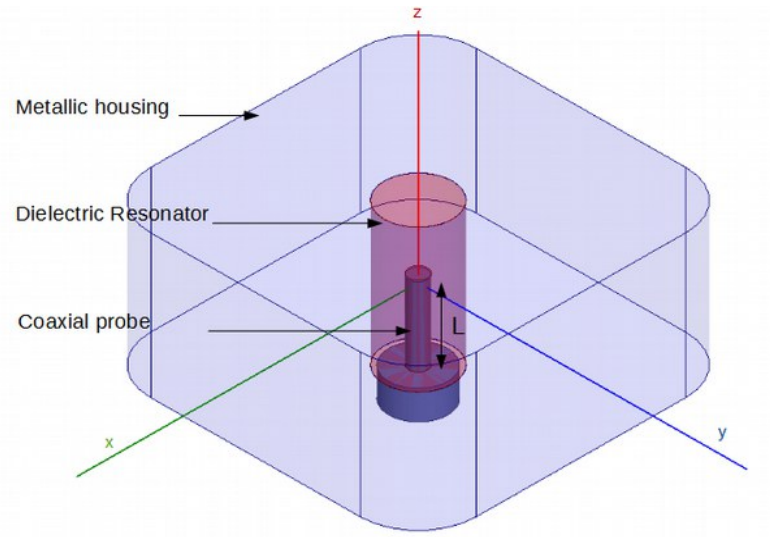


Figure 95: Input/Output coupling system

resonator. Studying the electromagnetic field inside this structure, we see that we can create a very strong interaction between the dielectric resonator and the coaxial probe as shown in the Figure 96.

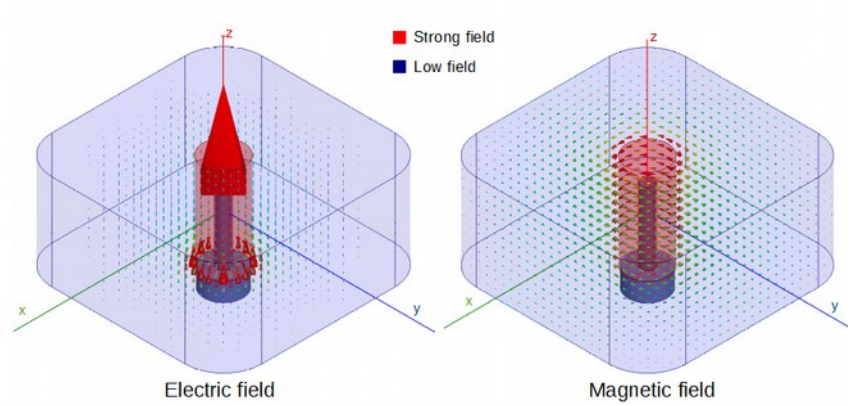


Figure 96: Electric and magnetic fields - interaction between the dielectric resonator and the coaxial probe

Moreover, the probe will be used like a support system to maintain the dielectric element in the cavity. A Teflon support is therefore not needed for the TM_{010} dielectric resonators.

The Figure 97 presents the variation of the Qe-factor as a function of the length of the coaxial probe inside the dielectric resonator. We observe that for a length greater than 1.5mm we have a very high Input/Output coupling. A very low Qe-factor around 3.5 can be obtained here. As a reminder, for a 4-pole filter, we would need a Qe-factor around 10. We thus have a coupling system fully satisfactory for our purpose.

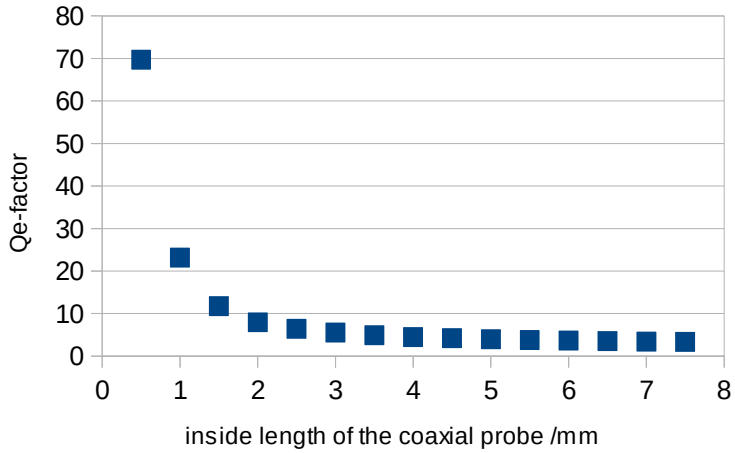


Figure 97: Evolution of the Qe-factor depending of the length of the coaxial probe

4 Designs for coupling between resonators

In order to get a maximum coupling between two stacked DRs, we propose the configuration shown in Figure 98. A dielectric element between the two dielectric resonators is placed in Figure 98.

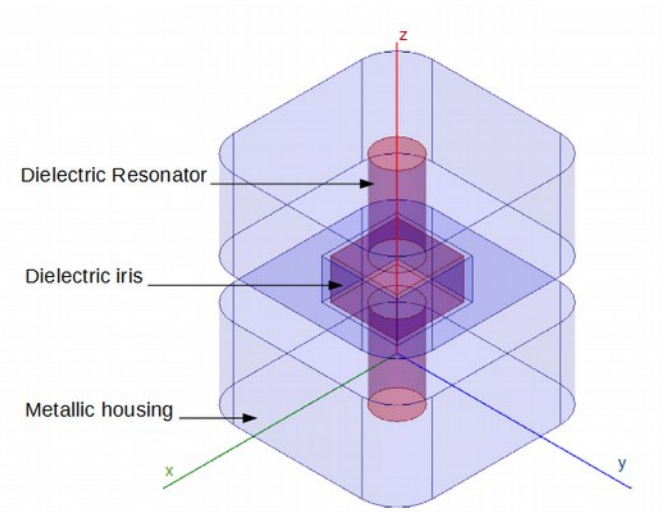


Figure 98: dielectric element for strong coupling and connecting two resonators

We have chosen a cubic dielectric element and this part connects both dielectric resonators together, Figure 98. It is an interesting solution because all these dielectric elements are made with the same material within one single part. At the level of the iris, we insert a gap between the dielectric material and the metallic cavity to take in account the manufacturing tolerances for the ceramic part and also for the metallic housing as we can see in the Figure 98.

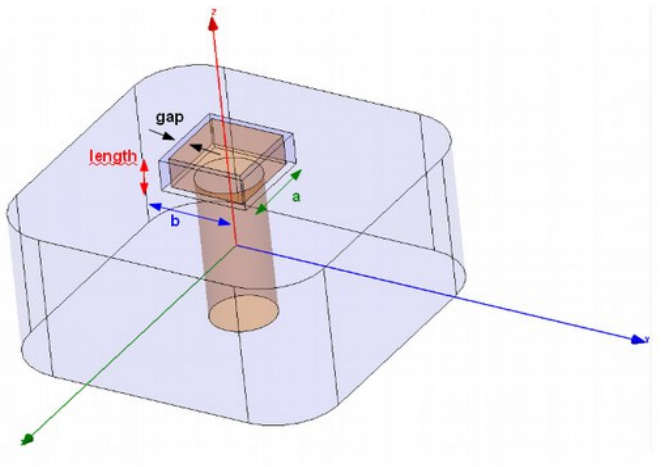


Figure 99: configuration to have a strong K_{12} coupling – TM_{010} mode

A study showing the variation of the K_{12} coupling as a function of the different dimensions of the dielectric element (see Figure 99) is provided in the next section.

1 Variation of the length of dielectric element (axis z)

To have a better idea of the behavior of the dielectric part in the iris, we will see the impact of its length on the K_{12} coupling coefficient. We consider this initial set of dimensions:

- axis x: a = 9 mm
- axis y: b = 9 mm
- gap dielectric element/cavity = 0.7 mm

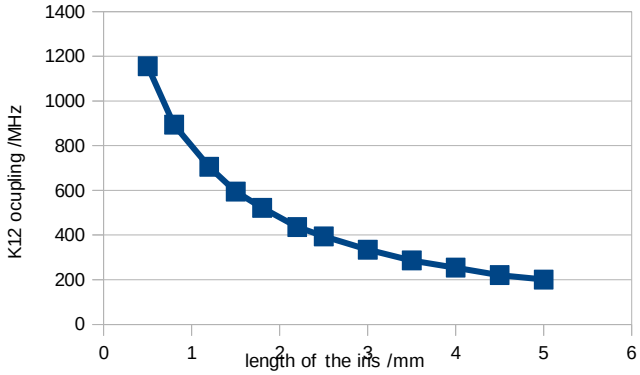


Figure 100: K_{12} coupling versus the length of the dielectric coupling element

We deduce that when the length of the element increases, the K_{12} coupling decreases (Figure 100). For a length of 0.5mm, we expect a coupling of 1150 MHz which is more than we want and therefore a very good way to have a strong coupling between cavities based with DRs.

8.1.2 Variation of the dimensions of the dielectric element (axis x and y)

After the length, we study now the evolution of the coupling as a function of the dimensions a and b following the axis x and y. In order to arbitrary keep a square cross-section, we do the simulation with the same value for a and b.

Dimensions of the dielectric part:

- axis z: length = 2.2 mm
- gap dielectric element/cavity = 0.7 mm
- a = b

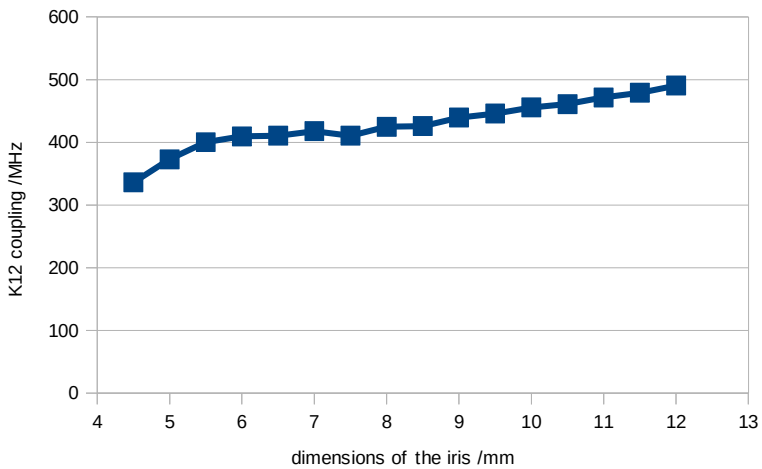


Figure 101: K_{12} coupling versus the dimensions a and b of the dielectric coupling element

The K_{12} coupling (Figure 101) increases with the dimensions but it is less sensitive. Indeed, the K_{12} coupling moves from 350 to 500 MHz.

2 Variation of the gap between the dielectric element and the cavity

The last parameter is studied in order to take into account the gap between the dielectric element and the metal cavity. To do this study, we set the others dimensions of the dielectric part as follow:

- axis x: a = 6 mm
- axis y: b = 6 mm
- axis z: length = 2.2mm

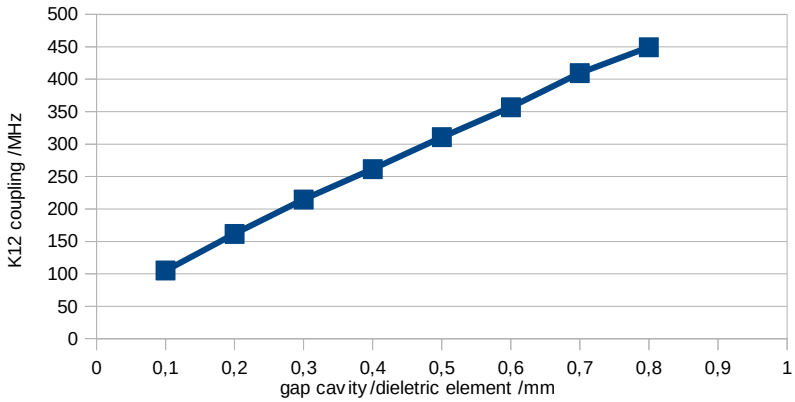


Figure 102: K_{12} coupling versus the gap metallic housing/dielectric element

The gap between the dielectric and the metallic parts appears to be a very sensitive parameter since a modification of just 100 µm induces a great change in the k12 coupling parameter (Figure 102). Considering the SLA manufacturing tolerances (±100µm typically) and the inaccuracy of the placement of the dielectric part in the housing, we therefore expect a limited control of this. Thus, we expect that it will be difficult to obtain the right value of coupling for this element. It is therefore strongly advised to find a tuning way for this coupling element.
Considering that a cylindrical connecting element instead of a cubic one could be used as well, we have decided to keep using the cubic shape because it is more easy to manufacture by the stereolithography process (self supported element that does not requires any supporting parts when the part will be made horizontally). Indeed, the layers composing this part will have the same length so they have a better stability. However, in the future, it may be necessary to

study a circular shape if we see better properties or to have a same general cylindrical form for the whole dielectric part.

5 Conclusion

We have studied the TM_{010} mode to obtain the required strong Input/Output couplings and between two close resonators.

On the first hand, we design a solution to achieve efficiently a strong coupling. The proposed solution consists in having a forceful interaction between the dielectric element and a coaxial probe. That is why we decide to study the impact of a hole inside the dielectric part where it will be possible to put a standard coaxial probe. The main advantage of this configuration is the proximity of the two elements which will provide a strong electromagnetic interaction between them. Furthermore, it is possible to tune the value of the Input/Output coupling by adjusting the length of the coaxial probe inside the dielectric part. If the length is shorter, the coupling decreases because the interaction between the both elements are less important and vice versa.

On the other hand, we have studied how it should be possible to achieve a strong coupling between two dielectric resonators. The first idea was to put between them a dielectric part able to guide more efficiently the electric field. Thus, we connected two resonators by way of a cubic dielectric element whose the dimensions could be modified to tune the coupling at the right value. This solution appears extremely efficient because, even if we succeeded in reaching the target 400MHz k12 parameter, we were also able to get a coupling bigger than 1000 MHz.

Conclusion

The stereolithography process is now an understood additive manufacturing technology, available and capable to make microwave components made of ceramic. Thanks to its freedom of fabrication, this latter is initially chosen among others as the technology used for the thesis first prototypes. For our work, we characterized three dielectric materials: Zirconia, Alumina and BMT. With the obtained results, we were able to set up realistic simulations for our project filter working around 4 GHz.

As a reminder, we did this study to have the possibility to achieve a wideband filter at 4 GHz with a bandwidth of 10%. To obtain these characteristics, we need strong coupling in Input and Output but also between the different resonators composing our filter. To this end, we decided to study different structures to know which one will more adapted for our application.

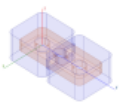
Configuration	Maximal K12 coupling	Observations
	80 MHz	Spurious mode close to our working frequency, monolithic element
	280 MHz	Spurious modes close to our working frequency, monolithic element
	Small coupling	Spurious mode close to our working frequency, monolithic element
	270 MHz	Spurious modes close to our working frequency, monolithic element

Figure 103: Summary of the different configurations using TE01δ mode dielectric resonators

Firstly, we oriented our work to use the $TE_{01\delta}$ mode because it has interesting properties like high Q-factor, compactness and compact spurious free range with the objective to achieve wide bandwidth as the ones achievable with combline filters. Two kinds of study were realized, the first one for the Input and Output coupling and the second one for the inter-resonator coupling. Different configurations were designed to achieve the strong Input/Output coupling represented by the Qe-factor. The target Qe-factor is 10 for our 10% bandwidth bandpass filter. Among the studied configurations, only one achieved this requirement using a bended coaxial probe.

On the inter-resonator coupling side, we presented several ideas as presented in Figure 103 to try to couple efficiently two resonators working on the $TE_{01\delta}$ mode. We encountered different problems. The main one is the difficulty to guide the electric field inside the dielectric material. In fact, the behavior of the $TE_{01\delta}$ mode is not the best one to realize this. Then, a solution using a dielectric part inside the iris linking two cavities was explored but it ended up exciting spurious modes close to our working frequency. Following this assessment, we have decided to move to another mode and we choose the TM_{010} mode for the main reason that the electric field should be more easy to lead inside the dielectric part connecting two DRs. In this way, we did a new study for the Input/Output coupling and the found solution consists in putting a coaxial probe inside the dielectric resonator. As a consequence, we designed a hole in this dielectric part and we can tune the Input/Output coupling by adjusting the length of the coaxial probe.

This first part achieved, we moved to the study of the inter-resonator coupling. A simple idea was to put a cubic dielectric element between two resonators made of the same material. The tuning of the coupling values is possible by modifying the dimensions of this connecting element. This configuration gave us very good result. We were able to have more than 1000MHz of bandwidth, so a coupling sufficient for our application (we need 400MHz only). Thus, we should be able to design a filter with a more important bandwidth if needed. Using Zirconia material for the manufacturing of the next first prototypes, initial simulations show that we can obtain a Q-factor better than 1200. If we use the BMT material in a second time, we can expect much thanks to its lower loss tangent. Moreover, the filter design we are targeting will be a monolithic structure so we may expect to reduce the inaccuracy due to the positioning of this one, contrary to some dielectric filter where a single DR is placed in each cavity. However, our first trial show that the proposed coupling mechanism may be very sensitive to the proximity of the metallic housing and that a great attention should be paid here.

Bibliography

[1] A. H. Khalil *et al*., "3-D pyramidal and collective Ku band pass filters made in alumina by ceramic stereolithography," *Microwave Symposium Digest (MTT), 2011 IEEE MTT-S International*, Baltimore, MD, 2011, pp. 1-1.

[2] R.J. Cameron, C.M. Kudsia, R.R. Mansour. 2007. Microwave filters for communication systems. John Wiley & sons, INC., PUBLICATION. Design and physical realization of the coupled resonator filters; p.507-509.

[3] Kobayashi, Y.; Minegishi, M., "Precise Design of a Bandpass Filter Using High-Q Dielectric Ring Resonators," in *Microwave Theory and Techniques, IEEE Transactions on,* vol.35, no.12, pp.1156-1160, Dec 1987

[4] Harrison, W.H., "A Miniature High-Q Bandpass Filter Employing Dielectric Resonators," in *Microwave Theory and Techniques, IEEE Transactions on,* vol.16, no.4, pp.210-218, Apr 1968

[5] Guillon, P.; Garault, Y., "Coupling Between : A Microstrip Transmission Line and a Dielectric Resonator and Between Two Adjacent Dielectric Resonators for Application to Bandpass Filter," in *Microwave Symposium, 1976 IEEE-MTT-S International* , vol., no., pp.200-202, 14-16 June 1976

[6] Uchida, H.; Nakayama, J.; Ikeda, H.; Yshikawa, Y.; Imai, Y.; Yoneda, N.; Miyazaki, M., "Dielectric Resonator Elliptic-Function Band Rejection Filter with External Coupling Waveguide," in *Microwave Conference, 2003 33rd European* , vol., no., pp.183-185, Oct. 2003

[7] Kaneki, T.; Konishi, K., "External Q of probe-coupled dielectric resonator," in *Electronics Letters* , vol.22, no.11, pp.606-607, May 22 1986

[8] K. V. Srivastava, V. V. Mishra and A. Biswas, "A modified ring dielectric resonator with improved mode separation in MIC environment," *Microwave Conference, 2004. 34th European*, Amsterdam, The Netherlands, 2004, pp. 609-612.

[9] Feng He and Qing-xin Chu, "Mode separation in ring dielectric resonator with cavity environment," *Microwave Conference Proceedings, 2005. APMC 2005. Asia-Pacific Conference Proceedings*, 2005, pp. 4 pp.-.

[10] L. Carpentier, N. Delhote, S. Verdeyme, L. Estagerie, H. Leblond and D. Pacaud, "Compact Ku band filter based on BMT dielectric resonators made in a single part using 3D ceramic stereolithography process," *Microwave Symposium Digest (MTT), 2012 IEEE MTT-S International*, Montreal, QC, Canada, 2012, pp. 1-3.

[11] Kobayashi, Y.; Yoshida, S., "Bandpass Filters Using TM_{010} Dielectric Rod Resonators," in *Microwave Symposium Digest, 1978 IEEE-MTT-S International* , vol., no., pp.233-235, 27-29 June 1978

CHAPTER III

First Generation of filters

Introduction

The previous study of the different achievable coupling values lets us move to the design step of the required filter. We can now achieve a strong coupling in its Input and Output and also between two resonators, making us capable to achieve the wide bandpass filter we are searching for. In this part, we present a 2-pole filter as a first step and then a 4-pole filter.
Their design as well as their fabrication and S parameters measurements are presented in the next paragraphs. The first part of this chapter will firstly give more details on the selected manufacturing technology in order to integrate its constraints for the filter designing step.

I. Manufacturing process

The design obtained in the previous chapter appear to be rather complex to build if we want to make it in a simple dielectric part. Since we want to avoid any assembling of single ceramic parts, additive manufacturing appears to be a good choice as seen in Chapter 1.
The principle of the 3D stereolithography process used in this chapter resides in the polymerization of a photosensitive liquid monomer in a layer by layer process. For this purpose, an ultraviolet laser beam scanning path is driven by computer to fabricate a 3D part. The first step is the conception of the element to manufacture with a CAD software, a 3D CAD file (.iges or .step format) being obtained. The second step is to convert this file in a special format, the stl format. The characteristic of this format is to transform all the faces of the object to an assembly of elementary triangles. The last one is to cut this 3D part in fine layers at a desired thickness.
According to the material and the required precision, the thicknesses ranges from 10 to 100µm. The layers will be create one after another to obtain the final 3D element. The detailed steps of the manufacturing are presented in the thesis works of N. Delhote [1] and A. Khalil [2].

1 Technology used in the CTTC

The first step is to prepare the ceramic paste used for the chosen technology (Figure 104).
Then, it is to sieve more and more thinly the ceramic powder to keep only the smaller particles. This powder presents a flawlessness better than 99%. The dimensions and the geometry of these particles can change the properties of the material and consequently the

quality of the final structure. Usually, we try to have the diameter of the particles between one and few micrometers to have a satisfactory compromise.

If some thin particles still present aggregates we have to eliminate them. With a ball grinding step, the powder is the mixed with ethanol and a scattered product. This latter does not change the properties of them but modifies the interaction forces between the particles.

After that, this mixing is grounded by ceramic marbles during several minutes to several hours as a function of the used powder. Then, we warm up to eliminate the ethanol. We have now a very thin ceramic powder.

At this moment, we realize the ceramic paste by mixing different elements together:

- Photosensitive resin: composed of a monomer sensitive to ultraviolet light. The energy brought by a laser beam for example triggers the polymerization of the resin.
- Photo initiator: it absorbs the ultraviolet ray and helps the resin to have enough energy to trigger the polymerization.
- Binder: this role is to bring a strong cohesion between the powder particle and the mechanical strength of the piece before the firing step, called the green part. For the stereolithography process this is realized by the monomer.
- Plasticizer: thanks to this element, the green part is flexible enough to make the part under fabrication capable to bear the paste spreading by a blade.
- Solvent: to maintain the paste sufficiently liquid
- Wetting agent: it increases the bonding between the powder and the binder.

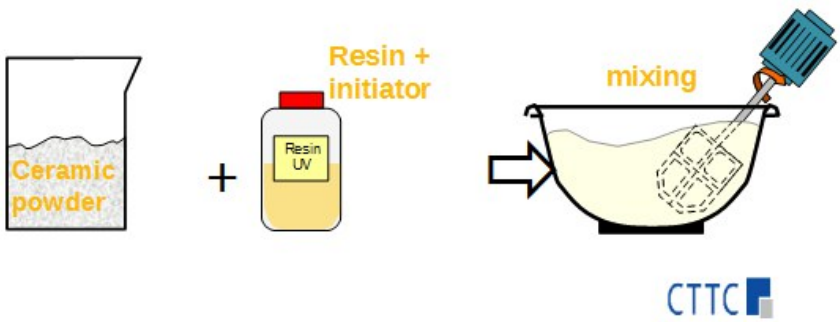


Figure 104: paste making for stereolithography process (cttc.fr)

The obtained paste goes through different rollers to break a last time the agglomeration of particles. Then, the paste need some rest during few hours to eliminate the gas trapped inside. Now, we can use the paste.

The used paste having a high viscosity, a special scraper system has been specifically developed and patented.

2 Manufacturing

An ultraviolet argon laser beam (λ=351nm) is used to polymerize the paste. In order to define the right surface to be scanned, the laser beam is reflected on a galvanometric mirror driven by computer. It is essential to spread a very uniform layer with no bubbles trapped inside a layer.
The paste system is composed of a tank and a scraper. It was developed and patented by the french society Optoform in 1999, which has been bought by 3D Systems©.

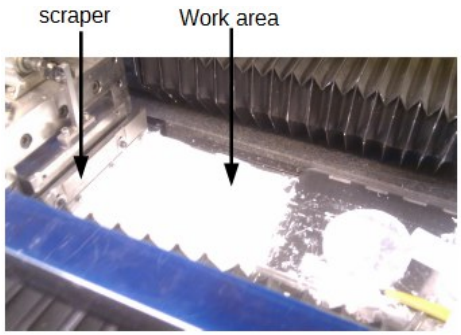


Figure 105: stereolithography process - view of the scraper and the work area

In this way, the paste (Figure 105) is spread on the work area by the scraper to create a layer with the right thickness. The scraper has a special shape (a double-edged blade) compatible with the highly viscous paste.
The work area (25cm x 25cm) is also the support for the manufactured element and is fixed on a piston that controls the descent of the platform to create a next layer with the required thickness.
Once the paste is scraped, the laser beam lights the paste to create a layer of the 3D part under fabrication (Figure 106). The typical diameter of this beam is 30µm. After that, the piston descends of one thickness, and another layer of paste layer is spread over the previous one. These steps are repeated until the last layer. The final object can reach a height of 25 cm. The typical process time is one hour for 100 layers.

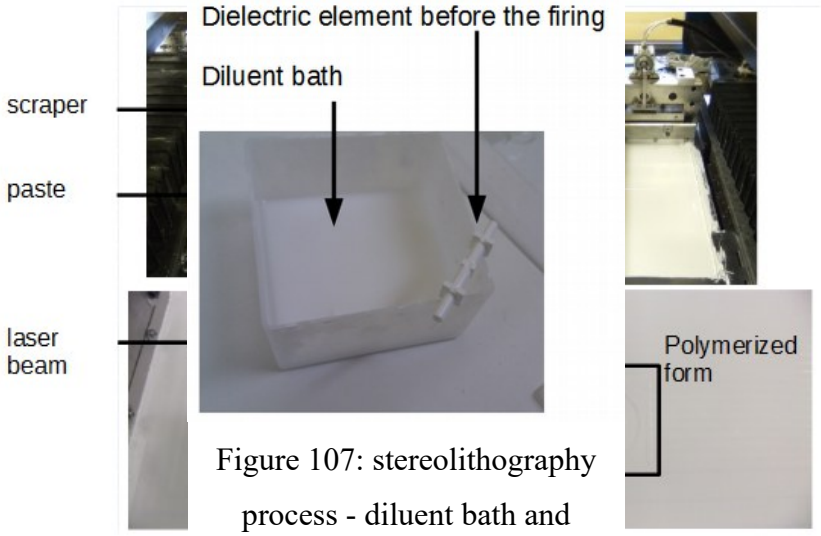


Figure 107: stereolithography process - diluent bath and dielectric part before firing

Figure 106: st ıg of the paste

After this step, the polymerized part is swallowed in the non-polymerized paste. We have to retrieve our part and we clean it to eliminate the paste in excess with a brush and different diluent baths.

The cleaned piece is called the green part (Figure 107). Different firing cycles are realized to obtain the final dimensions and properties. The Figure 108 summarizes the different steps of the stereolithography process.

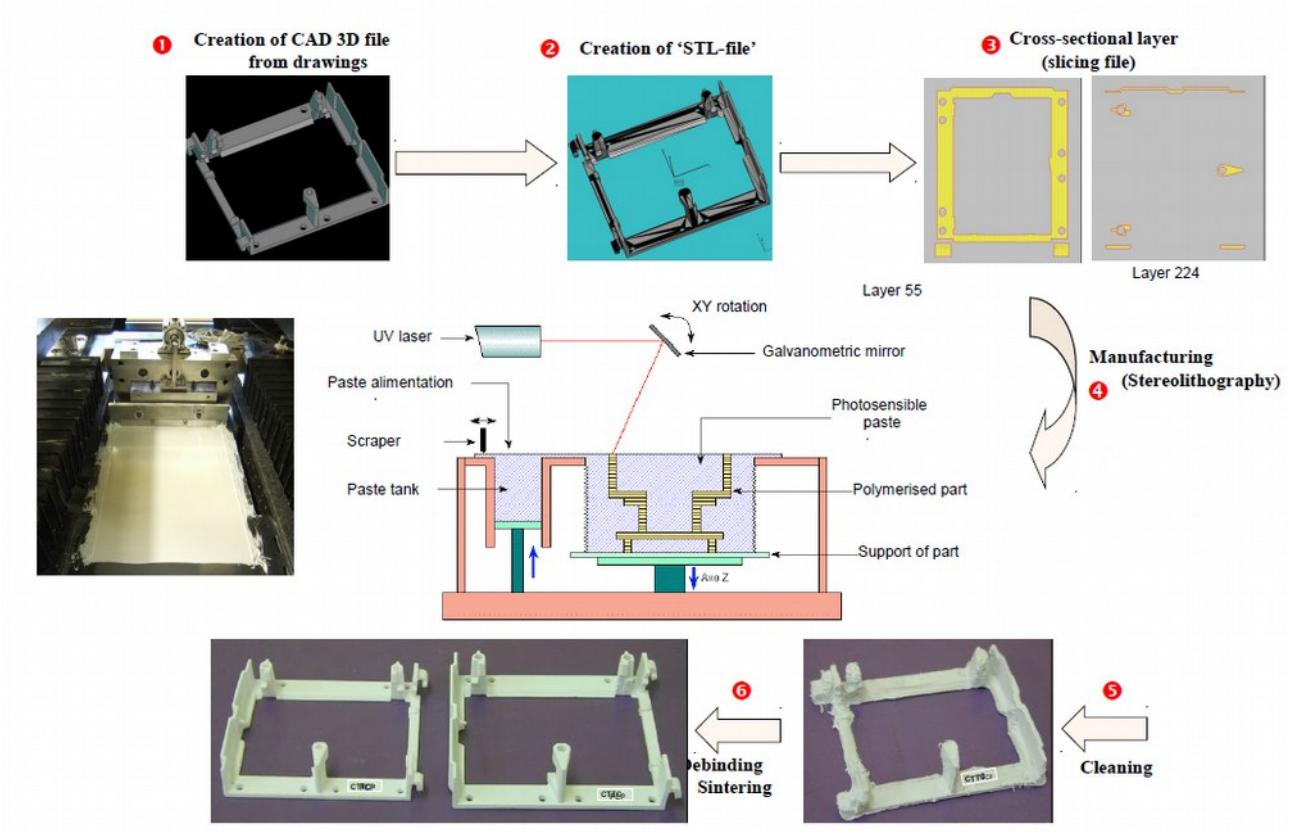


Figure 108: the different steps of the stereolithography process

3 Mechanical support for part under fabrication

The paste has to present an optimized viscosity to be correctly and uniformly spread on the work area by the scraper. It must have a constant thickness and homogenous aspect. The concentration of each element that composed the paste is very important and can be modified to reach these characteristics. This high viscosity permit to have a layer of non-polymerized paste that supports several other layers without to subside itself and to deform their stacking. Besides these properties and to avoid some deformations due to the scraper movement, it can be necessary to add some dielectric supports for a given structure. These "extra" elements are polymerized and they are not connected to the principal dielectric piece.

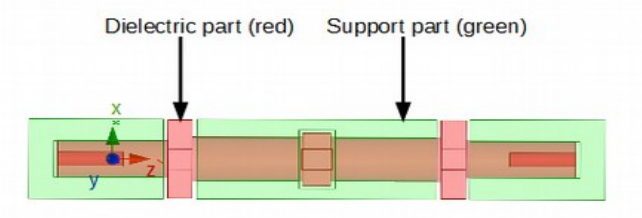


Figure 109: Example of a structure with support

In the Figure 109, we see an example of this extra elements made during the manufacturing process. A gap between our dielectric piece and the supporting elements is necessary to avoid contact between them (Figure 110). However, we can notice the gap can be different as a function of the manufacturing element. For example in the Figure 110, the gap 2 depends on the thickness of the paste layer when the gap 1 is related to the laser beam. At this end, the unconnected parts can be separated during the cleaning step.

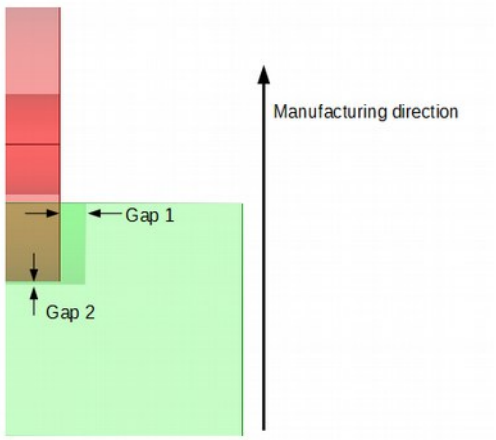


Figure 110: Example of gaps between
the support and the element

4 Shrinkage

First, we notice that for a strong concentration of ceramic particles in the paste, a high level of energy is needed to trigger the polymerization. Then, the other elements that composed the paste have an impact of the level of UV insolation. The definition of the dielectric part is therefore strongly dependent on the concentration of these elements in the paste. Moreover, when the ratio of ceramic particles increases, the definition decreases due to a light scattering

effect. However, a high concentration of the ceramic particles is essential to limit the strain of our structure during the manufacturing process.

Other mechanic constraints are brought by the different firing steps.

The first firing step is realized to eliminate the binders initially present in the paste. The polymers are also removed with this step. During several hours, the dielectric parts are put in an oven that heats up to 600°C. During this step, the different organic elements migrate to the outside of the piece. It is a critical step because we can observe important mishaping, and sometimes even some cracks if the temperature raises to quickly. Usually, the temperature raise is around 0.1°C per minute.

The second step can then be done. Now the oven goes up to 1700°C (5°C per minute). This phase is called sintering. The element obtains its final dimensions, properties, and resistance. The density of our dielectric part is usually better than 97%.

During these two firing steps, the ceramic element shrinks and increases its density. The shrinking percentage is connected to the particle concentration in the paste.

Currently, the process is well known and we are able to predict the shrinking for different paste recipes. In this way, we oversize the element before launching the manufacturing process. Then, we will have the right dimensions of our element after the firing steps. However, this phenomenon may not be isotropic for some complex designs, and at least two fabrications can be needed to come closer to the required dimensions.

5 Conclusion

The knowledge of the stereolithography process is very important to know what exactly to do to have the right element that is conform to the initial design. Among different manufacturing parameters, the composition of the paste has a direct impact on the manufacturing tolerances and the dielectric part final properties (permittivity, mechanical strength, etc). Then, the ratio of ceramic particles has an important function because it directly determines the properties of the final element as its density, dimensions (shrinkage), etc. Thus, the study of the paste is essential to obtain our object with the right behavior.

High ceramic particles concentrations lead to higher density for the sintered part and a high robustness of the piece but at the price of a lower resolution.

The current value of the manufacturing tolerances is about 50µm to 100µm in the CTTC in Limoges, and it is satisfactory with our application. Moreover, the steps take into account the fragility of the polymerized paste to avoid cracks and split during all the process.

The stereolithography is a pertinent choice to realize complex and original design for dielectric parts, and will be therefore firstly used for this chapter initial prototypes.

II. 2-pole filter

1 Characteristics

A simple 2-pole filter is firstly design to be made out of Zirconia with the stereolithography process that has previously been described.
The central frequency of this filter is arbitrary fixed at 3.3 GHz and the bandwidth is fixed at 14 % (500 MHz). We use Zirconia material for the dielectric part and the housing around it will be made out of machined copper. The theoretical matrix is shown in the Figure 111.

$$M_{/MHz} = \begin{vmatrix} 0 & 612 & 0 & 0 \\ 612 & 0 & 580 & 0 \\ 0 & 580 & 0 & 612 \\ 0 & 0 & 612 & 0 \end{vmatrix}$$

Figure 111: theoretical matrix of the 2-pole filter - f_0=3.3GHz - bandwidth 14%

Coupling values are therefore high but the previous chapter has shown that the selected topology, e.g. stacked TM_{010} DRs, can make them reachable. The theoretical response of this filter is presented in the Figure 112.

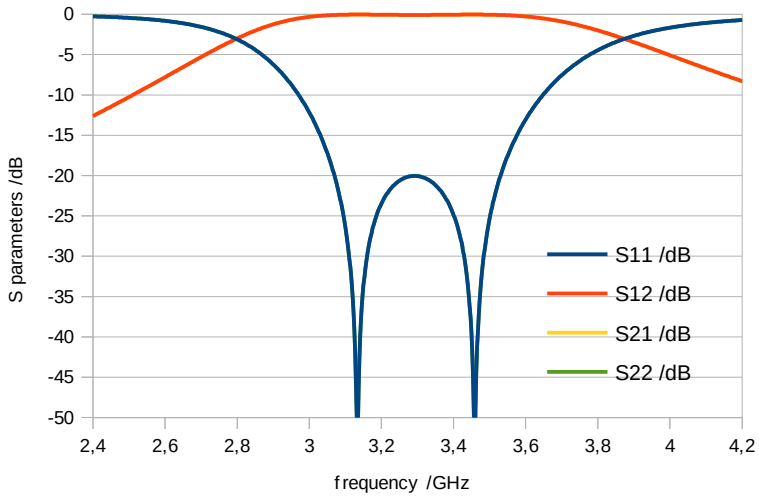


Figure 112: theoretical response of the 2-pole filter - f0=3.3GHz - bandwidth 14%

2 Simulation

We use HFSS© to perform our design. To realize a 2-pole filter, we have to couple two dielectric resonators together. In this way, we use our previous studies on the Input/Output and inter-resonators couplings. The resulting filter is shown in Figure 113.

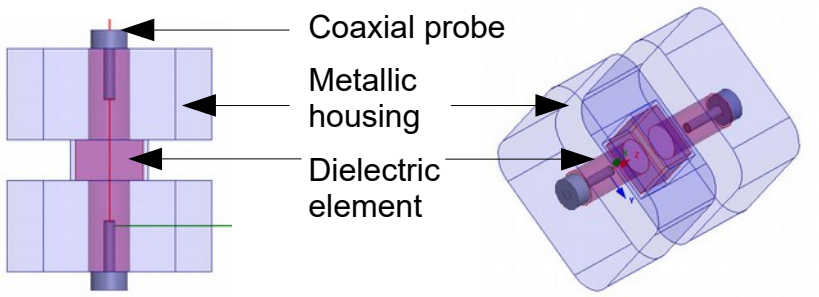


Figure 113: design on HFSS of the 2-pole filter

We recognize the coupling system for Input/Output with the coaxial probes inside the dielectric resonators. Then, a dielectric element connects both resonators inside an iris. The three dielectric elements (2 DR and a connecting part) will be made in a single part and will be placed in a metal housing. The design and optimization procedure presented in chapter II is applied to get the optimized dimensions.

To take in account the manufacturing tolerances, we chose to add to this structure some tuning screws (Figure 114) to obtain the required response in measurement.

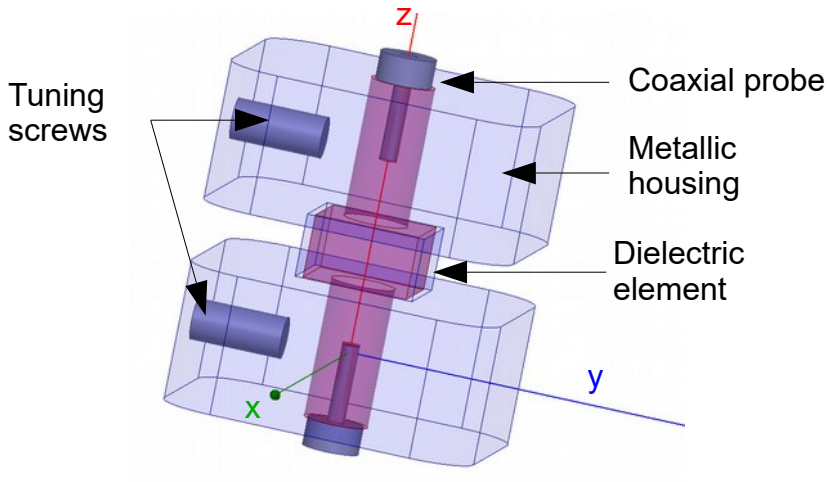


Figure 114: design of the 2-pole filter with tuning screws

We saw that when the tuning screws are close to the dielectric resonators, the resonance frequency of each cavity decreases. The diameter of the screws is 3mm. The dimensions of the DR are set up to be easily tuned by such screws even if simulations shows their moderate impact of the resonance frequency (e.g. a change of 150MHz when the screws are very close to the DR).

We achieve the response depicted in the Figure 115 for the structure taking into account these screws. The dielectric element length is 24,5 mm and the length of each resonator is 10mm while the diameters are 5mm for the first one and 4.8mm for the second. The iris element dimensions are $4.5\times7.5\times7.5mm^3$.

The metallic housing measures $38.5\times46.5\times46.5mm^3$.

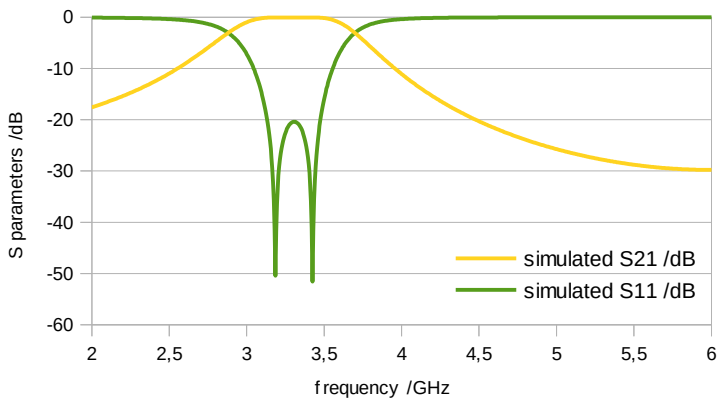


Figure 115: full wave response of the 2-pole filter

We have a 500MHz bandwidth at 3.3 GHz with a return-loss better than 20dB and a spurious free range up to 6GHz.

3 Manufacturing dispersion on permittivity

During the stereolithography process, it may be possible that the permittivity is not exactly what we obtained during the material characterization step (see chapter II). We decide to realize some complementary studies by simulating the response of the 2-pole filter for different permittivities around the initial value ($\varepsilon_r = 33$).

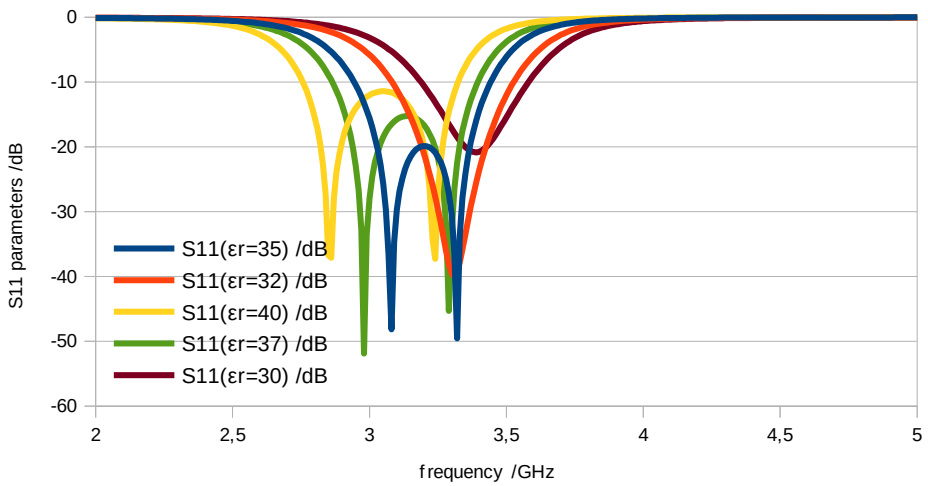


Figure 116: study of the permittivity value on the 2-pole filter response - S11 parameters

Figure 116 and Figure 117 summarize the S_{11} and S_{21} parameters of the 2 pole filter for the Zirconia permittivity ranging from 32 to 40. It may be possible during the process that pollutants can modify the properties of the dielectric material or that a lower density (and therefore ε_r) can be obtained. The structure of the paste can also disrupt the right spread and some air bubbles can appear between the layers, changing the part final density. In this way, we decide to study the impact of the permittivity of the response of our filter. For a small dispersion of the permittivity ($\varepsilon_r = 32$ and 35), the frequency shift is less than 100MHz and the bandwidth narrowing is around 30MHz. We notice for a permittivity higher than the initial value, the frequency goes down and the coupling between the resonators increases. However, for the lower permittivity we observe the opposite effect as expected.

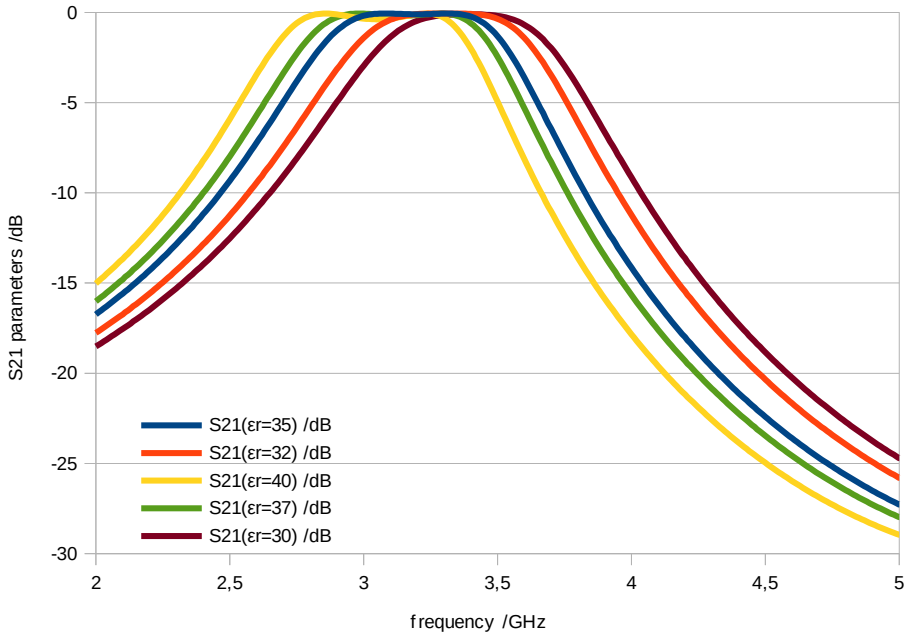


Figure 117: study of the permittivity value on the 2-pole filter response - S21 parameters

4 Manufacturing

1 support for the manufacturing and dielectric manufacturing

The dielectric element to manufacture is a compact but bulky part so we have to take care of the bearing of each layer during the fabrication process. In this case, we have to support both resonators because they are not touching the work surface contrary to the central part of the whole support.

We will have additional elements that will be polymerized at the same time as our dielectric piece. In this way, we decrease the risk of the deformation of the suspended resonators but we must take care that supporting elements are not touching the DRs.

The support is shown in Figure 118.

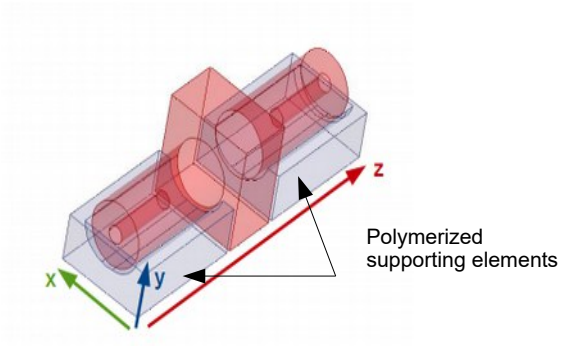


Figure 118: dielectric part with the support made during the manufacturing

A gap is necessary between the support and the main element to avoid the polymerization of these two parts together. Due to the manufacturing process, the gap is not the same for each direction:

_for x axis: 500µm

_for y axis: 75µm

_for z axis: 500µm

Then, taking into account the shrinkage due to the firing of our element, we oversize the part provided by the simulator by about 30% before its actual fabrication by stereolithography.

The manufactured part is shown in Figure 119. We recognize the different elements that constitute the 2-pole filter. The dimensions of the filter are :

_total length: 23,20mm

_iris length: 4.20mm

_diameter of the resonators: 4.36mm

_side of the iris: 7.32×7.30mm²



Figure 119: dielectric part of the 2-pole filter

2 housing

The housing is composed of two cavities and an iris. It is split in two parts (body and cover) to insert the dielectric element inside (Figure 120). In relation with our machine shop, we modify some shapes due to the drawing rules. Indeed, the used tool is a drill bit, consequently the corners of the cavities have to be circular to be machined. Then, we put a small rim between the two mechanical parts to increase the metallic contact and to insure that we will not have field leakage out of the filter.

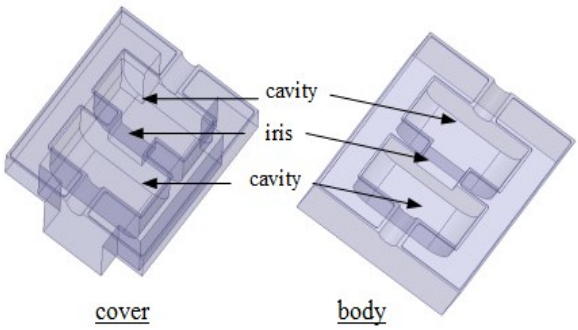


Figure 120: housing of the 2-pole filter

This element is machined by the Xlim machine shop and the material used is copper. Then, different holes are drilled to assemble the parts together and also to maintain the coaxial probes and to insert the tuning screws. The mechanical part is presented in the Figure 121, we recognize the different elements of this housing: the two cavities, the iris, the holes for the mounting screws, the holes for the tuning screw and for the connectors.

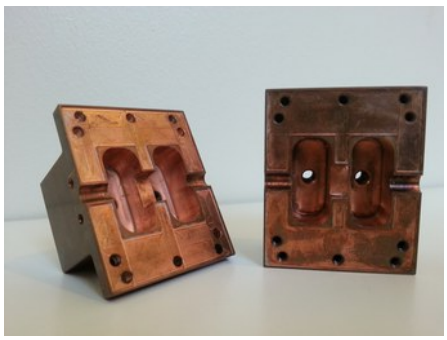


Figure 121: copper housing for the 2-pole filter

The assembled filter is shown in Figure 122, the different tuning and fixing screws are visible on this picture.



Figure 122: metallic housing for the 2-pole filter

5 Measurements

The different elements of the filter are put together (Figure 123) before we realize the measurement. The tuning screws are not shown.

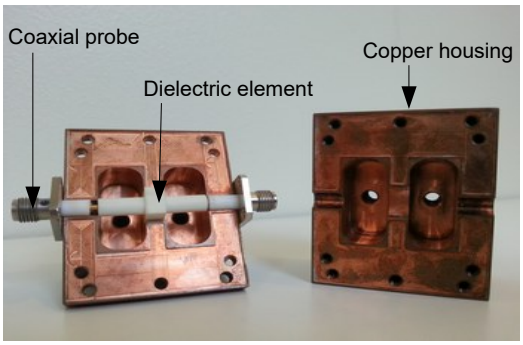


Figure 123: copper housing with the dielectric element between the Input/Output connectors

After some tuning of the screws as well as of the length of the coaxial probes, we present in Figure 124 the best response we have obtained.

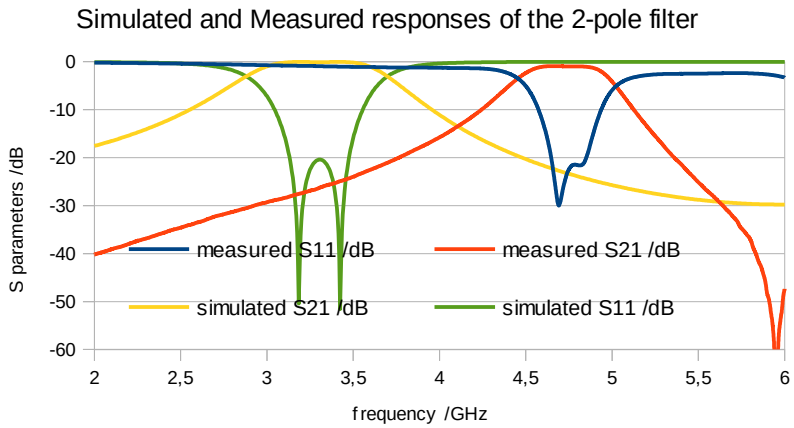


Figure 124: simulated and measured response of the 2-pole filter

The first thing we can notice is the difference between the simulated and measured central frequency. Our filter is centered at 4.75 GHz instead of 3.3 GHz. Several points can explain this value: a post fabrication checking shows we have smaller dimensions for the dielectric element than expected, so it resonates at higher frequencies. We also suspect the permittivity of the material to be lower than predicted. We think the internal structure has some defects, maybe the element contains air bubbles and in this way decrease the overall permittivity. Then, the coupling value has also an impact in the central frequency of the filter

In the Table IX, we see the different characteristics of the measured filter compared to the simulated one.

	Measured filter	Simulated filter
Δf /MHz	350	500
F_0 /GHZ	4.75	3.5
Insertion losses /dB	1	0.2
S_{11} /dB	21	20
1st spurious mode /GHz	6.5	11

Table IX: characteristics of the 2-pole filter

The measured bandwidth is 350 MHz (7% of the central frequency) which is only 70% of the expected value. We have a good in-band return loss and insertion losses around 1 dB. Then, the first spurious mode is closer than expected.

The tuning screws are not very efficient for this configuration. The electromagnetic field is strongly concentrated inside the dielectric part so it is difficult to perturb it. Moreover, to change the value of the Input/Output coupling by changing the coaxial probe length, we need to open the cavity each time we have to tune it. A more practical solution is then suggested: we can fix the coaxial probe to the cavity, but letting some movement inside the dielectric element. We also see that the other feature provided by these probes, e.g. centering the dielectric part in the cavity, is not very efficient because we have some gaps on both sides between the dielectric element and the coaxial. Moreover, it is difficult to center the piece in the right location making the dielectric element not perfectly centered in the iris, this latter point contributing to a frequency different from the expected one.

III. 4 pole Tchebitchev filter

1 Characteristics

Done in parallel with the 2-pole filter, another bandpass filter is designed to work at 4 GHz with a bandwidth of 10% (400 MHz). A 4-pole Chebychev topology is used to achieve these specifications with dielectric part made of Zirconia. We will evaluate here two kinds of metal housing, the first is made of machined Aluminum and the other one is made of plastic receiving a metallization done by a silver painting. We see the theoretical matrix of the 4-pole topology in the Figure 125.

$$M=\begin{vmatrix} 0 & 414 & 0 & 0 & 0 & 0 \\ 414 & 0 & 364 & 0 & 0 & 0 \\ 0 & 364 & 0 & 280 & 0 & 0 \\ 0 & 0 & 280 & 0 & 364 & 0 \\ 0 & 0 & 0 & 364 & 0 & 414 \\ 0 & 0 & 0 & 0 & 414 & 0 \end{vmatrix}$$

Figure 125: theoretical matrix of the 4-pole filter - f_0=4GHz - bandwidth 10%

This filter has a higher order than the previous one with the required coupling values naturally smaller than with the previous 2-pole filter. We then expect to have no specific problem to reach the required couplings. The theoretical response based on the matrix in the Figure 126.

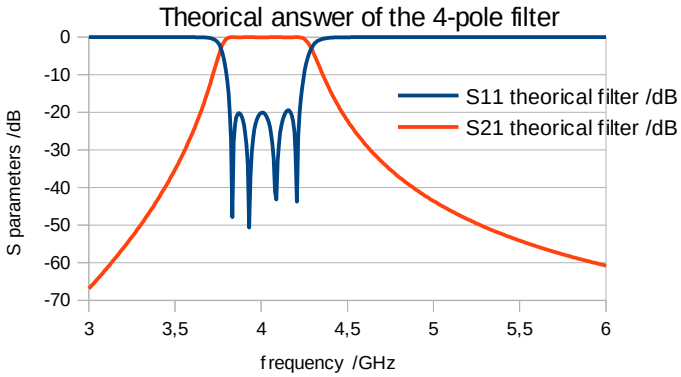


Figure 126: theoretical response of the 4-pole filter-f0 = 4GHz -bandwidth 14%

2 Simulation

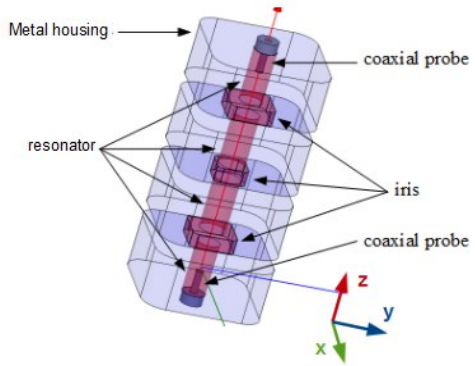


Figure 127: design on HFSS of the 4-pole filter

The design is performed with HFSS© using the same procedure we used for the 2-pole filter. We are now using four dielectric resonators connected together by three irises. The excitation is realized by coaxial probes inside the first and the fourth resonator, and the length of these probes are optimized to get the needed Input/Output values. The structure is shown in Figure 127. Then, we have changed the shape of the dielectric connecting elements between two adjacent resonators to have the possibility to tune the value of the coupling in the iris. The tuning is realized by a screw here again. The dielectric element has therefore a notch where the screw can be placed (Figure 128).

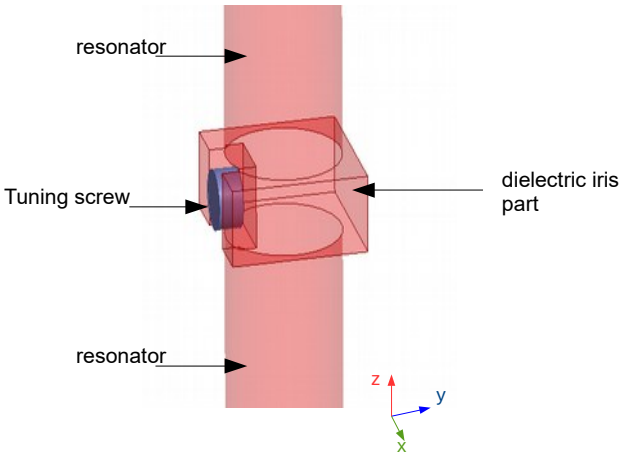


Figure 128: closer view of the tuning screw placed between two resonators

The diameter of the screw is 2mm and the hole inside the dielectric part is 2.2mm. The depth of the hole is 3mm, consequently the excursion of the screw is 3mm. As a first step, we primarily studied ceramic screw with Alumina material and we observe a maximum tuning range of 30 MHz for the coupling. Metallic screws can provide up to 190 MHz. Therefore, we will use metallic screws to tune the coupling in the iris thanks to their higher tuning range. During this study, we notice that the coupling decreases when the screws are deeper in the dielectric part. Thus, we have to overestimate the coupling between the resonators to have the possibility to tune the value.

Another set of screws are included to tune the central frequency of each resonator. The diameter of these screws is 3mm and they can be moved very close to the DR if needed (Figure 128).

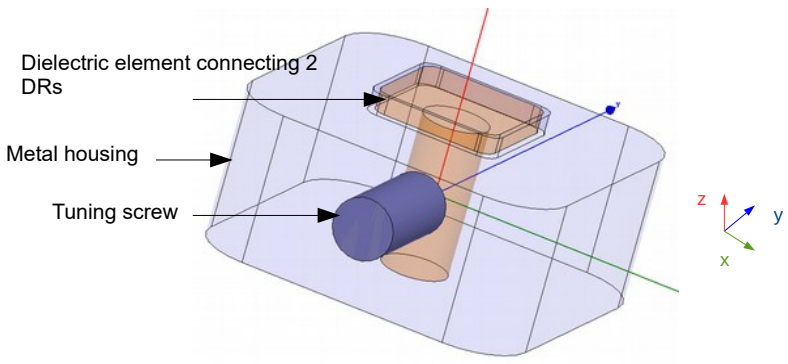


Figure 129: tuning screws for the central cavity of each cavity

The optimized response attained with HFSS© of the filter is presented in Figure 130 as well as the theoretical response linked to the matrix seen in Figure 125. Even if only three poles can be seen on the S11 and S22 parameters obtained by full wave simulation, the optimized filter

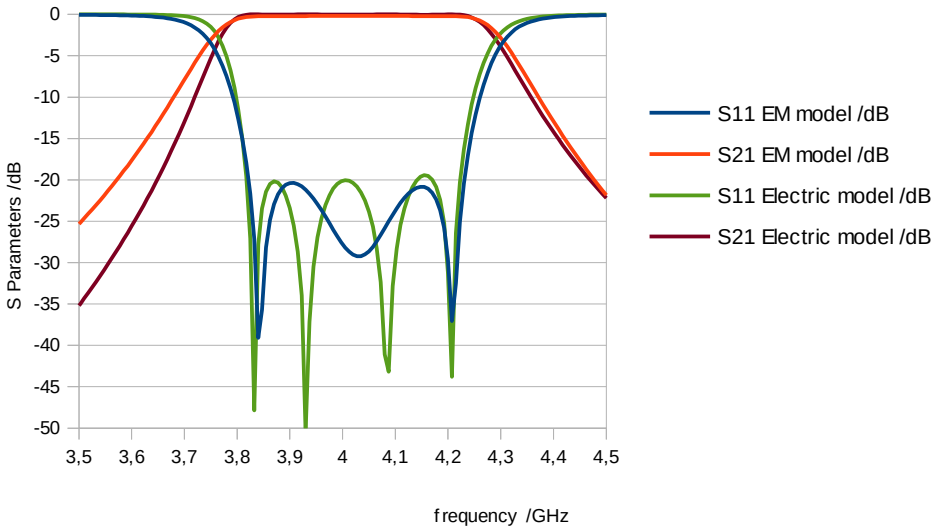


Figure 130: simulated response of the 4-pole filter and comparison with the electric model

is truly composed of four poles as seen in the extracted matrix (Figure 131).

In the Figure 131, we observe the coupling matrix extracted from a full wave simulation considering tuning screws. We can see that the coupling between the resonators are a bit stronger than we need (Figure 125) but the overall response is satisfactory.

$$M_{simulated}/MHz = \begin{Bmatrix} 0 & 448 & 0 & 0 & 0 & 0 \\ 448 & 9 & 398 & -2 & 1 & 0 \\ 0 & 398 & 18 & 298 & -2 & 0 \\ 0 & -2 & 298 & 21{,}1 & 394 & 0 \\ 0 & 1 & -2 & 394 & -18 & 470 \\ 0 & 0 & 0 & 0 & 470 & 0 \end{Bmatrix}$$

Figure 131: extracted matrix of the 4-pole filter - f_0=4GHz - bandwidth 10%

The wideband response of the 4-pole filter is shown in Figure 132 showing a spurious free range more than one octave. Thanks to the used TM_{010} mode, a rather high spurious free range is achieved with this kind of dielectric resonator.

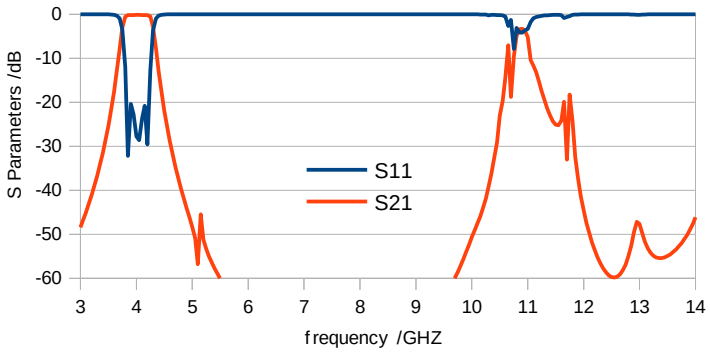


Figure 132: simulated wideband response of the 4-pole filter

In order to anticipate the manufacturing tolerances, we add more screws in the design to tune the made filter. On the Figure 133, we see the different screws, some of them are to control finely or coarsely the central frequency of each resonator and other ones are placed to modify the value of the coupling in the irises.

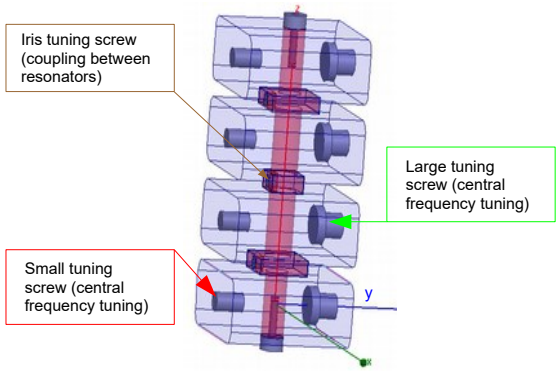


Figure 133: 4-pole filter with tuning screws

Based on this result we can launch the manufacturing of the different elements.

3 Manufacturing

1 support for the manufacturing

We follow the same steps as for the 2-pole filter. We thus design a similar manufacturing support (Figure 134) for the dielectric element.



Figure 134: designed and manufactured dielectric part of the filter with support

2 Housings

The Aluminum cavity in the Figure 135 was made by the ESTEC workshop.

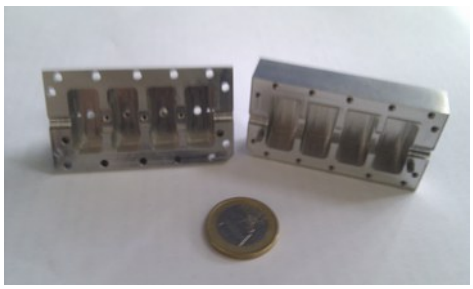


Figure 135: manufactured Aluminum housing for the 4-pole filter

In order to evaluate a low cost and fast prototyping alternative, we have manufactured another housing made with a plastic 3D printer. We realize the same structure knowing that with this method many traditional design rules do not exist like the rounded corner for the different rectangular cavities.

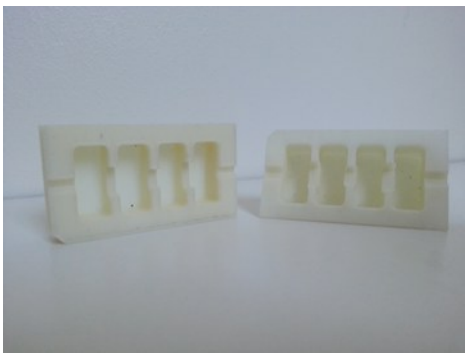


Figure 136: plastic housing for the 4-pole filter

When the manufacturing is done, we have to cover the internal structure with a silver paint to efficiently confine the electromagnetic field inside the cavities. We put several layers in order to get a satisfactory conductivity of about 2 S/µm. The view of the final obtained housing is presented in Figure 137.



Figure 137: plastic housing covered by the silver paint

4 Measurements

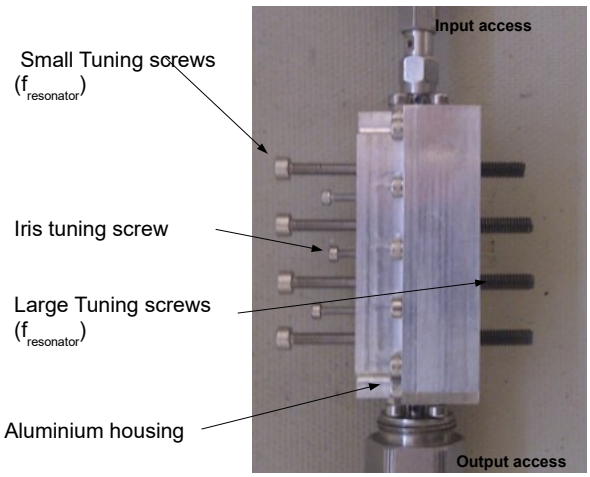


Figure 138: measurement of the 4-pole filter

We put the different elements together (Figure 138) and we tune the filter to have the best possible response.

The experimental response of the filter is shown in Figure 139 and in Table X with a comparison with the theoretical simulation. We realized the same measurements with the plastic housing and we obtained similar results proving the possibilities to use this kind of

material to have a quick prototype. The conductivity of the housing then appears to bring a small contribution to the filter insertion loss.

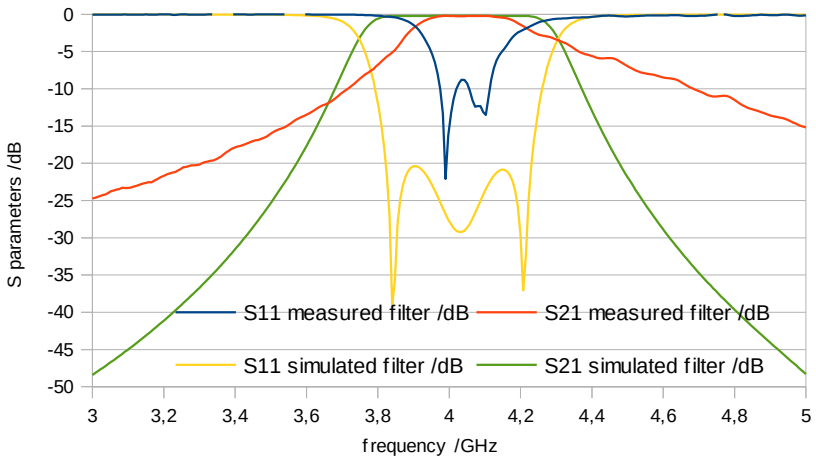


Figure 139: simulated and measured response of the 4-pole filter

The larger screws (6mm diameter for their head) are mainly used to tune the filter. These screws are actually 4mm screws with a 6mm diameter head: this geometry helps having a wide control of the resonator frequency without the appearance of spurious mode because the screw insertion remains small.

	Measured filter	Simulated filter
ΔF /MHz	200	400
F0 /GHz	4.05	4.0
Insertion losses /dB	0.3	0.2
S11 /dB	-9	-20
1st spurious mode /GHz	10	11

Table X: characteristics of the 4-pole filter

The extracted measured coupling matrix is shown in Figure 140.

$$M_{measure}(MHz)=\begin{Bmatrix} 0 & 697 & 0 & 0 & 0 & 0 \\ 697 & 599 & 545 & 3 & 32 & 0 \\ 0 & 545 & 64 & 199 & 3 & 0 \\ 0 & 3 & 199 & 89 & 560 & 0 \\ 0 & 32 & 3 & 560 & 624 & 672 \\ 0 & 0 & 0 & 0 & 672 & 0 \end{Bmatrix}$$

Figure 140: extracted coupling matrix of the 4-pole filter

The measured S parameters may let think that only two poles are appearing; however, the extracted coupling matrix does confirm that all four resonators are coupled.

The frequencies of the first and fourth resonators are too high because of a slit appearing on each side of the corresponding dielectric resonators. These cracks (Figure 141) that have appeared during the firing of the ceramic part have obviously modified their resonance frequency. The reason of these cracks is linked to the cleaning step (after the polymerization process) of the holes in resonators 1 and 4. Indeed, some liquid paste was still inside the holes of the dielectric part and, when it was remove using bellows, it weakened the wall of these resonators. The firing step was the one that definitively finished to increase this defect.

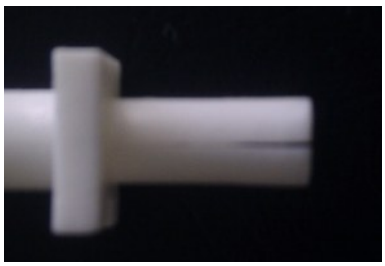


Figure 141: crack on the dielectric element of the 4-pole filter

Then, the Input/Output couplings are too strong so their values have been decreased by reducing the depth of the coaxial probes inside the dielectric part. However, it was not possible to obtain a response better than the one shown in Figure 139. The analysis of the coupling matrix also shown that the coupling between resonators 1 and 2 and between 3 and 4 are too high, however confirming that our design do provide a very high coupling between resonators. Resonators 3 and 4 are close to their respecting frequency and as expected non adjacent resonator cross coupling remains small. The matrix is finally not purely symmetric explaining the asymmetric measured S parameters.

The presented concept, besides the unexpected manufacturing problem, shows that high coupling values between dielectric resonators can be achieved. Indeed, the M12 coupling of 545 MHz do confirm that a wide bandwidth filters made of dielectric resonators can be achieved.

5 Post fabrication simulation

To analyze the behavior of the manufacturing filter, we measured the dimensions of the housing and the dielectric element. The tolerance of the housing is ±20µm, however we observe a noticeable difference between the theoretical and measured dimensions for the dielectric element. The measured dimensions of this element are shown in Figure 142.

	Simulation values	measured value 1	measured value 2	measured value 3	measured value 4	measured value 5	measured value 6		
diameter of the resonator 1		**4,317**	**4,148**	**4,129**	**3,831**	**3,883**	**3,9**	Maximum deviation	standart deviation
	4	0,317	0,148	0,129	0,169	0,117	0,1	0,31700	0,1918714848
diameter of the resonator 2		**4,843**	**4,816**	**4,428**	**4,676**	**4,553**	**4,598**		
	4,76	0,083	0,056	0,332	0,084	0,207	0,162	0,33200	0,1592766984
diameter of the resonator 3		**4,806**	**4,807**	**4,807**	**4,4616**	**4,585**	**4,635**		
	4,76	0,046	0,047	0,047	0,2984	0,175	0,125	0,298400	0,1461538915
diameter of the resonator 4		**4,088**	**4,129**	**4,084**	**3,877**	**3,857**	**3,811**		
	4	0,088	0,129	0,084	0,123	0,143	0,189	0,18900	0,1405612559
length of the resonator 1		**10,255**							
	10,2	0,055						0,05500000000000150	
length of the resonator 2		**10,069**							
	10,2	0,131						0,13099999999999800	
length of the resonator 3		**10,125**							
	10,2	0,075						0,07499999999999300	
length of the resonator 4		**10,072**							
	10,2	0,128						0,12800	
Iris 1 height (axis y)		**8,432**							
	8,5	0,068						0,06799999999999600	
Iris 1 width (axis x)		**8,257**							
	8,5	0,243						0,24300	
Iris 1 thickness (axis y)		**2,167**							
	2,3	0,133						0,13300	
Iris 1 hole height		**2,25**							
	2,2	0,05						0,04999999999999800	
Iris 2 height (axis y)		**5,643**							
	5,6	0,043						0,04300000000000200	
Iris 2 width (axis x)		**5,38**							
	5,6	0,22						0,22000	
Iris 2 thickness (axis z)		**2,51**							
	2,6	0,09						0,09000000000000300	
Iris 2 hole height		**2,183**							
	2,2	0,017						0,01700000000000300	
Iris 3 height (axis y)		**8,452**							
	8,5	0,048						0,04800	
Iris 3 width (axis x)		**8,218**							
	8,5	0,282						0,28200	
Iris 3 thickness (axis z)		**2,242**							
	2,3	0,058						0,05799999999999800	
Iris 3 hole height		**2,281**							
	2,2	0,081						0,08100	
Input (hole for coaxial)		**4,55**							
	6	1,45						1,4500	
Output (hole for coaxial)		**4,37**							
	6	1,63						1,6300	

Figure 142: measured dimensions of the 4-pole filter

The green values are the dimensions where a tolerance of ±20µm is respected and in red when it's not right. Following this result, we supposed the oversizing step before manufacturing is not accurate enough.

6 Tuning screws: return of experience

During the measurement, we tuned the filter with some screws but we clearly saw that when the screws came very close to the dielectric element some spurious mode quickly appear. The effects is shown in the Figure 143 (simulated 4 pole filter with tuning screws very close to the DRs).

When we initially simulated the filter with the tuning screws, we did not observe this phenomenon because we did not expect to put them very close to the DR.

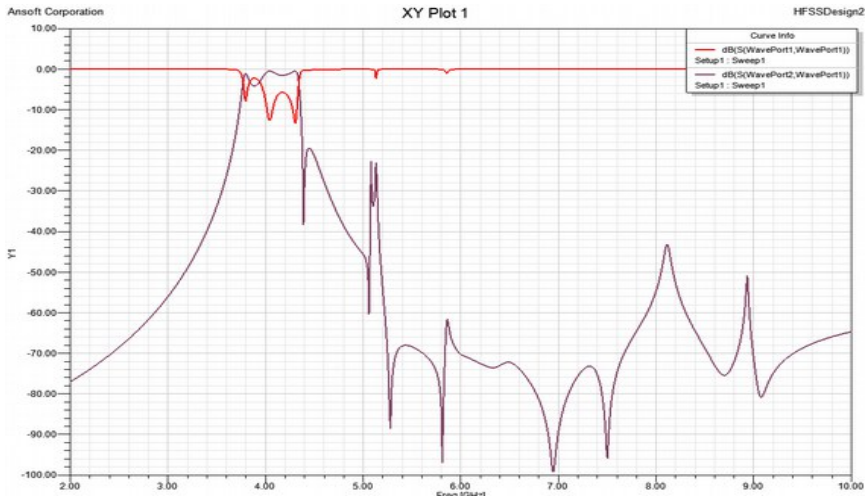


Figure 143: spurious mode created by the screws - 4-pole filter

Simulating now them in such a position, we can clearly observe spurious modes in the Figure 143.

Conclusion

In this part, we designed two filters using the coupling elements studied in the Chapter II. Firstly, we realized a 2-pole bandpass filter with a bandwidth of 500MHz at 3.3GHz (14% of f_0). Once optimized, we manufactured the dielectric element by stereolithography. This process permits us to have an important freedom for the design of the dielectric part. It more particularly makes possible the fabrication of the whole dielectric piece within just one part, i.e. without assembly of gluing. The dielectric resonators and different dielectric parts realizing the filtering function (Input/Output couplings, couplings between nearby resonators) are therefore embedded in this monolithic approach. However, when we measured the response of the filter, we had a frequency shift of more than 1.2 GHz towards the lower values. Two main reasons may explain this, the first one is the dimensions of the dielectric

element that are smaller than expected and the second one is the possibility of a lower permittivity of our element due to a possible lower density of the fired part (air bubbles trapped during the layer by layer spreading of the ceramic paste).

We decided to move to a 4-pole bandpass filter at 4GHz with a bandwidth of 400MHz (10% of f_0). We studied the behavior of some tuning screws in order to compensate the manufacturing tolerances observed in the previous 2nd order filter. We made the dielectric element by stereolitography and we measured the response of the complete filter. Again, we obtained unsatisfying result. Only two pole were identifiable on the graph and we had a lower bandwidth (only 5%). We tried to tune the response with the screws but their proximity with the dielectric resonators (needed for an efficient frequency tuning of the filter) just led to create spurious modes. Then, the manufacturing tolerances were around ±200µm, more than the expected ±50µm. Moreover, the dielectric element is not well hold in the housing and it is possible that we have spurious contacts between the dielectric part and the metallic housing bringing uncontrollable spurious modes. Then, the Input/Output coupling system has to be modify because we have to open and remove the elements in order to have access to the coaxial probe and to cut it at the right length during the experimental step.

Even if the obtained measurements have confirmed that very high couplings can be obtained with this stacked TM_{010} dielectric resonators, three critical upgrades have to be made on:

- the Input/Output couplings that should not be used as supporting elements while still maintaining very high values
- on efficient tuning systems for the resonators frequencies
- more accurate manufacturing technologies if such tuning device is not achievable.

The next Chapter will then deal with these different critical points upon creating a new generation of this wide band compact filters.

Bibliography

[1] N. Delhote, D. Baillargeat, S. Verdeyme, C. Delage and C. Chaput, "Ceramic Layer-By-Layer Stereolithography for the Manufacturing of 3-D Millimeter-Wave Filters," in *IEEE Transactions on Microwave Theory and Techniques*, vol. 55, no. 3, pp. 548-554, March 2007.

[2] A. H. Khalil *et al*., "3-D pyramidal and collective Ku band pass filters made in alumina by ceramic stereolithography," *Microwave Symposium Digest (MTT), 2011 IEEE MTT-S International*, Baltimore, MD, 2011, pp. 1-1.

CHAPTER IV

Second Generation of filters

Introduction

In this part we will present the new generation of our filter. The first wave of prototypes helped us to validate the possibility to achieve strong coupling in Input and Output accesses and between two resonators. However, we identified several critical points on the different results we obtained. That is why we work on these weaknesses to eliminate them.
First, we present a new solution to realize the Input and Output coupling, because currently we have to open the housing to modify the length of our coaxial probes. It has also appeared to be a poor supporting element for the dielectric part inside the cavity. For these reasons we decide to study another way to achieve this coupling.
Secondly, we will investigate a tuning system for our filter. Indeed, we saw on the previous chapter the difficulties to tune it with usual screws. The field of this selected TM_{010} mode is very concentrated inside the dielectric part so it is problematic to use them and to obtain a proper tuning.
This Chapter will thus present 2^{nd} and 4^{th} bandpass order filters made by machining a ceramic block in order to experimentally validate the mentioned evolutions.
To finish, we will present an original concept of a metalized dielectric filter. A silver coated 3-pole filter will be designed and measured, its results showing a promising evolution of the very initial concept of this thesis.

I. 2-pole filter with new Input/Output system

The first generation of filter has shown a weak point on its Input/Output system. In this part, we will focus on the Input/Output coupling system. The principal drawback of the previous one was the impossibility to experimentally finely optimize the coupling without opening the metallic housing. Then, the connectors were also used to support the dielectric element in a way which was poorly efficient. For these different reasons, we need to find another less invasive way to tune the Input/Output coupling.

1 Characteristics

In this part, we develop a 2-pole filter at 4GHz with a very wide bandwidth of 1.5GHz (37% of the central frequency) in order to take full benefit of the actually possible couplings with

our concept. The return loss is 20dB. The Figure 144 presents the theoretical coupling matrix of this 2-pole filter.

$$M(/MHz)=\begin{Bmatrix} 0 & 1837 & 0 & 0 \\ 1837 & 0 & 2487 & 0 \\ 0 & 2487 & 0 & 1837 \\ 0 & 0 & 1837 & 0 \end{Bmatrix}$$

Figure 144: Theoretical coupling matrix of the 2-pole filter - f0=4GHz - BW=1.5GHz

As previously we use Zirconia as dielectric material for the dielectric part.

2 Simulation

We are not starting all over again and we have based this work of the first design, trying to improve it. The two main developments concern the Input/Output coupling system and the spurious contact than can appear between the cavity and the dielectric parts.

1 New Input/Output coupling system

We study another concept for the Input and Output coupling. Indeed, the previous filter permit us to identify some drawbacks of the actual system. At the moment, when we want to modify the length of the coaxial probe we need to open the housing so it is not a good solution to have a stability for our measurement. This new concept is based on magnetic coupling. We have two surfaces face to face: the first one is a metallic one and corresponds to the coaxial probe and the other one is a dielectric one connected to the resonator. The design is presented in Figure 145.

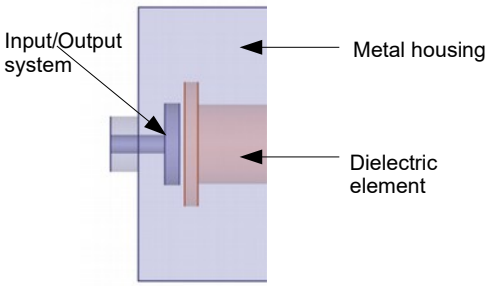


Figure 145: New Input/Output coupling

Several parameters can be modified to obtain the right coupling:

_ the diameter of the metallic disk

_the diameter of the ceramic disk

_the gap between the both elements

So we study the impact of these different dimensions and we determinate the related achievable coupling values.

Firstly, we observe the variation of the coupling for different radii of the metallic disk (Figure 146). The gap is fixed at 1.5mm and the radius of the dielectric disk at 7mm. The diameter of the DR is 3,8 mm. For this study, the value of the Input/Output coupling (Kin) extracted from the filter coupling matrix will mainly be used as an indicator of the achievable coupling values. As a reminder, Kin of many hundreds are researched here.

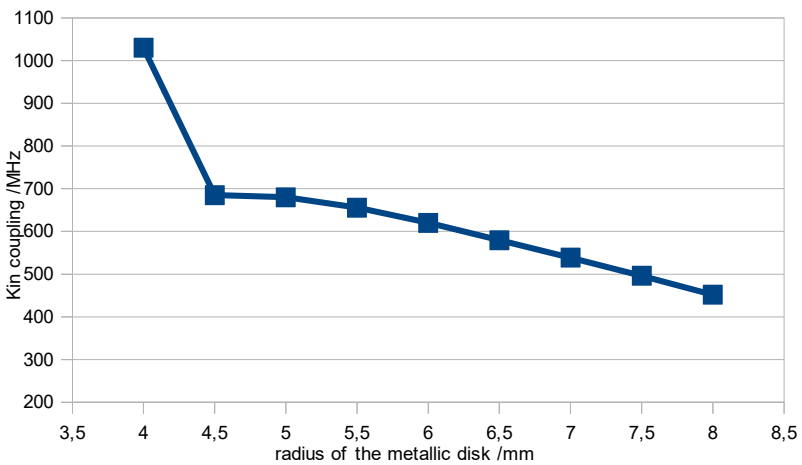


Figure 146: Kin coupling versus metallic radius

We remark the coupling decreases when the radius increases. Indeed, the surface increases and we increase the losses due to the area and the magnetic field concentration is lower.

Secondly, we study the behavior of the coupling as a function of the gap between the both elements. In this case, we fixed the metallic radius at 5mm and the dielectric one is still 7mm.

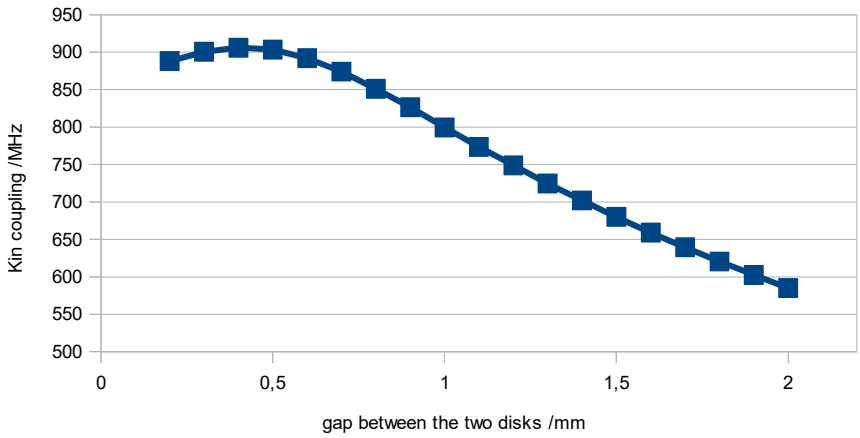


Figure 147: Kin coupling versus the gap between the dielectric and metallic radii

We observe a maximum for a gap around 0.4mm, then the coupling decreases logically when the probe is further from the DR.

Thirdly, we calculate the Input coupling for several radii of the dielectric disk. The gap is fixed at 1.5mm and the metallic disk at 5mm.

The variation of the Input coupling is lower than for the two previous parameters.

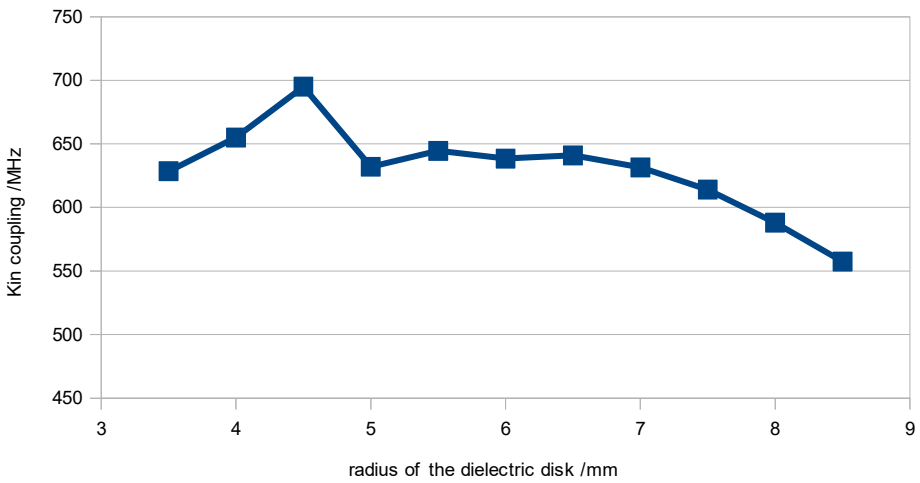


Figure 148: Kin coupling versus the radius of the dielectric disk

These initial simulations show a good potential of this excitation probes.

We can notice that we have now to think about a support for the dielectric element in order to assure its centering inside the cavity.

2 complete structure

This new filter is for some parts similar to the previous one. We have the both dielectric resonators connected by a dielectric element. The disk for the Input coupling is circular, the resonators are circular, so we chose to design a connecting with the same shape. Then, for this filter we decided to manufacture the dielectric piece by machining tools which can ensure a better and required accuracy to what was achieved in the previous chapter. In this way, the

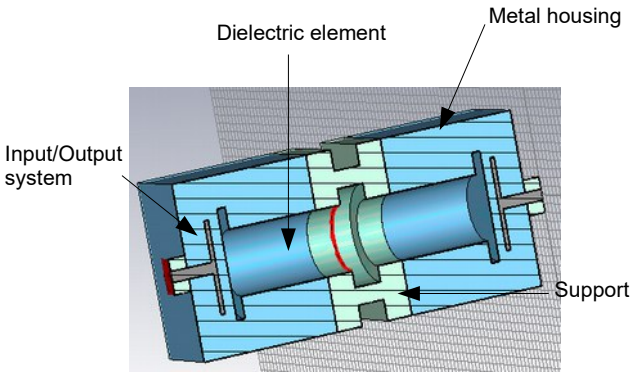


Figure 149: design of the 2-pole filter with the new Input/Output system

obtained design (Figure 149) is fully realized by this manufacturing technique.

We decide to put a support made out of Teflon at the level of the iris. The positioning is important for the dielectric element in the iris because we do not want contact between the dielectric and the metallic parts. Then it allows to keep a constant gap all around the central part of the dielectric element and the housing.

In this way, we choose to put the support in the iris to insure the position of the dielectric element in the center of the housing (Figure 148). The simulated response is presented in Figure 150. The dimensions of the dielectric element are:

- total length: 32.2 mm
-diameter of the Input/Output disk: 12.6mm
-diameter of the resonator: 7.6 mm
-diameter of the inter-resonator disk: 11.3mm

Then, the dimensions of the housing are $64.2\times42\times41.6mm^3$.

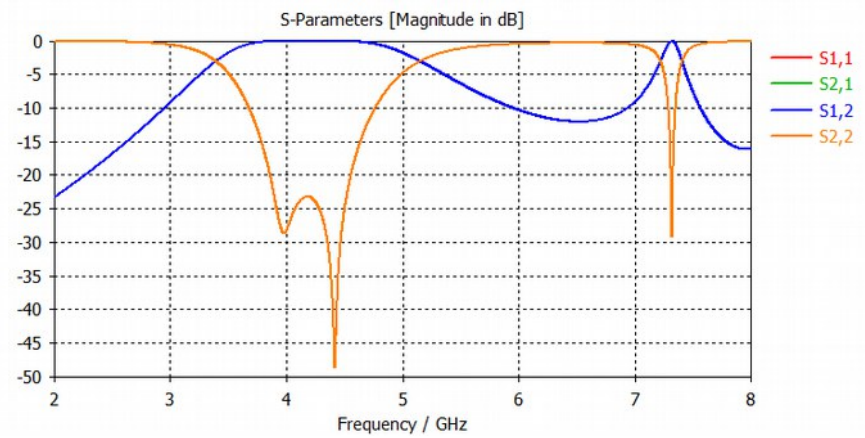


Figure 150: 2-pole filter - new Input/Output coupling system - simulated response

We observe a spurious mode at 7.3GHz. The plot of its electromagnetic field inside the structure shows that the E-filed is strongly concentrated inside the dielectric part. This mode was therefore impossible to get rid off without destroying the TM_{010} mode.

Moreover, we realize a study of the impact of the manufacturing tolerances, so we apply ±50µm at the optimized dimensions and we obtain the result presented in . We remark the small impact on it.

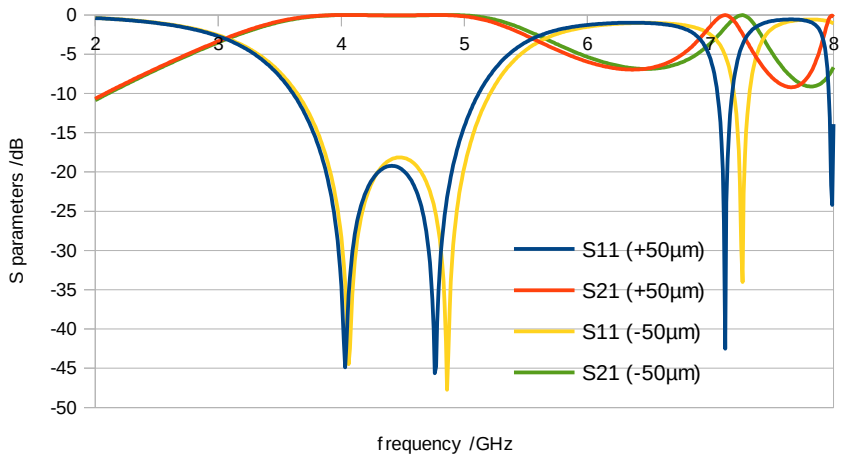


Figure 151: study of the manufacturing tolerances on the filter response

3 Manufacturing

Following what we said in the previous part, we have decided to manufacture the dielectric element by machining a Zirconia block. The announced manufacturing tolerance is ± 20µm.

In light of the small dimension drift and the poor tuning obtained in the previous chapter with screws, we decide to remove tuning screws for this filter. However to prevent problems, we performed some simulations will all the dielectric part dimensions changing by +/- 20µm. We still have a return loss better than 20dB and an acceptable response.

The manufactured dielectric part made of machined Zirconia is shown in Figure 152.

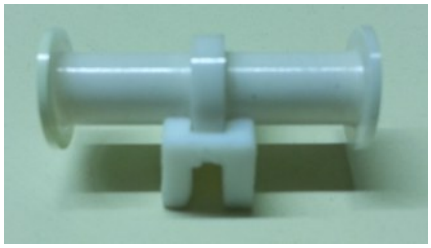


Figure 152: 2-pole filter - new Input/Output coupling system - dielectric element on this support

The metallic housing is made of copper by the machine shop of XLIM.

To realize the connectors, we used the same coaxial probes as previously but this time we soldered a Copper disk to the probe end. We manufactured a set of several diameters of copper disks to have the possibility to tune our filter Input/Output coupling. In Figure 151 we see the realized probes.



Figure 153: coaxial probe for the new Input/Output system

A part of the Teflon material is cover by silver paint (Figure 151)in order to avoid electromagnetic leak between the cavity and the ground of the connector. Indeed, during the tuning of the Input/Output coupling, we have to push or to pull back the probe but still want to have a proper grounding. The impact of the possible gap between the housing and the connector is therefore minimized.

4 Measurements

The measured element is presented in Figure 154.

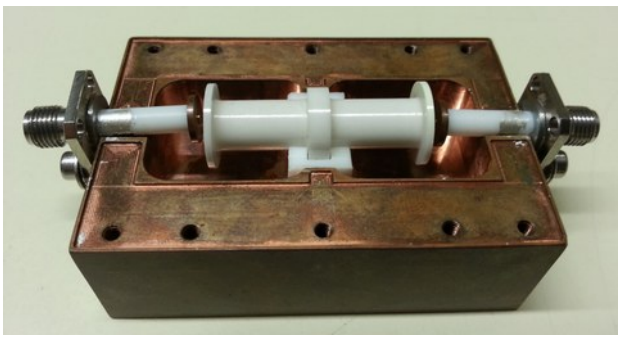


Figure 154: 2-pole filter - new Input/Output coupling system - manufactured structure without top plate

As seen in simulation, we measured a spurious mode at 7GHz, and we do not have the possibility to remove it or to shift up this frequency. The response is presented in Figure 155.

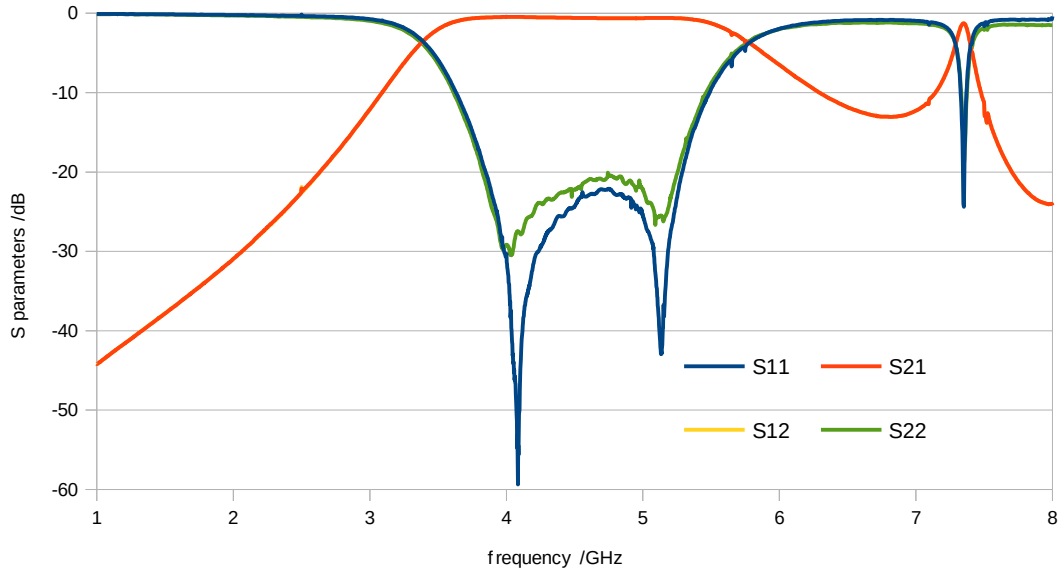


Figure 155: Response of the 2-pole filter with the new Input/Output system

The Table XI lists the different measured parameters. We have obtained a bandwidth of 1900 MHz (40% of the central frequency). The central frequency is a little bit higher in frequency than expected by our simulations and regarding the manufacturing accuracy, the expected +/- 20µm value was indeed obtained. The frequency shift can be explained by the wider bandwidth we have obtained. The behavior of this new generation is very efficiently working and represents a great improvement over the previous concept.

	Measured filter	Simulated filter
Δf /MHz	1900	1500
F_0 /GHZ	4.75	4,2
Insertion losses /dB	-1	-0.2
S_{11} /dB	-20	-23
1er spurious mode /GHz	7	7,3

Table XI: Results of the measured 2-pole filter

II. 2-pole filter with tuning system

In this part, we will present an alternative design with a tuning system for our filter. We saw in chapter III the difficulties to tune with regular screws. Indeed, the magnetic field is concentrated inside the dielectric element so it is not easy to perturb its distribution. That is why, we study a solution to realize some frequency tuning in our filter.

1 Characteristics

The solution we realized here is based on extra dielectric rings we can put on the dielectric main part to modify the coupling values and/or the frequency resonances of each pole. The resonator will be composed of two parts: the first half being cylindrical and the second one is composed of a cubic rod.

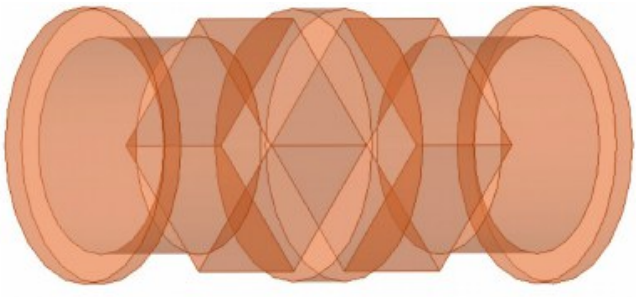


Figure 156: Design for the tuning system with
regular section (circular) and tuning one (cubic)

With this second section it is possible to put dielectric “rings” on it to modify some values of the coupling matrix. We actually intend to change the equivalent quantity of dielectric material in certain locations of the part. Two different dielectric materials will be used for this study: Zirconia and Alumina. The filter main dielectric part will be realized using Zirconia material and the rings will be made of Alumina and Zirconia. Alumina material has a lower permittivity than Zirconia so we expect a finer tuning with this set.

To achieve the tuning function, we design several rings of different diameters and different thickness. In this way, we expect to have more freedom to obtain the right coupling value. The different parameters we can change are:

_the diameter of the ring

_the thickness of the ring

_the position of the ring on the cubic zone of the Zirconia part as seen in Figure 156.

2 Simulation

In order to decrease the manufacturing time, we decide to use the same cavity as for the previous structure and we therefore have to take into account that constraint for the design of our dielectric element. In this way, we realize a 2-pole filter with the central frequency at 5GHz and a bandwidth of 1.8GHz (being 36% of f_0). The coupling matrix is presented in Figure 157.

$$M(/MHz)=\begin{Bmatrix} 0 & 2196 & 0 & 0 \\ 2196 & 0 & 2970 & 0 \\ 0 & 2970 & 0 & 2196 \\ 0 & 0 & 2196 & 0 \end{Bmatrix}$$

Figure 157: Coupling matrix for the 2-pole filter with tuning system

We design a 2-pole filter with the tuning system described previously in order to modify the coupling between the cavities and to tune the frequency of each resonator. To realize this tuning function, we use as explained before a dielectric resonator composed of two definite parts, the first one is a circular cross-section as we have for the previous design and the second one is has a square cross-section (cubic section).

We choose this form in order to easily maintain a dielectric ring on the square section. Moreover, this element could be placed at different locations on this part. Then, we design a set of disks (rings) with different radius and different thickness. By this way, the ring impacts on the filter response will be more or less important.
This tuning system permit to tune the coupling value between the two resonators and also the resonance frequency of the pole.

The Figure 158 explains in details the structure of the 2-pole tuning filter. We recognize the different parts of this filter maintained in the metallic housing by two Teflon supports.

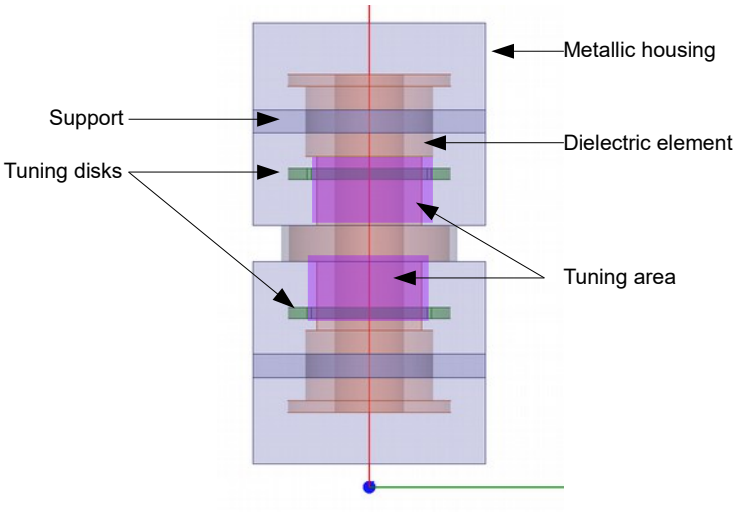


Figure 158: 2-pole filter with the extra rings tuning system

The tuning system however creates a spurious mode very close to our band. In this way, we have to find a solution to try to increase the spurious free range. In the part of this manuscript dedicated to the study of the $TE_{01\delta}$ mode dielectric resonator (see Chapter II), we saw that the ring shape provides a greater spurious free range as well as a good Q-factor. A similar study has been performed with this TM_{010} DR.

We study the behavior of the resonator frequency for several values of an internal hole added to the DR as presented in Figure 159.

We do not observe an increasing of the spurious free range by this way. However, we remark

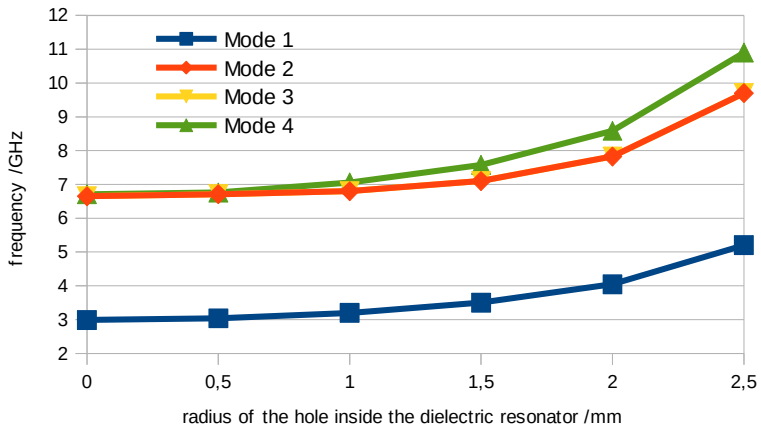


Figure 159: Behavior of the frequencies of the modes as a function of the radius of the hole

that the Q-factor slightly increases with the radius of the hole (Figure 160). Based on that conclusions, we will not use this configuration for two reasons: the first one is that no

significant improvement for the Q and spurious free range is obtained, the second one is that this design is not compatible with the machining process, even it can be possible to realize this form with the stereolithography process.

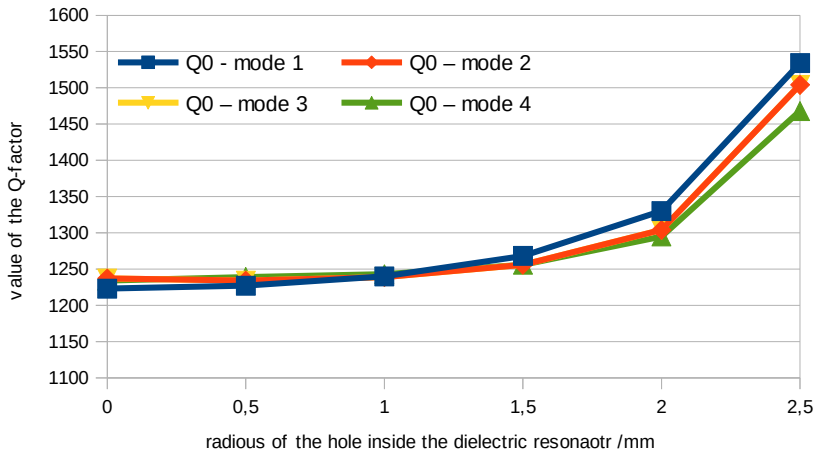


Figure 160: Variation of the Q-factor as a function of the radius of the hole

We optimized this 2-pole filter with one ring (for the first and second resonator) to have a tuning of each DR frequency with some control of the inter-resonators coupling.

The dimensions of the dielectric part are reviewed in Figure 161.

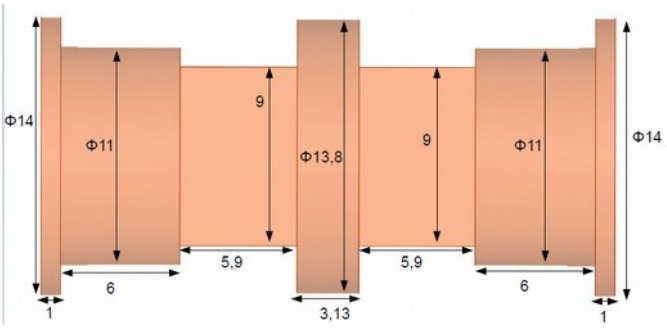


Figure 161: dimensions of the 2-pole filter with tuning system

The simulated response of our filter is presented in Figure 162 as well as the filter main dimensions.

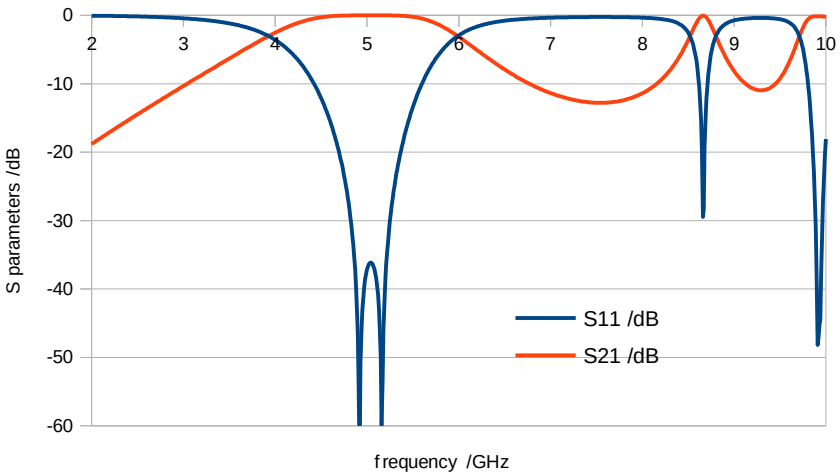


Figure 162: Simulated response of the 2-pole filter with tuning system

According to the constraint of using the same metallic housing, we obtain a central frequency at 5GHz and a bandwidth of 1,5GHz. We still have the spurious mode close to our bandwidth at 8,7 GHz. This filter is now ready for fabrication.

3 Manufacturing

1 Dielectric part and support for the manufacturing



Figure 163: Manufactured dielectric part - 2-pole filter with tuning system

As for the previous filter, the main dielectric part is made by machining a Zirconia block with a +/- 20µm accuracy. It is presented in Figure 163. We can identify the circular and square cross-sections on each DR.

Regarding the supports, they are made as usual in Teflon and two of them are supporting the dielectric main part in their cylindrical sections. The Teflon supports are actually cut in two parts in order to surround the dielectric part and make the assembly of the filter easy (Figure 165).

2 Dielectric rings

In the Figure 164, we can see one of the set realized, we easily identify the different radius (r_{min} = 7mm and r_{max} = 9mm) and the different thickness (t_{min} = 1mm and t_{max} = 3mm). This set and the main dielectric part are made with the same Zirconia material. A second set with the same dimensions is made of Alumina material with a lower permittivity. All the rings have been made with the SLA process.



Figure 164: a set of dielectric rings for the 2-pole filter with tuning

3 Housing

In order to decrease the manufacturing time, we decided to use as the same metallic housing as with the previous filter.

4 Measurements

The different elements are put together as we can see in the Figure 165. We observe that two dielectric rings are placed, one on each DR.

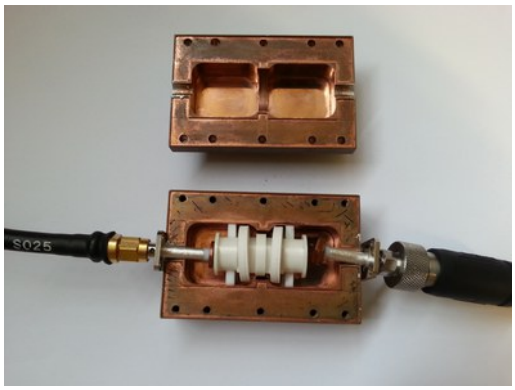


Figure 165: 2-pole filter with tuning system - manufactured elements

We measured the filter for all the configurations, all the radius and the different thickness.

1 First set of rings made of Aluminia material

In the Figure 166, we see the result of the S21 parameters of the filter for the different radius with a thickness of 3mm. They are the biggest tuning elements we have, so we expect to have the largest variation with these. We have some spurious peaks inside the bandwidth. Their origin is hard to tell but we remark a small damage in the metallic housing at the level of the iris. Maybe it is due to this defect but more investigations would be necessary.

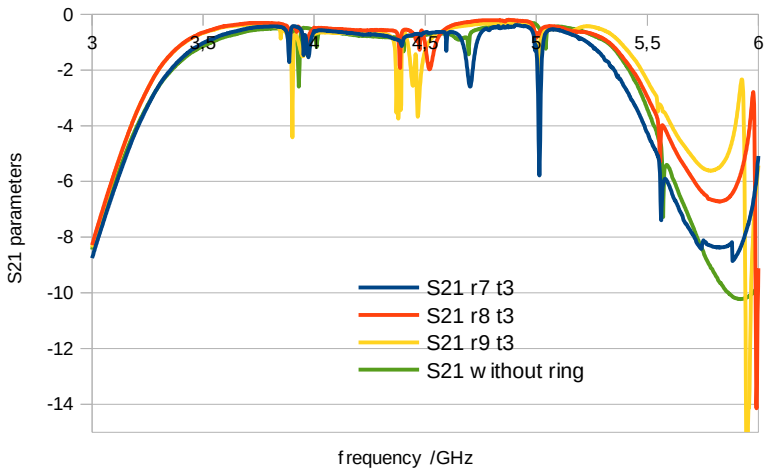


Figure 166: S21 parameters for different radius of the tuning rings (thickness = 3mm) – Alumina -2-pole filter with tuning system

The green curve is the response of the filter without ring.

Curve	Bandwidth /GHz
S_{21} without ring (reference)	2.15
S_{21} r7 t3	2.1
S_{21} r8 t3	2.3
S_{21} r9 t3	2.35

Table XII: Impact of the dielectric rings in the bandwidth – 2-pole filter with tuning system

We notice in the Table XII we increase the bandwidth, and consequently the inter-resonator coupling by using the rings with a radius of 8 and 9mm. However we have a lower bandpass with the 7mm radius rings.

This fact casts some doubts about the result obtained for the 8 and 9 mm radius. We identified several points during the measurements. Indeed, we do not have a good repeatable process because each time we want to realize a measure, we have to open the housing to change the rings. Then, the coaxial probe does not stay in the same exact position, and this brings the biggest mismeasurement. Another source of inaccuracy is the position of the ring on the cubic part that is not perfectly reproducible with the actual design.

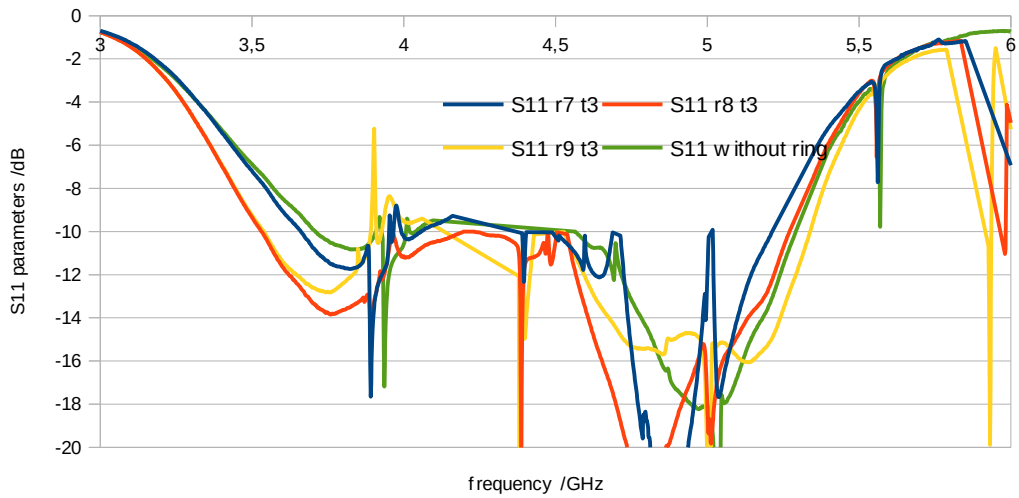


Figure 167: S11 parameters for different radius of the tuning rings (thickness = 3mm) – Alumina - 2-pole filter with tuning system

The same observations can be made for the S11 parameters (Figure 167).

We present in Figure 168 the result for a same radius but different thickness. In this graph, we see that the bandwidth increases with the thickness of the tuning element. However, the measurements are subject to the same observations as previously.

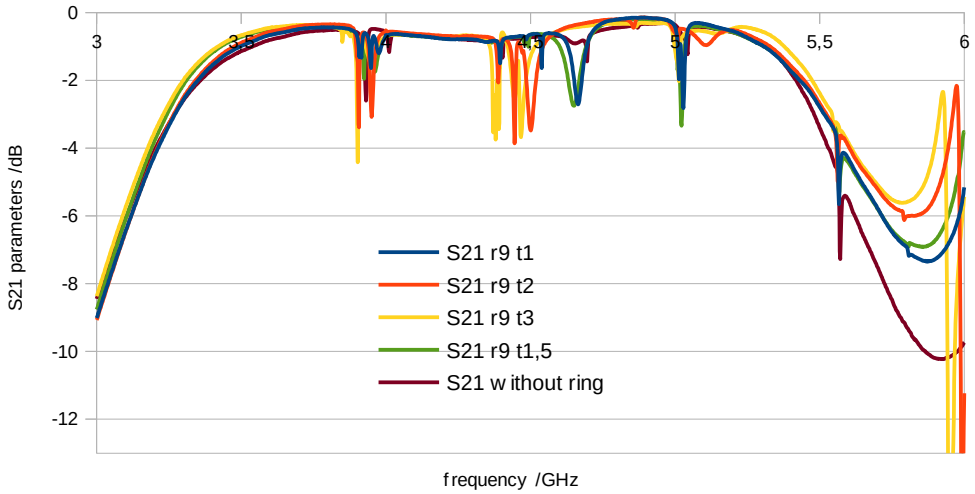


Figure 168: S21 parameters for different thickness of the tuning rings (radius = 9mm) – Alumina - 2-pole filter with tuning system

The different bandwidths are resumed in Table XIII.

Curve	Bandwidth /GHz
S_{21} without ring	2.15
S_{21} r9 t1	2.2
S_{21} r9 t1.5	2.25
S_{21} r9 t2	2.2
S_{21} r9 t3	2.3

Table XIII: bandwidths depending of the thickness of the tuning rings – 2_pole filter with tuning system

2 Second set of rings made of Zirconia material

The Figure 169 and Figure 170 show the S21 parameters depending of the thickness and the radius respectively.

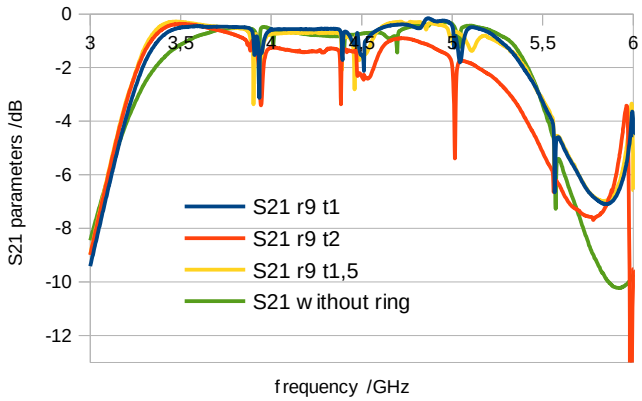


Figure 169: S21 parameters for different thickness of the tuning rings (radius = 9mm) - Zirconia - 2-pole filter with tuning system

The different bandwidths are resumed in Table XIV.

Curve	Bandwidth /GHz
S_{21} without ring (reference)	2.2
S_{21} r9 t1	2.3
S_{21} r9 t2	2.15
S_{21} r9 t1.5	2.25

Table XIV: bandwidths for different thickness of dielectric rings – Zirconia – 2-pole filter with tuning system

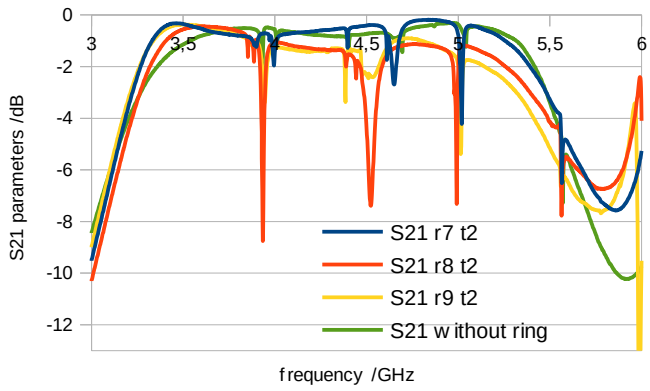


Figure 170: S21 parameters for different radius of the tuning rings (thickness = 2mm) – Zirconia -2-pole filter with tuning system

The bandwidths are summarized in Table XV.

Curve	Bandwidth /GHz
S_{21} without ring (reference)	2.25
S_{21} r7 t2	2.3
S_{21} r8 t2	2.2
S_{21} r9 t2	2,15

Table XV: Bandwidths depending of the radius of the tuning rings – Zirconia – 2-pole filter with tuning system

We have the same problems as mentioned in the previous paragraph. It is difficult to conclude about the efficiency of this tuning system.

We have to decrease the different mismeasurements, for example, we can design a metallic housing where we can fix the coaxial probe but we will have an access to the tuning part.

This tuning system seemed interesting because it offered the possibility to finely tune the filter response by putting different dielectric rings. Then, the different adjustments possible (radius, thickness and position) permit to have a better control of the filter response. However, we were confronted to many sources of mismeasurement, the major one being the non reproducible position of the coaxial probes for Input and Output coupling. Indeed, each time we wanted to realize a measurement, we had to remove the cover of the metallic housing, and during this step the coaxial prove moves a little bit but it is enough to have variations in the S parameters.

We saw for the different measurements that it is difficult to extract a clear effect of these tuning rings. However, we can notice the inter-resonator couplings increases when the tuning elements is bigger.

To efficiently complete this study, a better metallic housing is needed in order to remove the impact of the coaxial probe on the measurement. We also have to take into consideration the probable air gap between the DRs and the rings. Because of the high permittivity of the used ceramic materials, the ceramic-air interface is close to a perfect magnetic conductor. This underestimated factor may thus limit the changes brought by the rings more than expected by our initial simulations.

III. 4-pole filter with improvements

Following the previous results, we decide to move to a 4-pole filter using Zirconia material for the dielectric part but without the previously studied tuning rings. The manufacturing process used will be by machining once again. The previous result of the 2-pole filter has shown a good response without tuning screws and we want to know if we can have the same result with a higher order. A 4-pole filter is therefore designed in the next section.

1 Characteristics

The central frequency of our filter is 4GHz with a bandwidth of 1.8GHz (45% of the central frequency). The return loss is 20dB. We used Zirconia as dielectric material for the dielectric part and copper for the housing. The theoretical coupling matrix is shown in Figure 171.

$$M(/MHz)=\begin{Bmatrix} 0 & 1863 & 0 & 0 & 0 & 0 \\ 1863 & 0 & 1640 & 0 & 0 & 0 \\ 0 & 1640 & 0 & 1260 & 0 & 0 \\ 0 & 0 & 1260 & 0 & 1640 & 0 \\ 0 & 0 & 0 & 1640 & 0 & 1863 \\ 0 & 0 & 0 & 0 & 1863 & 0 \end{Bmatrix}$$

Figure 171: Theoretical coupling matrix of the 4-pole filter - f0=4GHz - Bd=1.8GHz

2 Simulation

The simulation is performed by HFSS©. The dielectric element is composed of four resonators and three connecting cylinders. We still have only one piece to insert in the metallic housing. The Input/Output coupling system is the one used previously because we expect the possibility to optimize more easily the value of the coupling by this mean.

The dielectric part is composed of four dielectric resonators and three connecting elements that permit to tune the value of the inter-resonator coupling. Still keeping a monolithic structure for our filter. It is very interesting because we eliminate many adjustment mistakes since no gluing or assembly is needed. We add two Teflon support in order to maintain our dielectric element inside the metallic housing. The complete filter is shown in Figure 172.

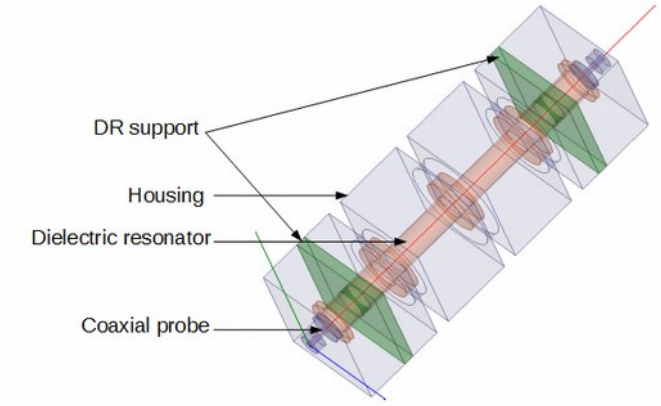


Figure 172: design of the 4-pole filter - new generation

The dimensions of the dielectric element are summarized in Figure 173.

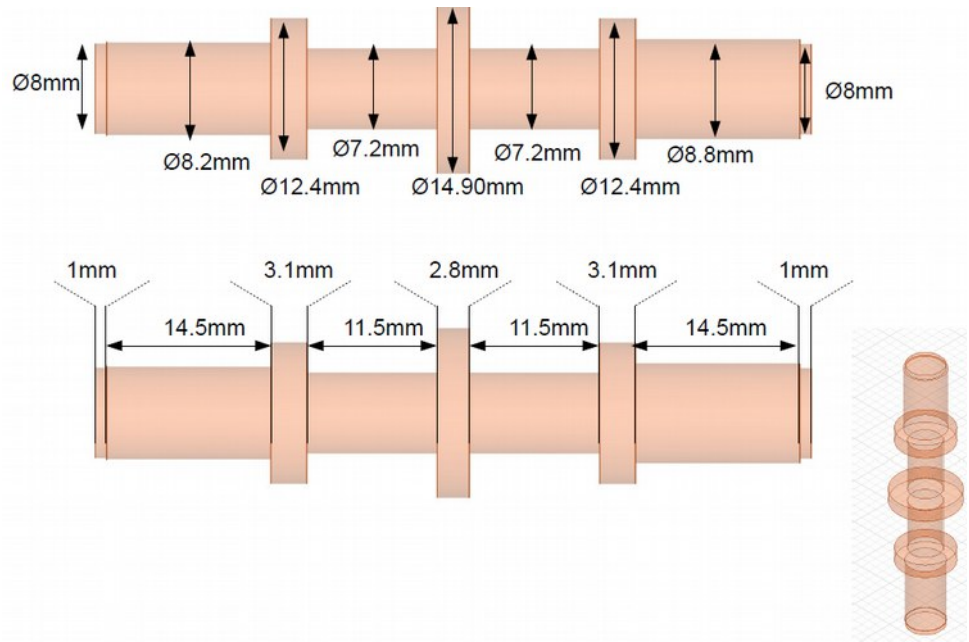


Figure 173: dimensions of the 4-pole filter new generation

The dimensions of the metallic housing are 83.4×41×23.9mm^3.

The simulated response of the filter is presented in Figure 174.

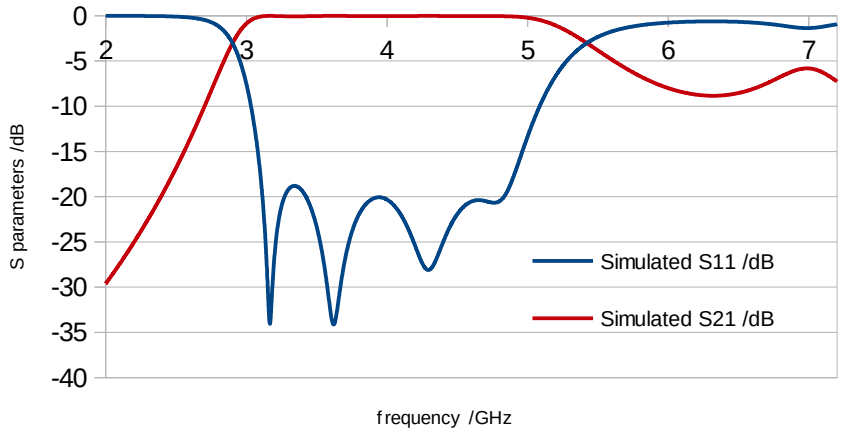


Figure 174: Simulated response of the 4-pole filter - new generation

We have a spurious mode at 7GHz. This latter is concentrated inside the dielectric part at the level of the first iris, making it not easily removable. However, one possible solution for this application is to cascade a lowpass filter in order to get rid of the spurious mode. At this point, we decide to move to the manufacturing step.

3 Manufacturing

1 Dielectric part

In light of the obtained manufacturing tolerances for the previous 2-pole filter, we decide to use the same fabrication process in order to have a very low dimension dispersion. In this way, we did not need to design tuning screws in our design. The dielectric element obtained by machining is presented in the Figure 175.

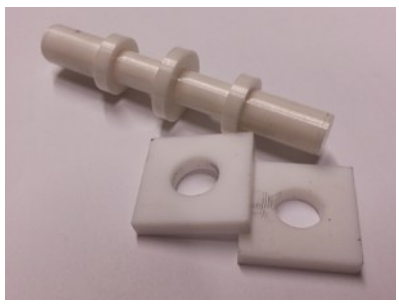


Figure 175: dielectric 4-pole filter with the Teflon supports

2 cavity

The metallic housing is made by milling using copper material and is manufactured by the XLIM machine shop.

4 Measurements

Once all the different elements are fabricated, we can assembly the filter to measure it. In the Figure 176, we see that it is very easy to center the dielectric element inside the cavity thanks to the Teflon supports.

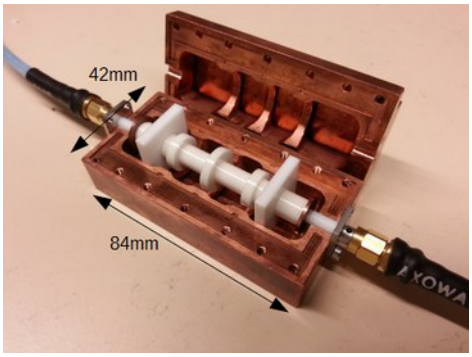


Figure 176: measurement of the 4-pole filter

The measured response is presented in the Figure 177 and compared to the simulated one.

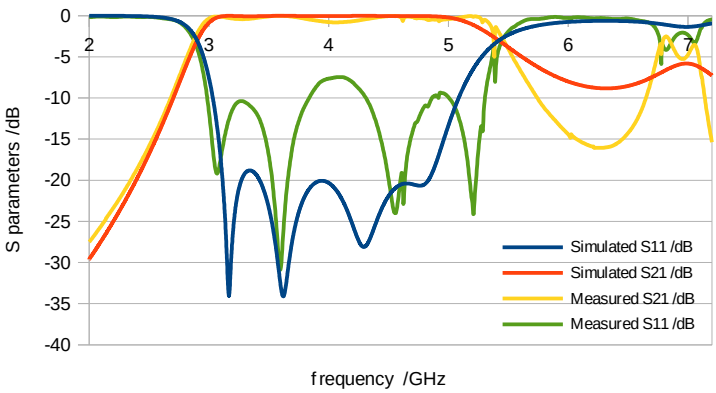


Figure 177: Measured response of the 4-pole filter -new generation

The results are presented in Table XVI.

	Measured filter	Simulated filter
Δf /MHz	2500	2400
F_0 /GHZ	4.157	4,1
Insertion losses /dB	-0.5	-0.2
S_{11} /dB	-8	-20
1st spurious mode /GHz	6.8	7

Table XVI: Comparison between measure and simulation for the 4-pole filter new generation

We obtain the expected bandwidth (60% of f_0) and central frequency. However, the In-band return-loss is around 8 dB, we have had some difficulties to get the right coupling value for the Input and Output couplings. As a consequence, the ripple is quite high (0.8 dB). This device still lack of fine tuning system for the setting of the Input/Output couplings. It will be an area of improvement for future devices.

We also realized a temperature study from 20°C to 80°C to check the behavior of our filter as a function of the temperature (Figure 178).

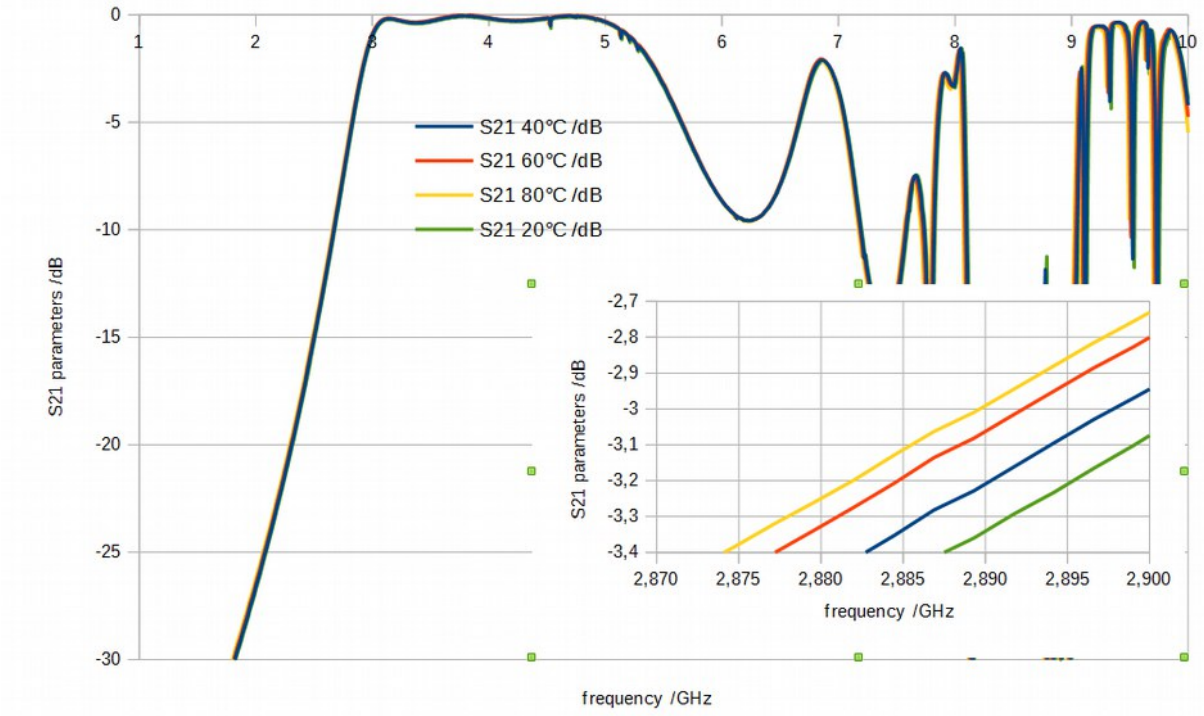


Figure 178: Behavior of the filter as a function of the temperature

We notice a frequency shift of about 15MHz between 20 and 80°C. This measurement takes into account the metallic housing and the dielectric element. Our filter is rather stable regarding the temperature variation.

IV. Filter with silver-plated dielectric part

Different observations made on the previous concepts lead us to an original evolution of this device. We saw that the impact of the metallic housing is low on the response due to the high permittivity of the Zirconia material. We then decide to design a 3-pole filter where the housing will be replaced by simply plating the external faces of the dielectric part in order to create a simple monolithic filter. By this way, we will be able to decrease drastically the weight of the entire structure as well as its size. We will only need a metallic housing to shield the coupling around the filter Input and in Output to avoid spurious signal and electromagnetic leaks.

1 3-pole silver-plated filter

1 Characteristics

In this part, we present a 3-pole filter centered at 3.5 GHz with a bandwidth of 2.6 GHz (74% of the central frequency). The coupling matrix is presented in Figure 179. The dielectric material is still Zirconia.

$$M(/MHz)=\begin{Bmatrix} 0 & 2800 & 0 & 0 & 0 \\ 2800 & 0 & 2678 & 0 & 0 \\ 0 & 2678 & 0 & 2678 & 0 \\ 0 & 0 & 2678 & 0 & 2800 \\ 0 & 0 & 0 & 2800 & 0 \end{Bmatrix}$$

Figure 179: coupling matrix of the 3-pole silver-plated filter

In the Figure 180, we can see the proposed the 3-pole filter. We identify the dielectric disks for Input and Output coupling and also the two disks for inter-resonator coupling. All the surfaces are covered by Silver (σ = 30 S/µm) with the exception of the front and rear disks faces in order to guide the electromagnetic field inside the structure.

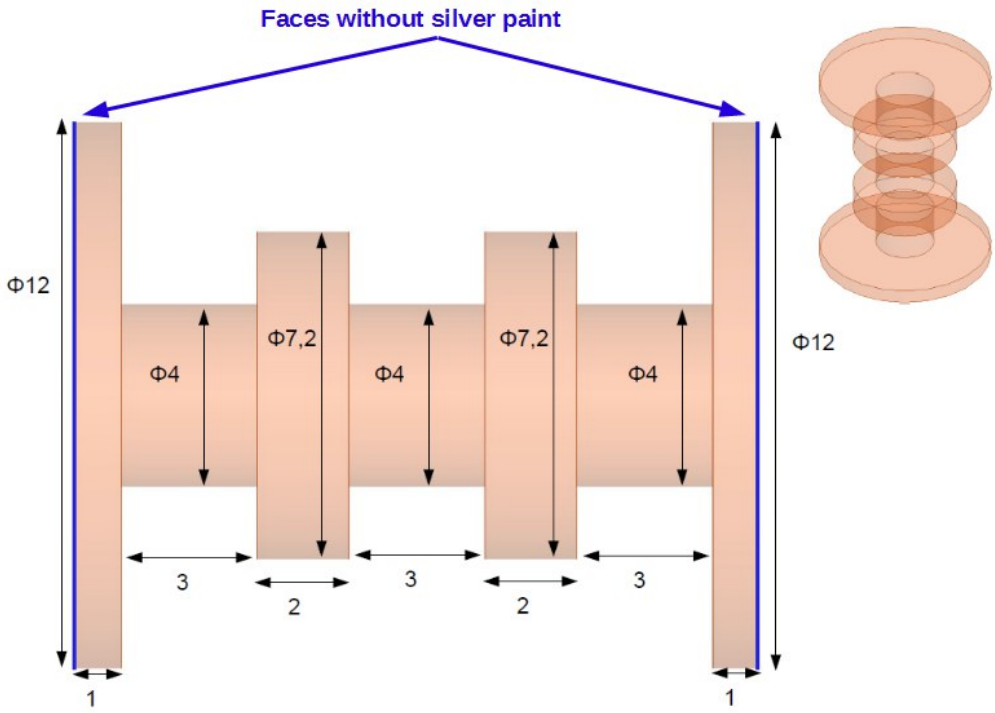


Figure 180: dimensions (in mm) of the 3-pole filter covered by silver paint

We will only use an external metallic housing in order to avoid electromagnetic leakage around for the Input and Output coupling.

The optimized response we obtain for this filter is presented in Figure 181 with a bandwidth of 2.6GHz, a central frequency of 3.5GHz, insertion loss about 0.3dB and 18 dB of return loss.

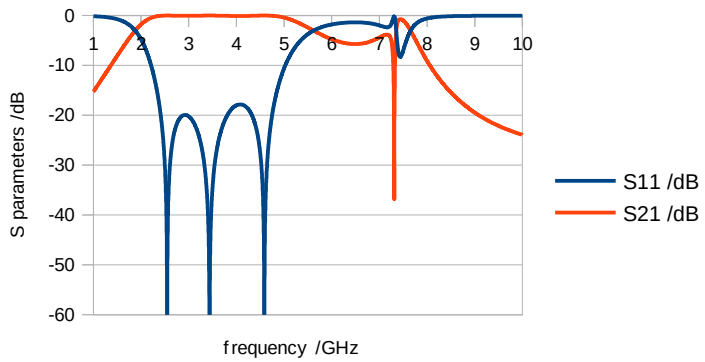


Figure 181: Simulated response - 3-pole filter covered by sylver paint

2 Manufacturing

1 Dielectric part

The dielectric part is obtained by machining a Zirconia cylinder as previously. Then, it was covered by a layer of silver whose conductivity is close to 30 S/µm.



Figure 182: Manufactured dielectric part - 3-pole filter

2 Housing

In order to be efficient, we realize the housing using a plastic 3D printer (Figure 183). Then, we covered the internal surfaces with a silver paint. The two cavities which can be seen are

made to avoid EM filed leakages around the coupling probes. To be noted that these cavities could be made smaller with more optimization of this early prototype.

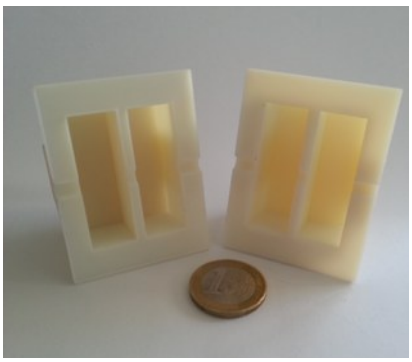


Figure 183: Plastic housing for the 3-pole filter silver-plated

3 Measurements

Once we painted the plastic housing, we are ready to measure the response of this filter. In the Figure 184, we can see the filter is assembled and we can do the measurements.

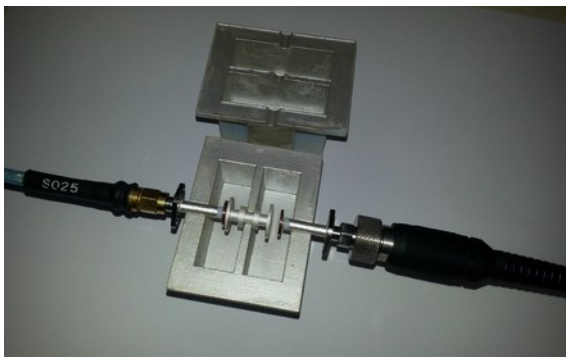


Figure 184: Dielectric silver-plated part inside the plastic housing cover of silver lacquer

The Figure 185 shows the result of the measurement of this filter. It is at the expected central frequency, however we have a smaller bandwidth (only 800MHz). Then, the insertion loss around 5dB is more important than expected. We notice that the spurious mode seen at 7GHz in our simulations is less coupled and slightly shifted around 6.5 GHz.

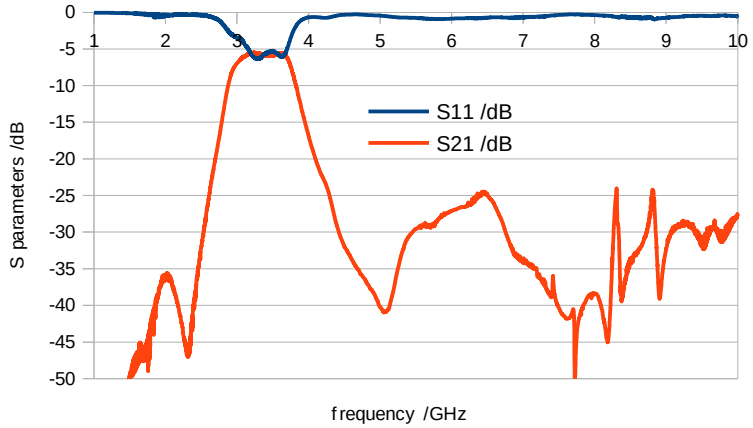


Figure 185: Measured response of the 3-pole silver-plated filter

We identify several critical points for this filter. The first one is the fixation for the coaxial probes. These latter were not efficiently blocked and they may have an angle of inclination that lead to a lower coupling. Thus, it is very likely that we did not achieve the right value for the Input/Output coupling, also explaining that the spurious mode is less coupled. This concept, even if functioning, still need to a precise tuning system for the coaxial probes.

Moreover, some electromagnetic leaks may be present even if we have apply many layers of Silver paint specially in the corners of the cavities where the paintbrush has more difficulty to get to this place. To put the dielectric element on the housing support, we finally had to file a little bit the plastic housing, so it is another source of error.

Finally, even if more improvements are still needed, this evolution of the proposed concept greatly improve the compactness of our filter and its weight, two key requirements for space applications.

3 2-pole filter covered by silver paint

Following the previous concept, we have just painted our previous tuning less 2-pole filter in order to create the same effect as we saw previously (Figure 185).



Figure 186: 2-pole dielectric part covered by silver lacquer

Then, we insert it inside as the same metallic housing.

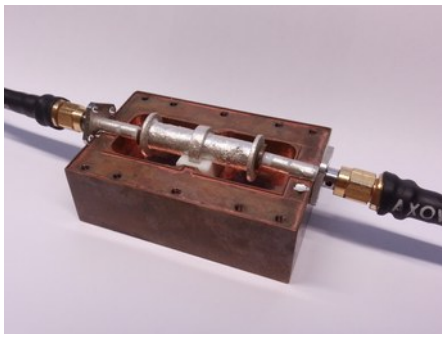


Figure 187: 2-pole silver-plated dielectric part inside the metallic housing

The response is shown in the Figure 188.

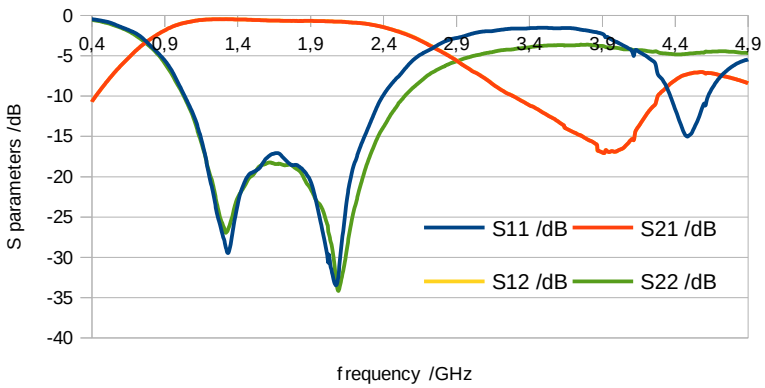


Figure 188: 2-pole filter covered by silver paint - measurement

We obtain a typical two pole response centered around 1.7 GHz. We have a lower central frequency as before (4.75 GHz, Table XI) but the bandwidth is maintained at 1,9 GHz, i.e.111% of f_0 is this case. The return loss is around 17dB without any tuning system and the insertion loss is around 0.8dB. Compared to the previous 3 pole filter, this example has a slightly better maintaining support for the dielectric part and for the coaxial probes.
This result confirms that this design has to be more studied and specially the housing supporting the different parts (dielectric part, probes) because it is truly possible to achieve very wide bandwidth and to increase the compactness of our concept.

4 Conclusion

The silver-plated filter is an original design that needs to be more studied to exploit its full potential. Indeed, the 3-pole filter did not achieved the requirements we were expecting from it. Because of the coaxial probes which require a more optimized supporting and tuning system, we still struggle with having the right bandwidth and a return-loss better than 5dB. However, we saw that this concept permits to have a more important compactness compared to the initial design with a metal housing around it.
Considering the result obtained with the 2-pole silver-plated filter, we have clear clues that tight manufacturing tolerances (±20µm by machining) and a stable supporting system for the dielectric part and probes are critical points to fully exploit this concept potential as the measured 111% bandwidth suggests. A highly accurate metal house (machined Aluminum for example) may be a better candidate than the 3D plastic printed housing we tried even if this latter was cheap and quickly made. Finally, these trials show that a fine tuning system for the coaxial probes is absolutely necessary to have a better control of the value of the Input and Output couplings during the experimental step.

Conclusion

In this part, we took into account the results of the previous chapters and we worked on the different problematics in order to increase the performances of our filter. Indeed, the support system using the coaxial probe as a blocking system showed its limitation in the previous Chapter. It was constraining because we had to remove all the element to have access to the coaxial probe. Then, the centering of our dielectric part was not optimum. In this way, we

designed new coaxial probes to have a better control of the coupling values and we created a Teflon support physically separated from the probes.

The new coaxial probes are based on the previous ones (metallic rod) but a metallic disk is soldered at its top. Then, we have several geometrical parameters to adjust the right coupling: the gap between the coaxial probe and the dielectric part, the diameter and the thickness of the disks. Great values of coupling are possible with this new probes and they appear to bring way more coupling than the previous generation.

Then, the dielectric part is now made by machining so we are able to have manufacturing tolerances of about ± 20µm. We adapted our structures for this process by designing them as cylindrical stacked blocks.

The measurement of the 2-pole filter show some very promising results with a bandwidth of 40% of the central frequency. We finally managed to achieve our main goal, i.e. wide bandpass filter using dielectric resonators. However, a spurious mode close to our bandwidth is present and it is difficult to remove it because the electromagnetic field of this mode is concentrated inside the dielectric part just as the used TM_{010} mode.

We studied a tuning system using dielectric rings made of Zirconia for one set and Alumina for the other. The mismeasurements do not permit us to conclude clearly about this impact on the coupling values. However, this design helped us to identify problems linked to the probes placement and we proposed to design another metallic housing with better features.

The result of the 4-pole filter attests of the relevance of this design. Indeed, we achieved for a more complex structure a bandwidth of 60%. The measurement and specially the only 10dB return loss show that we still have to work on a system to finely tune the Input/Output coupling.

Finally, we developed another concept where the dielectric part is coated with a silver layer. We saw during the study of the TM_{010} dielectric resonator placed in a metal housing that the electromagnetic field is mostly concentrated inside the dielectric element due to the high permittivity of the material. That is why we decided to apply the metallic housing directly on the dielectric object. One of the first effect was the improvement of the compactness of the filter: the relative permittivity of the entire structure increases, so for a given frequency, we will have a smaller piece. We designed a 3-pole filter, however the measurements show us some difficulties. We work at the right frequency but we have a smaller bandwidth and higher loss insertion. More investigations are necessary in order to better understand some observed effects. The final attempt done by silver painting the 2-pole filter designed in Chapter 3 experimentally brought an impressive 111% bandwidth with a 17dB return loss. This very last

device finally brings valuable information about the potential of this very compact and wide bandpass filter made with a single part composed of dielectric resonators.

Conclusion and perspectives

The telecommunication is still an important way of research. The data exchanges never stop growing. It began by transmitting phone communication, but now it is video, picture, etc. In this way, we have to increase the bandwidth of the signal in order to increase the data output. In this work, we focused on one function of the telecommunication satellite: the Input filters. We described our key requirements for the next generation of filter. We wanted wide bandpass filter with high Q-factor and compactness. Thus, we studied the existing solutions (combline and ridge filters mostly) but they did not complete all our specifications. This led us to another technology using dielectric resonators because they have the properties to obtain high Q-factor and compactness due to the material characteristics (respectively low loss tangent and high permittivity) but it was not possible to obtain wide bandwidth (only 5% of f0). We decided to create a hybrid solution using the best of both worlds.

To have wide bandpass filter, we need strong coupling in the filters' Input and Output but also between the different dielectric resonators. In this way, we studied different configurations to obtain these specifications, selecting coplanar probes and stacked dielectric resonators (DR merged in a single part) concepts. Solutions based on the TM010 mode were retained specifically for the DR. Then we designed a 2-pole and a 4-pole filters with the dielectric (Zirconia) parts both made by stereolithography. We obtained a maximal bandwidth of 7% when the single dielectric part is placed in a dedicated metal housing. It was a promising result. However, we identified several critical points about the Input/Output coupling system, manufacturing tolerances and spurious contact between our dielectric element and the metallic housing as well as not efficient tuning screws.

In this way, we moved to another generation. We studied a new Input/Output coupling system using modified coplanar probes. Thus, we designed a 2-pole filter with modified supporting elements made of Teflon. We fabricated the main single dielectric part of this filter by machining a block made of Zirconia in order to have low manufacturing tolerances (±20µm) and we measured the response of the fabricated filter. We obtained a very satisfactory bandwidth of 40%. It is a big step compared to the 5% obtained previously. We also studied a tuning system using dielectric rings that we can be added to our structure to modify the different couplings. However, the mismeasurements do not allow us to validate this method.

We decided to move to a more complex structure with the conception of a 4-pole filter and we obtained another satisfactory result with a bandwidth of 60%.

Following our observations, we decided to study a last concept based on the proposed dielectric element covered by silver paint. Considering the high permittivity of the dielectric material concentrating the electromagnetic field mainly inside the dielectric part, the

surrounded metal housing used previously could be directly “applied” on the dielectric part without modification of this concept functioning.

A 3-pole filter was designed, fabricated and measured following this idea. The principle was experimentally verified and we increased the compactness of our structure but we still have to work on a fine Input/Output coupling system to obtain the right value. By curiosity, we decided to paint our previous 2-pole filter to know the effect on it. It was working and we measured a clean response with a bandwidth of 111% of f0 (1,7GHz).

This very last concept is giving an innovative solution to the initial challenges set at the beginning of this project because:

1. very wide bandwidths can be obtained
2. the silver coated dielectric part is very compact even if small cavities have to be placed around the coplanar probes to limit leakages of the EM fields
3. insertion loss is rather low but could be really better using low loss ceramic instead of the Zirconia
4. a very low number of parts are used, of course mentioning the single dielectric part composed of stacked TM010 dielectric resonators

The future work to do on this thematic is the study of a fine coupling system for Input and Output in order to optimize more efficiently the response of the filters. Then, we have to work on a much more efficient tuning system. The different solutions tried here have not been satisfactory and compatible with the extremely well confined EM filed inside the DR, even if the very accurate machined dielectric part is limiting the use of a tuning device.

The silver-plated filter opens an innovative path to study because it is possible to achieve a good tradeoff between wide bandwidth and compactness for a bandpass filter for low frequency applications. The first result was promising but we need to understand better this structure.

To increase the Q-factor of the filter, we can move to the BMT material instead of Zirconia. Some structures were designed and manufactured for this material but the paste based on BMT ceramic was contaminated by pollutants and the BMT initial block cracked during the firing, preventing us to create a successful device at the end of the project. However, we already know that it is possible to machine this material as the same way as Zirconia

Another study could be made to try to create negative couplings with the proposed concept. Transmission zeros could then be used to have a better out of band rejection. This can be possible to do if two side by side resonators could be close enough. To do that, the general

structure of the filter should be change and we can imagine a curved structure as presented in Figure 189.

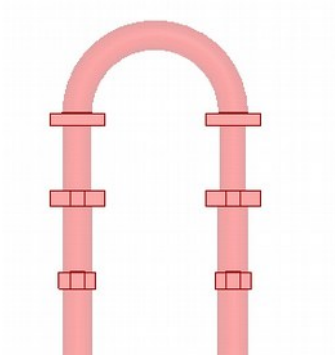


Figure 189: Example of a design of a curved 7-pole filter to realize negative couplings

Résumé :

Les télécommunications sont devenus indispensables dans notre monde actuel. De plus, le volume des données échangées ne cesse de croître. En effet, nous pouvons transmettre nos photos, nos vidéos au monde entier. Nonobstant, nous ne voulons pas attendre pour les avoir, ce qui exige un débit de données très important et par conséquent des signaux avec des bandes passantes plus larges. Les satellites de télécommunications doivent donc s'adapter, c'est pourquoi nous proposons dans ces travaux la recherche de filtre à large bande avec une recherche de compacité et de faibles pertes. Nous nous sommes intéressés à l'utilisation de matériaux céramiques qui permettent d'obtenir de bonnes performances vis à vis de nos besoins. Notre travail est aussi rendu possible par le développement de procédés de fabrication additifs, comme par exemple la stéréolithographie, qui va nous permettre de nous affranchir fortement de règles de dessin contraignantes que nous pourrions avoir en utilisant des procédés classiques. Nous avons développé des filtres avec de larges bandes passantes autour de 4GHz. Une première étude nous a permis de rechercher des concepts qui permettent d'obtenir de forts couplages, conditions sine qua non pour réaliser ces filtres. Plusieurs concepts sont présentés ainsi que leur fabrication et leur mesures. Nous avons ainsi démontré expérimentalement que les concepts proposés, à base de pièces monoblocs céramiques, sont capables de produire des filtres à bandes passantes supérieures à 60 % (voire même 110 % pour une version améliorée).

Mots clés : [stéréolithographie, résonateur diélectrique, filtre large bande, IMUX, mode $TE_{01\delta}$, mode TM_{010}, fabrication additive, forts couplages, Zircone, BMT, céramique]

Abstract :

Every day, the data exchanges increase thanks to the new technologies. We can keep our files, our pictures, our videos online to have an access anywhere on the planet (for now). In this way, the data output of the telecommunication systems has to be increased in order to satisfy the more and more demanding users. One way to allow this is to increase the bandwidths of the different signals, making possible to transmit more data at the same time. In this work, we will develop wide bandpass filters dedicated to space telecommunications. For that purpose, we need them to be compact, with low insertion loss and a limited number of parts to assemble. Consequently, we are interested to use resonators made with ceramic materials that permits to reach such properties. Moreover, these materials are compatible with stereolithography, an additive manufacturing process. Such technology is here very useful for our purpose since its design freedom allows the creation of almost all kind of geometries. To realize such wide bandpass filters, we need strong couplings between the different resonators and also for the accesses, so we will present our studies focused on reaching these specific objectives. Then, we will present different designs of wide bandpass filter around 4GHz. After different generation of ceramic based components, we are be able to experimentally create a 60% bandwidth (even 100% for our last version) very compact bandpass filter filling the objectives of this PhD thesis.

Keywords : [stereolithography, dielectric resonator, wide bandpass filter, IMUX, $TE_{01\delta}$ mode, TM_{010} mode, additive manufacturing process, strong couplings, Zirconia, BMT, ceramic]